A NEW PARABOLIZED NAVIER-STOKES SCHEME FOR HYPERSONIC REENTRY FLOWS

by

Bilal A. Bhutta

Dissertation submitted to the Faculty of the

Virginia Polytechnic Institute and State University

in partial fulfillment of the requirements for the degree of

Doctor of Philosophy

in

Aerospace Engineering

APPROVED:

Dr. Clark H. Lewis, Chairman

Dr. J. A. Schetz

Dr. B. Grossman

Dr. A. K. Jakubowski

Dr. W. L. Neu

April, 1985

Blacksburg, Virginia

A NEW PARABOLIZED NAVIER-STOKES SCHEME FOR HYPERSONIC RE-ENTRY FLOWS

by

Bilal A. Bhutta

Dr. Clark H. Lewis, Chairman

Aerospace Engineering

(ABSTRACT)

High Mach number, low-Reynolds number (high-altitude) reentry flowfield predictions are an important problem area in computational aerothermodynamics. Available numerical tools for handling such flows are very few and significantly limited in their applicability. A new implicit fully-iterative Parabolized Navier-Stokes (PNS) scheme is developed to accurately predict such low-Reynolds number flows. In this new approach the differential equations governing the conservation of mass, momentum and energy, and the algebraic equation of state for a perfect gas are solved simultaneously in a coupled manner. The idea is presented that by treating the governing equations in this manner (rather than eliminating the pressure terms in the governing equations by using appropriate differentiated forms of the equation of state) it may be possible to have an unconditionally time-like numerical scheme. The stability of a simplified version of this new PNS scheme is also studied, and it is demonstrated that these simplified equations are unconditionally time-like in the subsonic as well as the supersonic flow regions. A pseudo-time integration approach is used in addition to a new

second-order accurate fully-implicit smoothing, to improve the efficiency of the solution algorithm.

The new PNS scheme is used to predict the flowfield around a seven-deg sphere-cone vehicle under high- and low-Reynolds number conditions. Two test case, Case A and Case B, are chosen such that Case A has a large freestream Reynolds number (2.92×10^5), whereas Case B has a freestream Reynolds number of 1.72×10^3, which is smaller than the usual limit of applicability of the non-iterative PNS schemes ($Re\sim10^4$ or larger). Comparisons are made with other available numerical schemes, and the results substantiate the stability, accuracy and efficiency claims of the new Parabolized Navier-Stokes scheme.

ACKNOWLEDGEMENTS

The author wishes to thank his faculty advisor and Chairman of his Advisory Committee, Dr. Clark H. Lewis, for his kind guidance, encouragement and invaluable suggestions, which were instrumental in the conceptual and technical development of this research.

The author wishes to thank Dr. J. A. Schetz, Dr. B. Grossman, Dr. A. K. Jakubowski and Dr. W. L. Neu for their suggestions and review of the dissertation. Also, the author is grateful to his parents and his family for their faith in him, and for their patience and understanding.

Finally, the author humbly dedicates this work to his parents, friends and teachers.

TABLE OF CONTENTS

LIST OF ILLUSTRATIONS

LIST OF TABLES

NOMENCLATURE

a =speed of sound

CFS =streamwise skin-friction coefficient

DX =axial step size

e =total energy per unit volume

J =determinant of the transformation Jacobian

k =thermal conductivity

M =Mach number

m =slope of the $\log(\psi^n)$ curve

n =iteration number

P,p =static pressure

Pr =Prandtl number

PWALL =wall pressure

PINF =freestream static pressure, p_∞

QW =wall heat-transfer rate, $Btu/ft^2/sec.$

Re =Reynolds number, $(\rho^* V^* Rn^*)/\mu^*$

RN,Rn =nose radius

T =static temperature

t =time

U,u =x-component of velocity

UINF =freestream velocity, V_∞

V =total velocity

w =z-component of velocity

X,x =coordinate along body axis

ZB =z-location of the body surface

ZSHK =z-location of the bow shock

z =axis-normal coordinate

β =convergence rate, exp(-m)

ε =M_∞/Re_∞

θ =half cone-angle

ξ =marching or streamwise coordinate

ζ =coordinate measured from the body to the outer bow shock, either axis-normal or body-normal

ρ =static density

τ =average computing time per grid point

ψ =maximum local percentage change in the flowfield variables from one itertaion to the next iteration

$\bullet$ =vector dot product

superscript

$\rightarrow$ =vector quantity

$\sim$ =matrix quantity

n =index for iteration

j =index in ξ direction

$*$ =dimensional quantity

subscript

, =represents partial derivative

ℓ =index in ζ direction

∞ =freestream quantity

w =wall quantity

CHAPTER I. INTRODUCTION

Over the past several years, significant interest has been generated in applying Parabolized Navier-Stokes (PNS) schemes to study various aerodynamic and aerothermodynamic problems. Various researchers have used the PNS schemes to study supersonic/hypersonic external flows around realistic reentry configurations (Refs. 1-15). However, these studies have been typically limited to low-to-moderate reentry altitudes. Recent developments in Aeroassisted Orbital Transfer Vehicle (AOTV) and decoy technologies have focussed significant interest on the high-altitude (low-density and low Reynolds number) flows around complex multiconic and lifting reentry configurations under large angles of attack. The PNS schemes are elliptic in the crossflow direction and can treat the large crossflow separated regions that might occur under such flow conditions. Although under such altitude conditions the flowfield is more accurately that of finite-rate chemically reacting air, a stable high-altitude perfect-gas scheme is the basic stepping stone for such an effort.

1.1. PROBLEM IDENTIFICATION

High altitude reentry flows are characterized by low Reynolds numbers. The case of decoy-type reentry geometries is even more severe, as the nose radii for such geometries are typically much smaller than the AOTV-type geometries, and the characteristic Reynolds numbers (based on nose radius) are even smaller. The typical Reynolds numbers for these conditions

are well below the accepted lower bounds of the conventional (iterative or non-iterative) PNS schemes. Presently, the most widely used PNS scheme is the implicit non-iterative PNS scheme of Schiff and Steger.[1] For this scheme, Schiff and Steger[1] indicated that the results were valid for freestream Reynolds numbers (Re_∞) greater than 10^4; however, the basis for such an argument was not discussed. Thus, the author is led to believe that the aforementioned observation was largely based on numerical experiments. Over the past few years, the author has been extensively involved in the study and prediction of low-Reynolds number flows. Several numerical tests were conducted with various numerical schemes over a wide range of reentry conditions, and experience with the implicit non-iterative PNS schemes has shown that the low-Reynolds number limit suggested by Schiff and Steger[1] serves as a good rule of thumb.

In order to answer the question "Why do the implicit non-iterative PNS schemes fail under low-Reynolds number conditions?," the problem was split into various possible causes; namely, the Approximate Factorization scheme, the near-wall solution, the effects of implicit and explicit smoothing, and the sublayer approximation. Each of these possible sources of instability was studied separately and in great detail. In order to get away from the problems caused by the use of the Approximate Factorization scheme, it was decided to focus attention on axisymmetric flows, and we developed an equivalent axisymmetric version of the implicit non-iterative AFWAL PNS scheme.[2] Although the subsequent solutions were slightly more stable, the instability under low-Reynolds number conditions remained. This led to the belief that although the Approximate

Factorization errors do contribute to the solution instability, they are not the main cause of it.

Next, the near-wall solution and the impact of smoothing and damping parameters was examined. In this near-wall region the velocities in general are very small. Under high-Reynolds number conditions this low-velocity region is very thin and typically spans over a couple of grid points. Under laminar low-Reynolds number conditions, however, this region of low velocities may spread over a significant portion of the shock layer. The magnitudes of these velocities are significant because they directly impact the condition number of the solution matrices. Furthermore, the smaller the magnitude of these velocities the larger is the impact of the smoothing and damping terms on the form and accuracy of the solution matrices. On the other hand, the smaller the local velocities, the more are the solution oscillations caused by the use of central-differencing operators and, thus, require more smoothing to be added. Based on these arguments, the author believes that, while the inaccuracies in the solution procedure and the use of arbitrary smoothing parameters might not be the sole cause of instabilities, they certainly contribute significantly to the overall solution instability of a non-iterative PNS scheme under low-Reynolds number conditions.

After Studying the behavior of such non-iterative PNS schemes under high-altitude (low Reynolds number) conditions, the author also believes that the use of "sublayer approximations" (such as the sublayer approach of Schiff and Steger[1] and the approach of Vigneron et al.[3]) under

low-Reynolds number conditions may be another possible source of inaccuracies. All PNS schemes based on such sublayer approximations (and reported in the open literature) have been studied only under high-Reynolds number conditions where the subsonic sublayer region is typically very small in relation to the shock-layer thickness (of the order of 0.5%). However, under low-Reynolds number flows this subsonic sublayer region may become as large as 5% of the shock-layer region and may contain as much as 50% of the total grid points. Furthermore, the fact that the solution errors and oscillations can grow in the near-wall region, indicates that use of the conventional sublayer approximations is inadequate under low-Reynolds number conditions.

As a result of these studies, it is concluded that there are some serious deficiencies in the conventional non-iterative PNS schemes, especially when they are used under low-Reynolds number conditions. The problems are so basic that in order to resolve them one has to step beyond the limits of a simple non-iterative algorithm. Thus, with these ideas in the background, it was decided to look into the development of a new PNS solution scheme which will not only retain the main attractive aspect of the non-iterative PNS schemes (namely; efficient and fast solution), but will also be more stable and accurate.

This study deals with the mathematical development and numerical demonstration of a new implicit fully-iterative PNS solution scheme for the prediction of axisymmetric reentry-type flowfields. These numerical results suggest that the new iterative PNS scheme is not only superior to

the conventional non-iterative PNS schemes, but it is also stable in the imbedded subsonic regions and, thus, does not require any sublayer approximation. Furthermore, the scheme typically shows a cubic convergence rate, and the computing times for a full iterative solution are only fractionally larger than the corresponding computing times of a non-iterative PNS solution.

1.2. RELATIONSHIP WITH PREVIOUS PNS TREATMENTS

Over the past several years a number of parabolized Navier-Stokes (PNS) schemes have been developed to study the problem of hypersonic reentry flows. These PNS schemes can be broadly classified as (a) non-iterative PNS schemes and (b) iterative PNS schemes. Examples of non-iterative PNS schemes are the scheme of Schiff and Steger,[1] the AFWAL PNS scheme[2,4] and the scheme of Vigneron et al.[3] Examples of iterative PNS schemes are the schemes of Lubard and Helliwell,[5] Helliwell et al.,[6] and Lin and Rubin.[9] While the schemes of Refs. 1-6 solve the steady state equations, the scheme of Lin and Rubin[9] solves the unsteady equations by integrating them in the time direction until a steady state is reached. Actually, all iterative schemes may be viewed as integrating in some pseudo-time direction. Thus, we see that of the iterative PNS examples cited earlier, the schemes of Lubard and Helliwell,[5] and Helliwell et al.[6] are pseudo-unsteady formulations, whereas the scheme of Lin and Rubin[9] is an actual unsteady formulation.

All the aforementioned PNS schemes (Refs. 1-6 and 9) are conditionally time-like (hyperbolic/parabolic) in the streamwise marching direction. In the literature this problem of conditionally time-like character in the streamwise direction is also referred to as the problem of departure solutions. This departure behavior is in fact related to the streamwise stability of the solution scheme. In the available literature there are two ways in which the problem of departure (streamwise stability) has been analyzed; i.e, either from the point of view of the governing differential equations (Refs. 1-4) or from the point of view of the differenced form of these governing differential equations (Refs. 5,6 and 9).

The works of Schiff and Steger[1] and Vigneron et al.[3] are good examples of how to analyze the problem of departure (streamwise stability) by looking at the governing differential equations. They approach the problem by considering the fact that the solution scheme will be a valid marching scheme (stable in the streamwise direction) only if the governing differential equations are time-like (hyperbolic/parabolic) in the marching direction. In case the governing equations become locally elliptic, the use of a marching approach becomes invalid and any attempt to march through such locally elliptic regions will encounter numerical difficulties; in short, the problem of departure will occur. Although based on a simplified versions of the governing PNS equations, both Schiff and Steger[1] and Vigneron et al.[3] have shown that the character of the governing equations can be directly linked to the eigenvalues of the system of differential equations being considered. Their analyses (Refs. 1 and 3) indicated that the eigenvalues of the system become complex in

the subsonic sublayer region, indicating that the governing equations become elliptic in the subsonic sublayer region and a marching-like solution scheme becomes ill-posed. The supersonic outer flow region did not pose any problem because the eigevalues of the system in this region remained real. Thus, the governing equations were truely time-like (hyperbolic/ parabolic) in the outer supersonic region and, consequently, a marching-type solution scheme was well-posed.

On the other hand, Lubard and Helliwell[5] and Helliwell et al.[6] looked at the problem of departure (streamwise stability) by looking at the differenced form of the governing equations. Actually the analysis of Lubard and Helliwell[5] was also used as the basis for the stability constraints used in Ref. 6. In this approach a Fourier-type analysis is used to look at the growth of oscillations in the streamwise directions. The result of their analysis also indicated that the eigenvalues of the amplification matrix had magnitudes greater than 1 in the subsonic sublayer region, unless the marching step size was kept greater than a certain minimum value.

The work of Rubin and Lin[8] and Lin and Rubin[9] also confirms that a minimum step-size requirement is necessary to prevent departure. The earlier reported work of Lin and Rubin[7] had suggested that any time relaxation (unsteady formulation) could be used to prevent departure completely. However, analytic and numerical stability analyses were subsequently performed by Rubin and Lin[8] and Lin and Rubin[9], and they corrected the claim made in Ref. 7 by noting the existence of a minimum

step-size constraint if the solution was not globally iterated (i.e., attempted as a "single-sweep"). The results of these analyses indicated that for the time-relaxed (unsteady) PNS scheme of Rubin and his associates (Refs. 7-9) $\Delta x_{min} \sim O(y_m)$, where y_m is the extent of the sublayer region. This constraint was obtained analytically from a linear Von Neumann stability analysis of a simplified and incompressible form of the PNS equations (Ref. 9), and was qualitatively confirmed by numerical tests.

In order to get rid of the problem of departure, various researchers have devised different approaches. Most notable of these are the sublayer approximation used by Schiff and Steger,[1] the approach of Vigneron et al.,[3] and the step-size control methods of Lubard and Helliwell[5] and Lin and Rubin.[9] The departure analyses of Schiff and Steger[1] and Vigneron et al.[3] were based on looking at the character of the governing equations and the corresponding eigenvalues of the system in the viscous and inviscid limits. In the case of Schiff-Steger approach[1] the sublayer pressure was assumed to be known and a constant. By doing so it was observed that the resulting governing equations became time-like even in the sublayer region and the problem of departure was, thus, resolved. Vigneron et al.,[3] on the other hand, assumed that in the subsonic sublayer region only a fraction of the streamwise pressure derivative ($p_{,\xi}$) was to be included; i.e.,

$$p_{,\xi} = \omega p_{,\xi} \qquad (1.1)$$

With such an assumption the governing equations also became time-like in the subsonic sublayer region, as long as

$$\omega < \gamma u^2/[a^2+(\gamma-1)u^2] \tag{1.2}$$

In the case of Lubard and Helliwell,[5] it was observed that if the streamwise pressure derivative ($p_{,\xi}$) was estimated explicitly (i.e., it was estimated from the previous marching steps), convergent (stable in the iteration direction) and departure-free (streamwise stable) marching solutions were possible if:

$$\Delta x_{min} < \Delta x < \Delta x_{max} \tag{1.3}$$

where the lower bound was the constraint for a departure-free solution and the upper bound was the constraint for the iteration convergence.

The approach of Lin and Rubin,[9] for suppressing departure solutions, resembles that of Lubard and Helliwell[5] in suggesting a minimum step-size constraint if $p_{,\xi}$ term was backward differenced; i.e.,

$$\Delta x > \Delta x_{min} \sim O(y_m) \tag{1.4}$$

Rubin and Lin[8] and Lin and Rubin[9] also suggested that if $p_{,\xi}$ was forward differenced, departure could be prevented. Such a forward-differenced approach requires the use of a global relaxation procedure (global iter-

ations). However, the present study concentrates on "single-sweep" PNS procedures only, and not on globally iterated PNS methods.

In the aforementioned "single-sweep" PNS schemes we can see that the possibility of departure solutions (streamwise instabilities) exists, and the constraints developed to prevent departure involve a special treatment of either the sublayer pressure or of its streamwise derivative. This is where the present PNS approach starts to differ from the classical treatments. If we look into the aforementioned schemes for preventing solution departure, and the mathematical reasoning used to arrive at each one of them (Refs. 1, 3 and 5), we see that (in a way) they pre-suppose that the streamwise pressure derivative is the culprit and something needs to be done with respect to it. In each of these cases the reasoning is based on the original suggestion by Rubin and Lin[8] of an "elliptic pressure effect" in the streamwise direction. This suggestion by Rubin and Lin was based on a consideration of interacting boundary-layer theory and, also, assumed an incompressible flow (Ref. 8, pp. 24). At least in the case of Vigneron et al.[3] and Lubard and Helliwell[5] this pre-supposition about the treatment of $p_{,\xi}$ term is obvious. Consider the case of Vigneron et al.[3] and their eigenvalue analysis for analyzing the time-like character (streamwise stability) of the governing differential equations. The factor 'ω' was by choice placed in front of the streamwise pressure derivative term ($p_{,\xi}$), and conveniently appeared in the eigenvalues in the form:

$$\sigma_i \sim \{\gamma u^2 - \omega[u^2 + (\gamma-1)a^2]\}^{0.5} \qquad (1.4)$$

The criterion for the time-like character required these eigenvalues to be always real, and this led to the constraint on 'ω' as given in the Eq. (1.2). Now, it should be noted that the $p_{,\xi}$ term is not the only contributing factor to the quantity whose square root is involved in Eq. (1.4). Thus, from a purely mathematical point of view, it may be possible to have the factor 'ω' re-appear in the square root even if it was chosen as a multiplier for some term other than the streamwise pressure derivative. Consequently, some equivalent constraint on 'ω' may still be obtained to make the eigenvalues real, without neglecting part of the streamwise derivative.

Similarly, in the work of Lubard and Helliwell (Ref. 5, pp. 55-61) it was seen that if $p_{,\xi}$ term in the u-momentum equation and the energy equation was evaluated explicitly, certain contributions to the amplification matrix were removed and the corresponding eigenvalues were ≤ 1 as long as $\Delta x_{min} < \Delta x < \Delta x_{max}$. The approach of Schiff and Steger[1] to prevent departure is different only in the sense that it specifies the sublayer pressure directly rather than specifying its streamwise derivative ($p_{,\xi}$). Nevertheless, even in this case it is done so because certain problematic contributions to the eigenvalues of the differential system get removed, and the eigenvalues become always real. This in turn implies that the governing differential equations become always time-like.

Thus as can be seen form the above discussion, in all of the aforementioned "single-sweep" PNS treatments the problem of departure (streamwise instability) is removed by actually performing mathematical

manipulations (eliminating or changing certain terms) such that either the eigenvalues of the differential system (Refs. 1 and 3) or the eigenvalues of the amplification matrix (Ref. 5) have acceptable values. Now we pose a question --- "Is it be possible to do a mathematical manipulation of the governing PNS equations such that an acceptable time-like character of the governing equations can be obtained without having to neglect certain terms in part or in full ?" This question is the focal point of the new PNS scheme being proposed. In this new PNS scheme the following idea is presented:

If we consider pressure as an additional unknown quantity and solve the algebraic equation of state simultaneously (in a coupled manner) with the differential equations governing the conservation of mass, momentum and energy, it appears to be possible to have an appropriate time-like marching scheme without having to either specify a constant sublayer pressure (Schiff-Steger approach), or to neglect a part of the streamwise pressure derivative (approach of Vigneron et al.), or to estimate the streamwise pressure derivative explicitly (Lubard-Helliwell approach).

The present PNS approach differs from the previous PNS treatments mainly in the treatment of pressure terms. In almost all previous PNS treatments, typically, the pressure-derivative terms in the momentum equations are re-written in terms of the solution unknowns (typically, ρ, u, w and e) by using an appropriate differentiated form of the equation of state. In other words, pressure is considered as a "derived" quantity, and not as an additional unknown variable.

The conceptual development of the proposed PNS scheme uses the formulation of Schiff and Steger[1] as the starting point. In the case of Schiff-Steger scheme, the formulation requires the jacobians (in other words, the derivatives) of the pressure with respect to the unknown flowfield variables (ρ, ρu, ρw and e). Based on a "frozen coefficient" analysis (which is like a local linearization) of a simplified form of the governing equations, it was noted by Schiff and Steger[1] that the derivatives of pressure bring the contribution of speed of sound in the eigenvalues of the resulting system of equations. This speed-of-sound contribution causes the condition that some of the eigenvalues of the system, which dictate the character of the governing equations, are of the form:

$$\sigma_i \sim (u^2-a^2)^{0.5} \qquad (1.5)$$

where 'u' is the streamwise velocity and 'a' is the speed of sound. Thus, Schiff and Steger concluded that as long as u>a (i.e., supersonic flow) all eigenvalues were real and the resulting system was time-like and, consequently, the solution could be marched in the streamwise direction. However, when u<a (i.e., subsonic flow) the eigenvalues became complex and the resulting system showed an elliptic character and, thus, the solution could not be marched.

In order to eliminate this problem of complex eigenvalues, Schiff and Steger recognized (as can be seen in Ref. 1) that if they could some how get rid of this speed-of-sound contribution to the eigenvalues (at least

in the subsonic sublayer region), they would have a system which will be always time-like, and could be marched in the subsonic sublayer region as well as in the outer supersonic region. In order to do so they assumed that the pressure in the sublayer is specified as a constant, and as in their words ". . is not a function of $\vec{q}$ (the local vector of unknowns), . ." (Ref. 1, pp. 4). In doing so, it is indirectly assumed that the sublayer pressure (p_s) is an additional unknown quantity. In the literature, sometimes, the terminology of 'splitting the sublayer pressure' is also used to imply the same concept.

With such an assumption about the sublayer pressure, the derivatives of pressure (in the sublayer region) with respect to the remaining unknown variables (ρ, ρu, ρw and e) become zero; i.e.,

For $u > a$:

$$p = (\gamma-1)[e-\rho(u^2+w^2)/2] \tag{1.6}$$

and

$$p_{,e} = (\gamma-1) \tag{1.7}$$

$$p_{,\rho} = -(\gamma-1)(u^2+w^2)/2 \tag{1.8}$$

$$p_{,\rho u} = -(\gamma-1)u \tag{1.9}$$

$$p_{,\rho w} = -(\gamma-1)w \tag{1.10}$$

For $u < a$:

$$p = p_s = \text{sonic pressure} = \text{constant} \tag{1.11}$$

and

$$p_{,e} = p_{,\rho} = p_{,\rho u} = p_{,\rho w} = 0,\ p_{,p_s} = 1 \tag{1.12}$$

Thus, the contribution of the speed-of-sound to the eigenvalues in the subsonic region is removed (see Ref. 1, pp. 4). Now Schiff and Steger were faced with the problem of how to go from basically four unknowns (ρ, ρu, ρw and e) in the supersonic region to five unknowns in the subsonic region (ρ, ρu, ρw, e and p_s). This problem was resolved through an approximation in which the value of p_s was estimated by extrapolation from the previous steps, and this overall treatment was called the "sublayer approximation." It becomes clear from this discussion that the sublayer approximation is at the expense of satisfying the equation of state, in other words the equation of state in the sublayer region is replaced with the condition $p=p_s$, and the solution of the conservation equations in the sublayer region is not constrained to satisy the equation of state. Once this sublayer solution has been obtained, the updated sublayer pressures are recomputed from this solution using the equation of state. However, this application of the equation of state occurs after the solution has already been obtained, so that although the derived pressures may satisfy the equation of state, the solution of the remaining unknown variables (ρ, ρu, ρw and e) may not.

Now, the idea behind the treatment of pressure terms in the present scheme is conceptually an extension of the Schiff-Steger approach. That is to say, rather than just considering pressure as an additional unknown in the subsonic sublayer region, we consider it as an additional unknown all across the shock-layer (i.e., in the subsonic as well as the outer supersonic region). That is to say we retain the pressure terms in the conservation equations the way they are (i.e., we do not replace them with

appropriate differentiated forms of the equation of state), and include the algebraic equation of state as an additional equation to be solved simultaneously. Thus, the dimensions of the system of equations to be solved increases from five to six. However, from a simplified version of these PNS equations, we see that in doing so we are able to remove the contribution of the speed-of-sound from the eigenvalues of the system in much the same way as the sublayer approximation does, but without having to impose the constant sublayer pressure condition. Since we are not constrained to impose the $p=p_s$ condition anymore, we are able to retain the equation of state even in the sublayer region. In this way, instead of approximating the sublayer pressure by extrapolation from the previous marching steps (the Schiff-Steger approach), we are able to solve for these pressure values in a coupled manner by using the equation of state.

Thus, in general terms, it may be said for the present approach that it is an improvement on the Schiff-Steger approach, whereby we are able to calculate the sublayer pressure directly from the perfect-gas equation of state instead of approximating it by extrapolation from the previous marching steps.

1.3. OUTLINE

Chapter II of this dissertation deals with the description of the coordinate system chosen and, also, a summarized derivation of the governing PNS equations. These PNS equations are derived in detail in Appendix A. A simple and hypothetical problem consisting of three independent vari-

ables is also presented. The idea behind this model problem is to only suggest that for situtations where we have differential equations coupled through an algebraic relation, there may be cases where the time-like or elliptic character of the final solution may depend upon the way these equations are formulated. It is suggested that this model problem may provide some insight into the reason why the classical PNS treatments are conditionally time-like and the present scheme seems to be unconditionally time-like.

Chapter III deals with the numerical formulation and the finite-difference approximations of the governing PNS equations, used to reduce them to a block-tridiagonal system of equations. It is explained how a pseudo-unsteady approach can be used to improve the computing efficiency of the resulting iterative solution. The boundary conditions used to solve the final block-tridiagonal system are explained, and it is shown how the body-normal derivatives at the wall can be accurately calculated.

Chapter IV of this dissertation deals with a new smoothing and damping approach, which is used in the present scheme to damp solution oscillations generally associated with the use of central-differenced operators. It is demonstrated that this smoothing approach is mathematically consistent and second-order accurate.

Chapter V deals with a simplified analysis of the governing PNS equations. This analysis attempts to study the marching-like character

of the simplified PNS equations, and follows partly the approach used by Schiff and Steger in the study of their non-iterative PNS scheme (Ref. 1). It is suggested that (within the limitations of the assumptions and simplifications) the "simplified PNS equations" show an unconditionally time-like character.

Chapter VI of this dissertation provides some demonstrative numerical results based on the present scheme. A seven deg sphere-cone (with a nose radius of 0.041667 ft) is chosen as the test vehicle, and the flow over this vehicle is studied under 80 kft and 200 kft flight altitudes, and for a freestream Mach number of 25. The results of these cases suggest that the present scheme behaves more accurately under high-altitude (high Mach number and low Reynolds number) conditions, where the non-iterative AFWAL PNS scheme (Refs. 2 and 4) seems to encounter stability problems.

Finally, the general conclusions of the present study and their possible implications are presented in Chapter VII. Appendix A provides a detailed description of the governing PNS equations of Chapter II. Appendix B deals with the detailed analysis of the model problem presented in Chapter II. The expressions and details of the linearization processes used in Chapter III are given in Appendix C, and the details of the eigenvalue analysis used in Chapter IV for the "simplified PNS equations" are given in Appendix D.

CHAPTER II. MATHEMATICAL FORMULATION

2.1. COORDINATE SYSTEM

The present PNS scheme can be used for two-dimensional as well as axisymmetric perfect-gas flows. The coordinate system used is a general curvilinear coordinate system (ξ,ζ) shown in Fig. 1. Also, a body-fixed orthogonal (Cartesian) coordinate system is chosen such that the origin of the Cartesian coordinate system is at the tip of the blunt nose and the x-axis is aligned with the axis of the body. The z-axis is chosen as pointing downwards such that the windward surface of vehicle is on the positive z-axis side (see Fig. 1). The ξ coordinate is along the body and is also the marching direction. The ζ coordinate stretches from the body to the outer bow shock and can be either body-normal or axis-normal. In general, it is assumed that the (x,z) space is uniquely transformable to the (ξ,ζ) space through relations of the form:

$$\begin{aligned} \xi &= \xi(x,z) \\ \zeta &= \zeta(x,z) \end{aligned} \qquad (2.1)$$

The uniqueness property is automatically satisfied as long as coordinate lines of the same family do not cross, and this is important so that the inverse transform of Eq. (2.1) is definable. Suppose we denote the marching step at which we seek the solution as 'j+1' and the previous step as 'j', then the transformation of Eq. (2.1) is chosen such that the

physical (x,z) grid between 'j' and 'j+1' steps transforms to a rectangle in the computational (ξ,ζ) plane. The body surface corresponds to the ζ=0 curve, whereas the outer bow shock corresponds to ζ=LMAX curve (LMAX being the number of grid points in the ζ direction). Also, ξ=0 at the j-th step and ξ=1 at the j+1 step. Thus, at each marching step, every grid cell in the x-z space between the j and the j+1 step is transformed into a unit square in the ξ-ζ plane with $\Delta\xi$=$\Delta\zeta$=1.0 (see Fig. 2).

The transformation given by Eq. (2.1) is in general difficult to obtain. However, if we assume for the present that the (x,z) grid at the j+1 step is known (subsequent sections will discuss this in more detail), then the metric derivatives for the inverse transform

$$x = x(\xi,\zeta)$$
$$z = z(\xi,\zeta) \qquad (2.2)$$

can be easily obtained numerically. At each grid point, this information about the inverse-transform metrics is used to determine the transformation Jacobians (J) and the metric derivatives ($\xi_{,x}$, $\xi_{,z}$, $\zeta_{,x}$ and $\zeta_{,z}$) for the transformation given by Eq. (2.1).

2.2. PARABOLIZED NAVIER-STOKES EQUATIONS

The full Navier-Stokes equations governing three-dimensional compressible flows can be written in a nondimensional form as (see Appendix A):

$$\begin{bmatrix} \rho u^2+p \\ \rho uv \\ \rho uw \\ \rho u\Phi \\ 0 \end{bmatrix}_{,x} + \begin{bmatrix} \rho vu \\ \rho v^2+p \\ \rho vw \\ \rho v\Phi \\ 0 \end{bmatrix}_{,y} + \begin{bmatrix} \rho wu \\ \rho wv \\ \rho w^2+p \\ \rho w\Phi \\ 0 \end{bmatrix}_{,z} = \varepsilon\left(\begin{bmatrix} g_{12} \\ g_{13} \\ g_{14} \\ g_{15} \\ 0 \end{bmatrix}_{,x} + \begin{bmatrix} g_{22} \\ g_{23} \\ g_{24} \\ g_{25} \\ 0 \end{bmatrix}_{,y} + \begin{bmatrix} g_{32} \\ g_{33} \\ g_{34} \\ g_{35} \\ 0 \end{bmatrix}_{,z} \right) + \begin{bmatrix} 0 \\ 0 \\ 0 \\ 0 \\ \gamma p-\rho T \end{bmatrix}$$

Or

$$\vec{E}_{1,x} + \vec{E}_{2,y} + \vec{E}_{3,z} = \varepsilon(\vec{G}_{1,x} + \vec{G}_{2,y} + \vec{G}_{3,z}) + \vec{P} \qquad (2.3)$$

where the various components of the aforementioned viscous vectors ($\vec{G}_1$, $\vec{G}_2$ and $\vec{G}_3$) have been derived in Appendix A, and $\Phi=[T/(\gamma-1)+V^2/2]$. The aforementioned Navier-Stokes equations have been closed by using the equation of state, which is the last equation of the above vectorial equation. For a perfect gas this equation of state is given as:

$$\gamma p = \rho T \qquad (2.4)$$

Unlike the conventional PNS approaches, we choose our unknowns to be the density (ρ), the density-velocity products (ρu and ρw), the density-temperature product (ρT) and the pressure (p). The reason for choosing 'ρT' as the independent variable (instead of the total energy per unit volume, 'e') is that when one considers the eventual extension of the present scheme to real-gas flows, the temperature 'T' (or equivalently ρT) is a more convenient variable. Thus our vector of unkowns is:

$$\vec{q} = \begin{bmatrix} \rho \\ \rho u \\ \rho w \\ \rho T \\ p \end{bmatrix} \tag{2.5}$$

Following the approach of Peyret and Viviand,[16] it can be shown (see Appendix A) that Eq. (2.3) can be transformed into the following vectorial equation in the general curvilinear coordinate system (ξ,ζ), i.e.,

$$\vec{F}^{j}_{,\xi_j} = \varepsilon \vec{S}^{j}_{,\xi_j} + (1/J)\vec{P} \tag{2.6}$$

where 'J' is the determinant of the transformation Jacobian, and

$$\vec{F}_j = (1/J)\xi_{j,x_i}\vec{E}_i \tag{2.7}$$

$$\vec{S}_j = (1/J)\xi_{j,x_i}\vec{G}_i \tag{2.8}$$

In the above equations the indicies 'i' and 'j' represent 1,2 and 3, ξ_1 is ξ, ξ_2 is ζ, ξ_3 is the circumferential coordinate measured from the windward plane of symmetry, x_1 is x, x_2 is y and x_3 is z.

It has been shown in Appendix A that for axisymmetric or 2-D flows the crossflow convective derivatives can be analytically obtained. If we consider only the windward pitch-plane, we obtain

$$\vec{F}_{3,\xi_3} = (1/J)\begin{bmatrix} 0 \\ 0 \\ 0 \\ -\kappa p/z \\ 0 \\ 0 \end{bmatrix} \tag{2.9}$$

where κ=0 for 2-D flows and κ=1 for axisymmetric flows.

Furthermore, for axisymmetric/2-D flows the crossflow diffusion effects are zero; i.e.,

$$\vec{S}_{3,\xi_3} = 0 \tag{2.10}$$

Thus, if we define $\vec{H}$ as

$$\vec{H} = \vec{P} - \vec{F}_{3,\xi_3} \tag{2.11}$$

we obtain the axisymmetric/2-D Navier-Stokes equations in a general curvilinear coordinate system as:

$$\vec{F}_{1,\xi} + \vec{F}_{2,\zeta} = \varepsilon(\vec{S}_{1,\xi} + \vec{S}_{2,\zeta}) + \vec{H} \tag{2.11}$$

It should be noted that the third row of the above vectorial equation [Eq. (2.11)] consists of all zero terms and, thus, will be dropped. In other words, the vectors appearing in Eq. (2.11) are re-defined such that third row is removed, and all other terms are simplified using v=0.

Equation (2.11) is elliptic in both ξ and ζ directions. If we neglect the viscous diffusion and dissipation effects in the ξ direction and assume that the solution can be marched in the ξ direction (the validity of this marching assumption will be discussed later), Eq. (2.11) reduces to the parabolized Navier-Stokes (PNS) equations. The complete set of these PNS equations for axisymmetric and two-dimensional perfect-gas flows can be written in a vectorial form as:

$$
\begin{bmatrix} \rho U_1/J \\ (\rho u U_1+\xi_{,x}p)/J \\ (\rho w U_1+\xi_{,z}p)/J \\ \rho\Phi U_1/J \\ 0 \end{bmatrix}_{,\xi} + \begin{bmatrix} \rho U_2/J \\ (\rho u U_2+\zeta_{,x}p)/J \\ (\rho w U_2+\zeta_{,z}p)/J \\ \rho\Phi U_2/J \\ 0 \end{bmatrix}_{,\zeta} = \varepsilon\left(\begin{bmatrix} 0 \\ s_2 \\ s_3 \\ s_4 \\ 0 \end{bmatrix}_{,\zeta} \right) + \begin{bmatrix} 0 \\ 0 \\ \kappa p/Jz \\ 0 \\ \gamma p-\rho T \end{bmatrix}
$$

or

$$
\vec{F}_{1,\xi} + \vec{F}_{2,\zeta} = \varepsilon \vec{S}_{,\zeta} + \vec{H} \qquad (2.12)
$$

where U_1 and U_2 are the contravariant velocity components defined in Appendix A, and the form and derivation of the viscous vector $\vec{(S)}$ is also given in Appendix A.

2.3. A MODEL MARCHING PROBLEM OF A MIXED TYPE

The system of equations represented by Eq. (2.12) is not a pure differential system, it consists of five partial differential equations coupled through a sixth equation which is a purely algebraic relation. In the present treatment this set of governing equations is referred to as a 'mixed-type system'. The term 'mixed-type' is not to be confused with the character of the differential equations in the system (i.e., hyperbolic, parabolic, elliptic, etc.). In terms of character classi-

fication, a system whose differential equations change character will be explicitly called out as a 'mixed-character system'.

The most important view point to be presented in this section is that the character classification of a mixed type system is significantly different from the classical character classification of purely differential systems. In other words a purely differential system has a fixed character; i.e., it is either elliptic or time-like. By 'time-like' we mean that a differential system is either hyperbolic or parabolic or mixed hyperbolic-parabolic. However, as long as the differential system is time-like, the numerical solution can be marched in the time-like direction. On the other hand, if the differential system is elliptic in character, marching-like numerical solutions are invalid.

The case of mixed-type systems is, however, quite different. For such mixed-type systems the overall character of the system may depend upon the way in which the problem is formulated. That is to say, it may be possible to have a mixed-type system as elliptic or conditionally elliptic if one formulates the problem in one way, and have it unconditionally marching-like if one formulates the problem in another way. This idea is new and has given rise to a fair amount of controversy. Nonetheless, it may be analytically demonstrated on a model mixed-type system.

Consider the following system involving 3 unknowns, ϕ_1, ϕ_2 and ϕ_3; i.e.,

$$
\begin{aligned}
\phi_{1,x} - \phi_{2,y} &= 0 \\
\phi_{2,x} - \phi_{1,y} + 2\phi_{2,y} + \phi_{3,y} &= 0 \\
a^2\phi_1 - \phi_3 &= 0
\end{aligned}
\qquad (2.13)
$$

with initial condition specified at x = 0 and boundary conditions specified at y=0 and at y=1. Suppose we consider the following initial and boundary conditions:

$$
\begin{aligned}
\phi_3(0,y) &= a^2\phi_1(0,y) \\
\phi_1(0,y) &= \phi_2(0,y) = y
\end{aligned}
\qquad (2.14)
$$

$$
\begin{aligned}
\phi_3(x,0) &= a^2\phi_1(x,0) \\
\phi_{1,y}(x,0) &= \phi_{2,y}(x,0) = 1
\end{aligned}
\qquad (2.15)
$$

and

$$
\begin{aligned}
\phi_3(x,1) &= a^2\phi_1(x,1) \\
\phi_1(x,1) &= 1 + x \\
\phi_2(x,1) &= 1 - (a^2+1)x
\end{aligned}
\qquad (2.16)
$$

The solution to Eq. (2.13) for these boundary conditions [Eqs. (2.14), (2.15) and (2.16)] is (see Appendix B):

$$
\begin{aligned}
\phi_1(x,y) &= y + x \\
\phi_2(x,y) &= y - (a^2+1)x \\
\phi_3(x,y) &= a^2(y+x)
\end{aligned}
\qquad (2.17)
$$

It is suggested that the above model problem appears to bear some resemblence with the inviscid limit of the governing PNS equations. The model problem involves only first-order derivatives in the two spatial coordinate directions to simulate the convective derivatives of the inviscid limit of the PNS equations. The third equation of this model problem is an algeraic relation, and is used to simulate the role of the algebraic equation of state in the PNS equations. Just like the equation of state in the governing PNS equations, the algebraic relation of the model problem appears not only as a relation to be satisfied within the solution domain, but it also appears in the initial conditions and the boundary conditions. The variable ϕ_3 of the model problem plays a similar role as played by pressure in the governing PNS equations. Now consider the following two different formulations of the model problem.

2.3.1. Formulation I

In this approach we can substitute the third equation of Eq. (2.13) into the second equation and obtain

$$\begin{aligned} \phi_{1,x} \qquad\qquad - \phi_{2,y} &= 0 \\ \phi_{2,x} + (a^2-1)\phi_{1,y} + 2\phi_{2,y} &= 0 \end{aligned} \tag{2.18}$$

Or we may simply write

$$\vec{\phi}_{,x} + \tilde{A}\cdot\vec{\phi}_{,y} = 0 \tag{2.19}$$

where

$$\vec{\phi} = \begin{bmatrix} \phi_1 \\ \phi_2 \end{bmatrix} \tag{2.20}$$

and the eigenvalues of $\tilde{A}$ are

$$\lambda_1 = 1 + (2-a^2)^{0.5}$$
$$\lambda_2 = 1 - (2-a^2)^{0.5} \tag{2.21}$$

It is also shown in Appendix B that we can write Eq. (2.19) as

$$\psi_{1,x} + \lambda_1 \psi_{1,y} = 0$$
$$\psi_{2,x} + \lambda_2 \psi_{2,y} = 0 \tag{2.22}$$

where

$$\phi_1 = \psi_1 + \psi_2$$
$$\phi_2 = -\lambda_1 \psi_1 - \lambda_2 \psi_2 \tag{2.23}$$

Thus, we see that Eq. (2.22), and equivalently Eq. (2.18), is time-like if λ_1 and λ_2 are real ($a^2 \leq 2$). When λ_1 and λ_2 are not real ($a^2 > 2$), Eqs. (2.18) and (2.22) are elliptic in nature. In other words, a marching-like solution of Eq. (2.18) will be valid only if $a^2 \leq 2$. Fur-

thermore, Appendix B shows that for $a^2 \leq 2$ the analytic solution to Eq. (2.18) can be found, and it is the same as given by Eq. (2.17).

2.3.2. Formulation II

From the earlier discussion on Formulation I of the model problem we see that the variable 'a' of the model problem is like the speed of sound in the governing PNS equations. That is to say, like the classical PNS schemes where the speed of sound appears in the eigenvalues through the pressure terms and the accompanying equation of state (Refs. 1 and 3), in the model problem the variable 'a' appears in the eigenvalues through the variable ϕ_3 and the corresponding algebraic realtion. Now, for this model problem, if we can devise another formulation such that the variable 'a' no longer contributes to the eigenvalues of the system, it may provide us with a key to attempt a similar treatment of the governing PNS equations. It appears that such a re-formulation of the model problem may be mathematically possible, and will be called Formulation II.

In the aforementioned Formulation I, the overall mixed-type system was reduced to a pure differential system. In Formulation II we will attempt to solve directly the actual mixed-type system [Eq. (2.13)], and look at the character of the resulting system. At first glance it does not seem likely to be able to do that. However, it may be possible to do such an analysis if one looks at Eq. (2.13) as the limiting case of a small-perturbation problem. Such an approach might be valid as long as

the small-perturbation problem being considered allows us to take this limit without any singular behavior.

For this purpose, consider the following problem (were $\varepsilon \geq 0$)

$$\begin{aligned} \phi_{1,x} - \phi_{2,y} &= 0 \\ \phi_{2,x} - \phi_{1,y} + \phi_{2,y} + \phi_{3,y} &= 0 \\ \varepsilon\phi_{3,x} &= a^2\phi_1 - \phi_3 \end{aligned} \tag{2.24}$$

with

$$\begin{aligned} \phi_1(0,y) &= y \\ \phi_2(0,y) &= y \\ \phi_3(0,y) &= a^2 y \end{aligned} \tag{2.25}$$

$$\begin{aligned} \phi_{1,y}(x,0) &= 1 \\ \phi_{2,y}(x,0) &= 1 \\ \varepsilon\phi_{3,x}(x,0) &= a^2\phi_1(x,0) - \phi_3(x,0) \end{aligned} \tag{2.26}$$

and

$$\begin{aligned} \phi_1(x,1) &= 1 + x \\ \phi_2(x,1) &= 1 - (a^2+1)x \\ \varepsilon\phi_{3,x}(x,1) &= a^2\phi_1(x,1) - \phi_3(x,1) \end{aligned} \tag{2.27}$$

Thus, the small perturbation problem being presented has the correct initial conditions, and the boundary conditions at y=0 and y=1 are consistent with the governing equations [Eq. (2.24)].

The complete solution of this problem is given in Appendix B. However, briefly speaking, Eq. (2.24) can be written as:

$$\vec{\phi}_{,x} + \tilde{A}\cdot\vec{\phi}_{,y} - (1/\varepsilon)\tilde{B}\cdot\vec{\phi} = 0 \qquad (2.28)$$

The eigenvalues of $\tilde{A}$ are

$$\begin{aligned} \lambda_1 &= 1 + \sqrt{2} \\ \lambda_2 &= 1 - \sqrt{2} \\ \lambda_3 &= 0 \end{aligned} \qquad (2.29)$$

It is shown in Appendix B that we can write Eq. (2.28) as

$$\begin{aligned} \psi_{1,x} + \lambda_1\psi_{1,y} - \lambda_2 (f/\varepsilon) &= 0 \\ \psi_{2,x} + \lambda_2\psi_{2,y} + \lambda_1 (f/\varepsilon) &= 0 \\ \psi_{3,x} - (\lambda_1-\lambda_2)(f/\varepsilon) &= 0 \end{aligned} \qquad (2.30)$$

where

$$f = [a^2(\psi_1+\psi_2) + (a^2-1)\psi_3]/(\lambda_1-\lambda_2) \qquad (2.31)$$

and

$$\phi_1 = \psi_1 + \psi_2 + \psi_3$$
$$\phi_2 = -\lambda_1\psi_1 - \lambda_2\psi_2$$
$$\phi_3 = \psi_3 \qquad (2.32)$$

Since λ_1 and λ_2 are real [see Eq. (2.29)], we can see that Eq. (2.30) is unconditionally time-like, and a marching-type numerical solution of Eq. (2.30) will be unconditionally valid.

In order to answer the question, "How does the small perturbation problem of Eq. (2.24) relate to the original problem of Eq. (2.13)?", we can see that under the limiting condition

$$\varepsilon \to 0^+ \qquad (2.33)$$

Eq. (2.24) reduces to Eq. (2.13), and the boundary conditions given by Eqs. (2.26) and (2.27) reduce to the actual boundary conditions given by Eqs. (2.15) and (2.16). The initial conditions are the same anyway.

A question arises --- "Is it valid to take the limit of Eq. (2.30)?", or in other words "Does Eq. (2.30) behave singularly because of the $1/\varepsilon$ factor?" To answer to this question, the third equation of this system [Eq. (2.30)] shows that for all ε

$$f/\varepsilon = \psi_{3,x}/(\lambda_1 - \lambda_2) \qquad (2.34)$$

In other words, Eq. (2.34) indicates that 'f/ε' is always defined, if $\psi_{3,x}$ is defined for ε≥0.

The demonstration that $\psi_{3,x}$ is bounded for ε≥0 [i.e., Eq. (2.30) is not singular when $\varepsilon \to 0^+$], comes from the actual analytic solution of Eq. (2.30). It is shown in Appendix B that the analytic solution to Eqs. (2.30) and (2.32) is:

$$\begin{aligned} \phi_1(x,y) &= y + x \\ \phi_2(x,y) &= y - (a^2+1)x \\ \phi_3(x,y) &= a^2(y+x) - a^2\varepsilon[1-\exp(-x/\varepsilon)] \end{aligned} \tag{2.35}$$

where

$$\varepsilon \geq 0 \tag{2.36}$$

It should be noted that we are marching in the x direction, so that our x is always positive and increasing. Thus, we see that with $\varepsilon \to 0^+$, Eq. (2.34) does not appear to be singular [or, equivalently Eq. (2.30) does not appear to be singular] and, furthermore, this solution seems to be even valid for ε = 0 (see Appendix B). Also, we see that with $\varepsilon \to 0^+$, the solution to our hypothetical small perturbation problem appears to correctly approach the solution to our actual model problem; i.e.,

$$\phi_1(x,y) = y + x$$

$$\phi_2(x,y) = y - (a^2+1)x$$

$$\phi_3(x,y) \rightarrow a^2(y+x) \qquad (2.37)$$

The aforementioned mathematical exercise is only used to present the conclusion --- There may exist a class of 'mixed-type' system-of-equations where it may be possible to have a conditionally time-like behavior if one formulates the problem in one way, and it may also be possible to have the same problem as unconditionally time-like if one formulates the problem in a slightly different manner.

The model problem [Eq. (2.13)] presented herein, bears some similarity to the governing PNS equations [Eq. (2.12)]. The classical treatments of these PNS equations (Refs. 1-9) appear to correspond to the Formulation I presented earlier, which was conditionally time-like. The present scheme, however, seems to follow the approach of Formulation II, which had an unconditionally time-like character.

CHAPTER III. NUMERICAL FORMULATION

3.1. EXPANSION AROUND THE PREVIOUS ITERATION

The previous chapter discussed the derivation of PNS equations for axisymmetric and two-dimensional flows. It was shown that these PNS equations can be written in the following vectorial form:

$$\vec{F}_{1,\xi} + \vec{F}_{2,\zeta} = \varepsilon \vec{S}_{,\zeta} + \vec{H} \tag{3.1}$$

In the present approach, at each marching step the solution to Eq. (3.1) is sought in an iterative manner. Let us denote the iteration level by the index 'n', so that the iteration at which we seek the solution is represented by the superscript 'n+1' and the previous iteration (the solution to which is known) is represented by the superscript 'n'. Thus, for the j+1 marching step the governing PNS equations at the n+1 iteration level are written as:

$$\vec{F}_{1,\xi}{}^{j+1,n+1} + \vec{F}_{2,\zeta}{}^{j+1,n+1} = \varepsilon \vec{S}_{,\zeta}{}^{j+1,n+1} + \vec{H}^{j+1,n+1} \tag{3.2}$$

If we assume that the solution at the n+1 level is close to the solution at the n-th iteration, we can use a first-order Taylor series expansion around the previous iteration to write

$$\vec{F}_1{}^{j+1,n+1} \simeq \vec{F}_1{}^{j+1,n} + \tilde{A}_1{}^{j+1,n} \cdot \vec{\Delta q}^{n+1}$$

$$\vec{F}_2^{\,j+1,n+1} \simeq \vec{F}_2^{\,j+1,n} + \tilde{A}_2^{\,j+1,n} \cdot \vec{\Delta q}^{\,n+1}$$

$$\vec{S}^{\,j+1,n+1} \simeq \vec{S}^{\,j+1,n} + \tilde{M}^{\,j+1,n} \cdot \vec{\Delta q}^{\,n+1} \qquad (3.3)$$

$$\vec{H}^{\,j+1,n+1} \simeq \vec{H}^{\,j+1,n} + \tilde{A}_0^{\,j+1,n} \cdot \vec{\Delta q}^{\,n+1}$$

where

$$\vec{\Delta q}^{\,n+1} = \vec{q}^{\,j+1,n+1} - \vec{q}^{\,j+1,n} \qquad (3.4)$$

The matrices $\tilde{A}_0$, $\tilde{A}_1$, $\tilde{A}_2$, and $\tilde{M}$ are called the jacobian matrices (not to be confused with the transformation Jacobian matrix), and the expressions for these matrices are given in Appendix C. It should be noted that in evaluating the jacobian matrices and doing the Taylor series expansion around n-th iteration, we only consider the flowfield variables as the unknowns and assume that we know the grid at the n+1 step. This becomes possible if we use (as in the present case) some independent approach to predict the shock location (and thus the grid) at the j+1 marching step. This shock propagation will be discussed separately in a later section, along with the other boundary conditions.

Thus, we see that by expanding the solution around the n-th iteration and using a two-point streamwise differencing (explained in detail in the following section), the governing PNS equations at the n+1 iteration can be written as:

$$(\tilde{A}_1/\Delta\xi-\tilde{A}_0)^{j+1,n}\cdot\Delta\vec{q}^{n+1} + [\{\tilde{A}_2-\varepsilon\tilde{M}\}^{j+1,n}\cdot\Delta\vec{q}^{n+1}]_{,\zeta}$$
$$= -[\vec{F}_{1,\xi}{}^{j+1}+\vec{F}_{2,\zeta}{}^{j+1} - \varepsilon\vec{S}_{,\zeta}{}^{j+1}-\vec{H}^{j+1}]^n$$
$$= \vec{g}^{j+1,n} \qquad (3.5)$$

3.2. DIFFERENCING SCHEME

Equation (3.5) is a vectorial equation involving derivatives in the ξ and ζ coordinate directions. As we neglected the viscous diffusion in the marching direction, the viscous vector $\vec{S}$ only involves the derivates in the ζ direction. Since the problem is elliptic in the ζ direction, we use central-difference operators for all ζ derivatives.

The streamwise differencing, however, needs some explanation. It has been noted in the case of conventional non-iterative PNS schemes (Ref. 1,2 and 4) that a simple two-point backward differencing is non-conservative as it results in truncation errors of order $O[(q^{j+1}-q^j)^2]$. Thus, in order to cancel this truncation error the non-iterative PNS schemes of Refs. 1, 2, 3 and 4 use special three-point operators. They use the solution at the j and j-1 marching steps to estimate this truncation error as:

$$\vec{F}_{1,\xi}^{\,j+1} \approx [\vec{F}_1^{\,j+1} - \vec{F}_1^{\,j}]/\Delta\xi + O(\Delta\xi)$$
$$\approx [\tilde{A}_1^{\,j}\cdot\vec{\Delta q}^{\,j+1} + O(\vec{\Delta q}^{\,j+1\,2})]\Delta\xi + O(\Delta\xi)$$
$$\approx [\tilde{A}_1^{\,j}\cdot\vec{\Delta q}^{\,j+1} + \vec{F}_1^{\,j} - \vec{F}_1^{\,j-1} - \tilde{A}_1^{\,j-1}\cdot\vec{\Delta q}^{\,j})]/\Delta\xi + O(\Delta\xi)$$
$$\approx [\tilde{A}_1^{\,j}\cdot\vec{\Delta q}^{\,j+1} - \tilde{A}_1^{\,j-1}\cdot\vec{\Delta q}^{\,j}]/\Delta\xi + \vec{F}_{1,\xi}^{\,j} \qquad (3.6)$$

where

$$\vec{\Delta q}^{\,j+1} = \vec{q}^{\,j+1} - \vec{q}^{\,j} \qquad (3.7)$$

and

$$\vec{\Delta q}^{\,j} = \vec{q}^{\,j} - \vec{q}^{\,j-1} \qquad (3.8)$$

In contrast to the conventional non-iterative PNS schemes, for the present scheme the two-point backward differencing formula (at the n+1 iteration) involves truncation errors of order $O(\vec{\Delta q}^{\,n+1\,2})$, i.e.,

$$\vec{F}_{1,\xi}^{\,j+1,n+1} \approx [\vec{F}_1^{\,j+1,n+1} - \vec{F}_1^{\,j}]/\Delta\xi + O(\Delta\xi)$$
$$\approx [\tilde{A}_1^{\,j+1,n}\cdot\vec{\Delta q}^{\,n+1} + O(\vec{\Delta q}^{\,n+1})^2 + \vec{F}_1^{\,j+1,n} - \vec{F}_1^{\,j}]/\Delta\xi + O(\Delta\xi)$$
$$\approx [\tilde{A}_1^{\,j+1,n}\cdot\vec{\Delta q}^{\,n+1} + O(\vec{\Delta q}^{\,n+1})^2]/\Delta\xi + \vec{F}_{1,\xi}^{\,j+1,n} \qquad (3.9)$$

where

$$\vec{\Delta q}^{\,n+1} = \vec{q}^{\,j+1,n+1} - \vec{q}^{\,j+1,n} \qquad (3.10)$$

Thus, in the limit of convergence ($\vec{\Delta q}^{\,n+1} \to 0$) the two-point streamwise differencing of the present PNS scheme becomes conservative.

The fact that the present PNS scheme allows us to use a simple two-point backward differencing, may not only be important from a storage point of view but it may also give the present scheme some improved capability for treating strong compression discontinuities. Experience with classical non-iterative PNS schemes suggests that these schemes encounter severe numerical difficulties when trying to step across regions of sudden geometry changes (such as strong compression corners). This is may be because across such discontinuities (a) a simple second-order Taylor series expansion around the previous step is not accurate, and (b) the streamwise differencing of Eq. (3.6) is no longer conservative. For these reasons (and may be more), when marching across a strong compression corner with a non-iterative PNS scheme, typically, significant solution oscillations are observed, and in many cases the non-iterative schemes just fail to step across. This problem seems to become more pronounced under high-altitude (low-density) reentry conditions where even small body-slope changes have a strong impact on the solution.

3.3. PSEUDO TIME FORMULATION

The solution of Eq. (3.5) involves the use of central-difference operators in the ζ direction. Typically, such central-difference operators cause solution oscillations and additional higher-order smoothing terms need to be added to Eq. (3.5). For the present scheme, a new second-order accurate fully implicit smoothing has been developed. This new smoothing approach will be discussed in detail in the following chapter. Nevertheless, briefly speaking, the form of these higher-order terms is chosen

to be such that Eq. (3.5) is transformed into another equation in terms of an intermediate solution $\vec{Q}^{j+1,n+1}$ as:

$$
\begin{aligned}
(\tilde{A}_1/\Delta\xi-\tilde{A}_0)^{j+1,n}\cdot\Delta\vec{Q}^{n+1} + [\{\tilde{A}_2-\varepsilon\tilde{M}\}^{j+1,n}\cdot\Delta\vec{Q}^{n+1}]_{,\zeta} \\
= -[\vec{F}_{1,\xi}{}^{j+1}+\vec{F}_{2,\zeta}{}^{j+1} - \varepsilon\vec{S}_{,\zeta}{}^{j+1}-\vec{H}^{j+1}]^n \\
= \vec{g}^{j+1,n}
\end{aligned}
\tag{3.11}
$$

As can be seen, this equation is identical in form to the original equation [Eq. (3.5)], with $\vec{q}$ being replaced by $\vec{Q}$. The actual solution $\vec{q}$ is explicitly related to this intermediate solution (to be shown in Chapter IV) by:

$$
\vec{q} = \vec{Q} + \omega\vec{Q}_{,\zeta\zeta}\Delta\zeta^2/4 \tag{3.12}
$$

where ω=0 for no smoothing effects and ω=1 if smoothing effects need to be included.

As a result of the above discussion we see that by using a two-point backward differencing for the ξ derivatives, central-difference approximations for the ζ derivatives, including second-order accurate smoothing, and expanding the solution around the n-th iteration, the difference equations corresponding to the solution for the n+1 iteration at the j+1 marching step can be written in terms of an intermediate solution vector $\vec{Q}^{j+1,n+1}$ as:

$$(1/2\Delta\zeta)[\tilde{A}_2-\varepsilon\tilde{M}]_{\ell+1}{}^{j+1,n}\cdot\Delta\vec{Q}_{\ell+1}{}^{j+1,n+1}$$
$$+[\tilde{A}_1/\Delta\xi-\tilde{A}_0]_{\ell}{}^{j+1,n}\cdot\Delta\vec{Q}_{\ell}{}^{j+1,n+1}$$
$$-(1/2\Delta\zeta)[\tilde{A}_2-\varepsilon\tilde{M}]_{\ell-1}{}^{j+1,n}\cdot\Delta\vec{Q}_{\ell-1}{}^{j+1,n+1}$$
$$=-[\vec{F}_{1,\xi}{}^{j+1,n}+\vec{F}_{2,\zeta}{}^{j+1,n}-\varepsilon\vec{S}_{,\zeta}{}^{j+1,n}-\vec{H}^{j+1,n}]_{\ell} \qquad (3.13)$$

It should be noted that the the right-hand side of the above vectorial equation is the governing differential equation written at the n-th iteration for the j+1 marching step. We can simply write this block-tridiagonal system as:

$$\tilde{A}^{n}\cdot\Delta\vec{Q}_{\ell-1}{}^{j+1,n+1}+\tilde{B}^{n}\cdot\Delta\vec{Q}_{\ell}{}^{j+1,n+1}+\tilde{C}^{n}\cdot\Delta\vec{Q}_{\ell+1}{}^{j+1,n+1}=\vec{g}_{\ell}{}^{j+1,n} \qquad (3.14)$$

So we see that as we converge to the final result, the right-hand side of Eq. (3.14) approaches zero. Under this limiting case there is one unique solution to the above problem which is $\Delta\vec{Q}=0$ as long as $\tilde{B}^{n}$ is a non-singular matrix. This iteration can be viewed as marching in some fictitious time (pseudo-time) direction, so that the overall iterative solution is like solving a fictitious unsteady (pseudo-unsteady) problem. The steady-state solution of this pseudo-unsteady problem is the same as the converged solution to our actual iterative problem. Once we accept this pseudo-unsteady interpretation of an iterative procedure, we can take a step further and realize that slight changes in the solution algorithm, such that they do not affect the final steady state, are completely valid and acceptable. This is because it is not the physics of the pseudo-unsteady problem that we are interested in, rather it is only the final steady-state solution which has any meaning for us. Or, in

terms of the real iterative solution, we can modify the convergence path as long as we do not affect the final converged solution. This idea is the backbone of all pseudo-unsteady approaches which in most cases result in more efficient solution procedures.

Of course, the important assumption behind such a pseudo-unsteady scheme is that the modified transient problems also have a final steady state. (This is usually true, as long as the original solution scheme is convergent and, also, that the modified pseudo-unsteady problem only involves small perturbations on the original scheme.) Thus, by using the pseudo-unsteady concepts we see that as long as $\tilde{B}^n$ is non-singular, the accuracy of the matrices $\tilde{A}^n$, $\tilde{B}^n$ and $\tilde{C}^n$ really does not make any difference in the limit of convergence. Slight changes in these matrices would only change the nature of the pseudo-unsteady problem, which is of no concern to us except that it affects the convergence rates. As mentioned earlier, experience with the use of such pseudo-unsteady schemes shows that as long as we can come up with constant coefficient matrices $\tilde{A}$, $\tilde{B}$ and $\tilde{C}$ such that they closely resemble $\tilde{A}^n$, $\tilde{B}^n$ and $\tilde{C}^n$ at all iteration levels, the convergence characterictics of such iterative solutions are typically very good.

The present scheme has the advantage that usually the $\tilde{A}$, $\tilde{B}$ and $\tilde{C}$ matrices at the first iteration are a good approximation to $\tilde{A}^{n+1}$, $\tilde{B}^{n+1}$ and $\tilde{C}^{n+1}$, respectively. Consequently, $\tilde{A}$, $\tilde{B}$ and $\tilde{C}$ are evaluated only once for the first iteration and kept unchanged for the remaining iter-

ations. Thus, without affecting the steady-state solution, we can write the block-tridiagonal system of Eq. (3.14) as:

$$\tilde{A}\bullet\vec{\Delta Q}_{\ell-1}^{\,j+1,n+1}+\tilde{B}\bullet\vec{\Delta Q}_{\ell}^{\,j+1,n+1}+\tilde{C}\bullet\vec{\Delta Q}_{\ell+1}^{\,j+1,n+1}=\vec{g}_{\ell}^{\,j+1,n} \qquad (3.15)$$

where

$$\tilde{A}=\tilde{A}^{n=1}$$
$$\tilde{B}=\tilde{B}^{n=1}$$

and

$$\tilde{C}=\tilde{C}^{n=1}$$

From Eq. (3.15) we see that we need to invert the matrices only once and store their inverted forms. After this first iteration, all that is required for obtaining the solution $\vec{\Delta Q}_{\ell}^{\,j+1,n+1}$ is a simple back-substitution using $\vec{g}^{\,j+1,n}$ vector and the stored inverted forms of matrices $\tilde{A}$, $\tilde{B}$ and $\tilde{C}$. Since solving for $\vec{\Delta Q}_{\ell}^{\,j+1,n+1}$ in this manner requires simple vector multiplications, it is exceptionally fast as compared to the time taken for the first iteration. Usually, the time taken for each iteration after the first iteration is only 10-15% of the time taken for the first iteration. This order of reduction in computing time occurs on a serial machine (such as IBM 3081); however, it is conceivable that on a vector processor this reduction in time will be even more.

After having obtained the intermediate solution $\vec{Q}^{\,j+1,n+1}$, the actual solution $\vec{q}^{\,j+1,n+1}$ can be obtained very easily by using Eq. (3.12).

Equation (3.12) is an explicit expression for $\Delta\vec{q}^{j+1,n+1}$, and can be processed with a negligible amount of additional computing time and effort.

3.4. BOUNDARY CONDITIONS

The problem represented by Eq. (3.1) is a split-boundary-value problem, i.e., the equations are hyperbolic-parabolic in the ξ direction and elliptic in the ζ direction. Thus, in order to solve the problem completely we need initial conditions to be specified at the start of the marching procedure, and boundary conditions to be specified at the wall and at the outer bow shock.

3.4.1. Initial Conditions

For the present PNS scheme, the initial conditions to start the marching procedure are obtained from a Viscous Shock-Layer (VSL) blunt body solution. The quality of such VSL solutions has been discussed in great detail in Refs. 12-15. Briefly speaking, studies have shown that the quality of VSL blunt-body solutions is comparable to a corresponding thin-layer Navier-Stokes (TLNS) solution. However, the computing times required for a VSL solution are only a small fraction of the computing times required for the TLNS solutions. Furthermore, the storage requirements of a VSL code are a lot less than the TLNS codes, so that for the same blunt-body region the VSL solution can be obtained with a lot more grid points than the TLNS solutions with the same memory allocation.

In the afterbody region the PNS equations represent a more accurate scheme than the VSL schemes. Furthermore, due to their parabolized (marching) nature the PNS schemes are still a lot less expensive and a lot less time consuming than the thin-layer Navier-Stokes schemes. The PNS equations are a higher-order set of equations than the viscous shock-layer equations, and unlike VSL solution schemes do not require a prior knowledge of the outer bow shock location. Also, the need to globally iterate the solution (like in the VSL schemes) is also eliminated. Although the VSL solutions in the blunt-body region are very attractive due to their efficiency, accuracy and unconditional stability, in the afterbody region the PNS equations are more accurate, comparable in computing effort, and also have a greater capability for treating cahnges in body slope and curvature. For the present scheme, the VSL blunt-body solution was interpolated to obtain the starting solution at the initial data plane (IDP) for the PNS solution. Typically, we choose this starting location to be approximately 2 nose-radii downstream of the stagnation point.

3.4.2. Wall Boundary Conditions

For the present PNS scheme, the boundary conditions at the wall consist of five independent relations representing the nature of the gas and the physical conditions at the wall. These conditions are:

(1) Equation of state for a perfect gas ($\gamma p=\rho T$)

(2) No-slip condition for 'u' velocity component ($\rho u=0$)

(3) No slip condition for 'w' velocity component ($\rho w=0$)

(4) Specified wall temperature ($\rho=\gamma p/T_w$)

and

(5) Zero pressure derivative in the ζ direction ($p_{,\zeta}=0$)

The first four boundary conditions are easy to visualize as they represent the actual physical conditions at the wall. The fifth boundary condition on the pressure derivative comes from a boundary-layer-type analysis performed at the wall. The above set of boundary conditions are well-posed and form a linearly independent set.

3.4.3. Outer Boundary Conditions

The boundary conditions at the outer bow shock are more involved than the boundary conditions at the wall. As was mentioned earlier, the solution scheme described in the previous sections involves the assumption that we not only know the location of the outer bow shock at the j+1 step, but that we also know the conditions behind the shock. In order to make such a prediction, before we actually solve for the solution at the new marching step, a shock propagation approach very similar to the one used by Chaussee et al[4] was used. In their approach they use a combination of inviscid compressible flow equations to predict $p_{,\xi}$ value behind the shock at the j-th marching station. Using this pressure derivative and a simple Euler integration, they predict the pressure behind the shock at the j+1 marching step, and the remaining conditions behind the shock are determined from the Rankine-Hugoniot shock-crossing relations. The shock location at the j+1 step is then predicted using the conditions

behind the shock at the j+1 step and the fact that the shock is a ζ=constant curve. This procedure of Ref. 4 is deficient because, in predicting the pressure behind the shock, it does not account for a variable marching step size. Furthermore, in the aforementioned procedure there is no interaction between the shock location and the solution at the j+1 marching step. An additional criterion for checking the quality of a solution is the global conservation of mass. Typically, the use of Chaussee et al.'s (Ref. 4) shock propagation results in errors of the order of 2% in the global conservation of mass, which are not good for a fully-conservative scheme (iterative as well as non-iterative).

The mass flow out of the j+1 plane is a lot more sensitive to the shock location at the j+1 step than any other shock quantity. Using this as the basis, the shock propagation problem is split into (a) the prediction of behind-the-shock conditions from a knowledge of the solution at the j-th step, and (b) an iterative prediction of the shock standoff distance from a knowledge of the solution (for the n-th iteration) at the j+1 step and the use of the global conservation-of-mass criterion. As an initial guess for the shock location at the j+1 step, the approach of Chaussee et al.[2] is used with an iterative correction applied at each subsequent iteration to satisfy the global conservation of mass to within a specified limit. Typically, the tolerance limit for this is specified to be less than 0.1% of the freestream mass flow. Furthermore, such a correction can be made without disrupting the pseudo-time integration scheme discussed earlier. That is to say, the grid changes resulting from a correction on the shock standoff distance are small and have little impact

on the metric derivatives and the corresponding Jacobians (J). Thus, during the iterations, the corrected grid is used only in calculating the right-hand-side vector ($\vec{g}_{\ell}^{\,j+1,n}$) of Eq. (3.10), and the matrices $\tilde{A}$, $\tilde{B}$ and $\tilde{C}$ are not changed. This is possible because in doing so we only slightly change the nature of the pseudo-transient problem and not the final steady state. The final steady-state solution still corresponds to $\vec{\Delta Q}_{\ell}^{\,j+1,n+1} \to 0$ and $\vec{g}_{\ell}^{\,j+1,n} \to 0$, so that when we reach the final steady-state (i.e., the solution converges) we automatically satisfy the correct difference equations given by $\vec{g}^{\,j+1,n}=0$. In this way, without retarding the solution convergence, we are able to correctly account for the grid changes due to a change in the shock standoff distance.

3.5. CALCULATION OF THE BODY-NORMAL DERIVATIVES AT THE WALL

The wall heat-transfer and skin-friction calculations require a knowledge of the body-normal derivatives of temperature and the streamwise component of velocity. Although the coordinate system used may not be body-normal, one can analytically obtain expressions for the body-normal derivatives in terms of the 'ξ' and 'ζ' derivatives.

If we represent the body-normal direction by η, then at the wall the body-normal derivative of any general quantity (Ψ) can be written as:

$$(\Psi_{,\eta})_w = (-\mathrm{Sin}\theta_b \xi_{,x} + \mathrm{Cos}\theta_b \xi_{,z})_w (\Psi_{,\xi})_w$$

$$+ (-\mathrm{Sin}\theta_b \zeta_{,x} + \mathrm{Cos}\theta_b \zeta_{,z})_w (\Psi_{,\zeta})_w \qquad (3.16)$$

where θ_b is the local body slope (angle). In the present calculations, three-point forward-differenced approximations have been used for the ζ derivatives at the wall, and the ξ derivatives at the wall have been estimated using two-point backward-differenced approximations.

CHAPTER IV. HIGHER-ORDER SMOOTHING TERMS

4.1. A NEW SECOND-ORDER ACCURATE FULLY-IMPLICIT SMOOTHING

As noted in the previous chapter, the governing equations [Eq. (3.1)] are elliptic in the ζ direction so that we used central-differenced approximations for all ζ derivatives. However, as was also noted by Schiff and Steger,[1] the use of central-differenced schemes is typically associated with solution oscillations. This oscillatory behavior becomes more pronounced if the local velocities are small, so that the diagonal terms of the jacobian matrices become relatively small also. In order to damp these solution oscillations, it is necessary to add some additional higher-order diffusive terms to the governing PNS equations. In the course of this study it was noted that it is not only important that these additional diffusive terms be small, but even more importantly they should be consistently treated on the implicit and explicit sides (left-hand and right-hand sides) of Eq. (3.5). If we choose the form of these diffusion terms to be the same as the ones used in the non-iterative PNS schemes of Refs. 1, 2 and 4, we end up with a block-petadiagonal system of equations to solve. In case of the non-iterative PNS schemes, this problem is circumvented by dropping the order of the implicit diffusion terms such that a block-tridiagonal system is retained. If we were to proceed along the same lines also, we would end up with an inconsistent treatment of these diffusive terms on the left-hand side and the right-hand side of the difference equations. Experience shows that this

inconsistency has a tremendous negative effect on the convergence characteristics of the present iterative scheme, and in most cases it causes the iterations to finally diverge.

The search for an appropriate form of the higher-order diffusion-like terms which would permit a simple yet a fully-consistent and fully-implicit treatment, was very tedious and involved. However, briefly speaking, the use of central-difference formulas for ζ derivatives makes the solution of Eq. (3.1) second-order accurate, that is to say the leading truncation error is $O(\Delta\zeta^2)$. Thus, if we were to add $O(\Delta\zeta^2)$ diffusion-like terms to the right-hand side of Eq. (3.1), we would not affect the formal second-order accuracy of the difference scheme in the ζ direction. The governing equations can thus be written as:

$$\vec{F}_{1,\xi}{}^{j+1} + \vec{F}_{2,\zeta}{}^{j+1} = \varepsilon\vec{S}_{,\zeta}{}^{j+1} + \vec{H}^{j+1} + \omega[\vec{f}(\vec{q}^{\,j+1})](\Delta\zeta)^2 \qquad (4.1)$$

where ω is 0 for no smoothing, and 1 otherwise.

The proper choice of smoothing terms ($\vec{f}$) was actually based on a trial and error procedure. To start with, an explicit relation relating the smoothed ($\vec{q}$) and unsmoothed ($\vec{Q}$) variables was chosen such that it included some second-order diffusive effects. A back-tracking approach was used to obtain the corresponding smoothing terms that needed to be added to the governing equations to produce the desired result. Once these smoothing terms in the governing equations were obtained, the order of each of these terms was analyzed and lower order terms were eliminated.

Then, the governing equations with the modified smoothing terms were analyzed to see the impact of these changes on the final relationship between the smoothed and unsmoothed variables. After several iterations of this trial and error procedure, the author was able to find a proper choice of these smoothing terms such that not only a second-order accuracy was retained but a simple and explicit transformation between the unsmoothed and smoothed variables was also retained.

By choosing the form of the vector $\vec{\mathcal{L}}$ to be

$$\vec{\mathcal{L}}(\vec{q}) = (1/4)[\tilde{A}_1 \cdot \vec{q}_{,\zeta\zeta} + (\tilde{A}_2 \cdot \vec{q}_{,\zeta\zeta})_{,\zeta} - \varepsilon(\tilde{M} \cdot \vec{q}_{,\zeta\zeta})_{,\zeta} - \tilde{A}_0 \cdot \vec{q}_{,\zeta\zeta}] \tag{4.2}$$

one can re-write Eq. (4.1) as:

$$\begin{aligned}[\vec{F}_1+\tilde{A}_1\cdot(-\omega\vec{q}_{,\zeta\zeta}\Delta\zeta^2/4)]^{j+1}+[\vec{F}_2+\tilde{A}_2\cdot(-\omega\vec{q}_{,\zeta\zeta}\Delta\zeta^2/4)]_{,\zeta}{}^{j+1} \\ = \varepsilon[\vec{S}+\tilde{M}\cdot(-\omega\vec{q}_{,\zeta\zeta}\Delta\zeta^2]_{,\zeta}{}^{j+1} \\ + [\vec{H}+\tilde{A}_0\cdot(-\omega\vec{q}_{,\zeta\zeta}\Delta\zeta^2/4)]^{j+1}+\vec{F}_1{}^{j}+O(\Delta\xi,\Delta\zeta^2)\end{aligned} \tag{4.3}$$

Now, let us define a new intermediate quantity $\vec{Q}^{j+1}$ as:

$$\vec{Q}^{j+1} = \vec{q}^{j+1} - \omega\vec{q}_{,\zeta\zeta}\Delta\zeta^2/4 \tag{4.4}$$

So that

$$\vec{Q}^{j+1} - \vec{q}^{j+1} = -\omega\vec{q}_{,\zeta\zeta}\Delta\zeta^2/4 = O(\Delta\zeta^2) \tag{4.5}$$

and

$$(\vec{Q}^{j+1} - \vec{q}^{j+1})^2 = O(\Delta\zeta^4) \tag{4.6}$$

Using Eqs. (4.5) and (4.6) it can be shown that to a second-order accuracy we can also write Eq. (4.4) as:

$$\vec{q}^{j+1} = \vec{Q}^{j+1} + \omega\vec{Q}_{,\zeta\zeta}\Delta\zeta^2/4 \tag{4.5}$$

Now consider the Taylor series expansion of vector $\vec{F}_1(\vec{Q}^{j+1})$ around $\vec{q}^{j+1}$, i.e.,

$$\begin{aligned}\vec{F}_1(\vec{Q}^{j+1}) &= \vec{F}_1(\vec{q}^{j+1}) + [\vec{F}_{1,q}]^{j+1}\cdot(\vec{Q}^{j+1}-\vec{q}^{j+1}) \\ &\quad + [\vec{F}_{1,qq}]^{j+1}\cdot(\vec{Q}^{j+1}-\vec{q}^{j+1})^2 + \ldots . \\ &= \vec{F}_1(\vec{q}^{j+1}) + \tilde{A}_1\cdot(-\omega\vec{q}_{,\zeta\zeta}\Delta\zeta^2/4) + O(\Delta\zeta^4)\end{aligned} \tag{4.6}$$

Thus, to second-order accuracy we can write the above expression as

$$\vec{F}_1(\vec{Q}^{j+1}) \simeq \vec{F}_1(\vec{q}^{j+1}) + \tilde{A}_1\cdot(-\omega\vec{q}_{,\zeta\zeta}\Delta\zeta^2/4) \tag{4.7}$$

Similar expansions can be obtained for $\vec{F}_2$, $\vec{S}$ and $\vec{H}$, so that to second-order accuracy in $\Delta\zeta$ we can rewrite Eq. (4.3) in terms of an intermediate solution $\vec{Q}^{j+1}$ as:

$$\begin{aligned}\vec{F}_1(\vec{Q}^{j+1}) + [\vec{F}_2(\vec{Q}^{j+1})]_{,\zeta} &= \varepsilon[\vec{S}(\vec{Q}^{j+1})]_{,\zeta} \\ &\quad + \vec{H}(\vec{Q}^{j+1}) + \vec{F}_1{}^{j} + O(\Delta\xi, \Delta\zeta^2)\end{aligned} \tag{4.8}$$

The actual solution that we seek at the j+1 step is related to this intermediate solution by Eq. (4.5). If we use ℓ to denote the grid points in the ζ direction (i.e., ℓ=1,2,3... LMAX), we can further express $\vec{q}^{j+1}$ in terms of the intermediate solution $\vec{Q}^{j+1}$ as:

$$\vec{q}_{\ell}^{\,j+1} = (\omega\vec{Q}_{\ell+1}^{\,j+1})/4 + (1-\omega/2)\vec{Q}_{\ell}^{\,j+1} + (\omega\vec{Q}_{\ell-1}^{\,j+1})/4 \qquad (4.9)$$

Thus, we see that in order to introduce a second-order accurate fully-implicit smoothing, we solve a block-tridiagonal system of equations (Eq. 4.8) which is identical in form to the differenced form of the original PNS equations [Eq. (3.1)]. However, this solution is just an intermediate solution ($\vec{Q}^{j+1}$), and the final smoothed solution ($\vec{q}^{j+1}$) can be explicitly obtained by using Eq. (4.9). It should be noted that computationally this procedure is no more involved than the original (unsmoothed) differenced form of the PNS equations. Furthermore, another important feature of the present second-order smoothing is that the additional diffusive terms are proportional to $\Delta\zeta^2$, so that the magnitude of the aforementioned smoothing automatically decreases with a decreasing ζ grid size, while still successfully damping out the numerical solution oscillations. Also, despite its final simple form, the present smoothing approach is more accurate and performs considerably better than the conventional smoothing approaches of Refs. 1, 2, 3 and 4.

CHAPTER V. SIMPLIFIED ANALYSIS FOR DEPARTURE AND STREAMWISE-STABILITY

5.1. ASSUMPTIONS AND SIMPLIFICATIONS

Usually, the actual stability analysis of a nonlinear set of partial differential equations (such as the PNS equations being studied) can be prohibitively difficult and in many cases impossible with the present mathematical tools. The final validation and justification for a numerical scheme (which is as complicated as the present PNS scheme) is almost always based on actual numerical testing under various flowfield conditions. However, in many cases a simplified stability analysis can provide a reasonably good understanding of the general stability characteristics of the scheme, point out the various elements (if any) which contribute to the stability or instability of the scheme, provide an understanding of the impact of various approaches directed towards making an unstable scheme conditionally or unconditionally stable, etc. In short, even a simplified analysis (if possible to do) can be of great value in understanding the behavior of a complicated numerical scheme.

It was pointed out in Chapter I that mathematically there are two ways in which the problem of departure or streamwise stability of the PNS equations has been looked at. In one approach (to be referred to as Approach I) the streamwise stability of the differenced form of the gov-

erning equations is considered. Fourier- or Von-Neumann-type methods are then used to look at the amplification of disturbances in the streamwise direction. Examples of this approach are the work of Lubard and Helliwell[5] and Rubin and Lin.[8] In the other approach (to be referred to as Approach II) an attempt is made to directly study the time-like character of the governing equations with respect to the direction of marching (streamwise direction). The idea is to see if the governing equations become elliptic at any location in the flow domain, and thus make the marching scheme ill-posed. Examples of this approach are the work of Schiff and Steger[1] and Vigneron et al.[3]

Initially, an attempt was also made to use Approach I for the departure analysis of the present PNS scheme. This resulted in a 6×6 amplification matrix whose eigenvalues were to be studied. In the case of Lubard and Helliwell,[5] certain terms related to the streamwise pressure derivative were neglected, and the resulting system was relatively easy to analyze. Since in the present PNS scheme the idea is to retain all terms, such simplifications could not be made, and the resulting 6-th order equation was impossible to analyze for possible closed-form expressions describing the eigenvalues. Indeed a numerical solution of this eigenvalue problem could have been possible. However, this idea was not pursued because the main objective of the stability analysis was to obtain (if possible) some sort of a closed-form representation of the eigenvalues to see if the speed-of-sound contributions to these eigenvalues were indeed eliminated. Thus, Approach I was abandoned and Approach II was looked into. Fur-

thermore, the conceptual development of the present scheme used the formulation of Schiff and Steger[1] as the starting point. Since Schiff and Steger[1] had also used Approach II for the analysis of their scheme, the idea of looking at departure by considering the character of the governing equations became even more attractive.

In order to simplify the required mathematics, let us restrict ourselves to

(a) two-dimensional flows, and

(b) an evenly spaced square grid such that $\xi_{,x}=\zeta_{,z}=1$ and $\xi_{,z}=\zeta_{,x}=0$

Furthermore, we choose to approximate the equation of state for a perfect gas by

$$\gamma p - \rho T + \theta(p_{,\xi}+p_{,\zeta}) = 0 \qquad (5.1)$$

where the coefficient 'θ' is chosen such that $\theta \approx 0$ and for all practical purposes

$$\theta p_{,\xi}+\theta p_{,\zeta}+\gamma p-\rho T \simeq \gamma p-\rho T$$

It should be noted that the use of this coefficient θ is for the sole purpose of the following stability analysis, and not for the actual solution scheme. In other words, the actual solution corresponds to the use

of $\theta=0$. The reason for introducing this coefficient 'θ' is that it makes the streamwise jacobian matrix nonsingular, so that one can perform certain matrix operations to simplify the stability analysis. Furthermore, there are no mathematical tools available to directly look at the character of 'mixed-type' systems. The available mathematical tools are strictly for purely differential systems. Thus, by introducing the coefficient 'θ' in Eq. (5.1) we are able to transform our 'mixed-type' problem into a purely differential form, which can then be analyzed. It is hoped that the choice of 'small enough θ' will not adversly affect the resulting conclusions. This is indeed a heuristic approach, and the only possible justification (if any) comes from the model mixed-type problem discussed in Section 2.3. The use of 'θ' in Eq. (5.1) appears to correspond to the use of the 'ε' term in Formulation II of the model problem (Section 2.3.2). For this model problem it was demonstrated that the choice of $\varepsilon \to 0^{+}$ did not appear to produce any singularity in the final solution.

With the equation of state given by Eq. (5.1), and after neglecting the viscous terms containing the contributions of w and $w_{,\zeta}$, we can write the simplified PNS equations as:

$$\vec{f}_{1,\xi}^{\,n+1} + \vec{f}_{2,\zeta}^{\,n+1} = \varepsilon \vec{s}_{,\zeta}^{\,n+1} + \vec{h}^{n+1} \qquad (5.2)$$

The forms of these vectors are given in Appendix D.

By expanding Eq. (5.2) around the n-th iteration we obtain

$$(\tilde{a}_1^n \cdot \vec{d})_{,\xi} + (\tilde{a}_2^n \cdot \vec{d})_{,\zeta} - \varepsilon[\tilde{m}^n \cdot \vec{d}]_{,\zeta} - \tilde{a}_0^n \cdot \vec{d} = -[\vec{f}_{1,\xi}^{\,n} + \vec{f}_{2,\zeta}^{\,n} - \varepsilon \vec{s}_{,\zeta}^{\,n} - \vec{h}^n] \tag{5.3}$$

where

$$\vec{d} = \Delta \vec{q}^{\,n+1} \tag{5.4}$$

and $\tilde{a}_1^n$, $\tilde{a}_2^n$ and $\tilde{m}^n$ are the jacobian matrices.

If we assume that $\tilde{a}_1^n$, $\tilde{a}_2^n$ and $\tilde{m}^n$ do not change with ξ and ζ (a frozen coefficient analysis), we can write (see Appendix D):

$$\tilde{a}_1^n \simeq \tilde{a}_1^f \tag{5.5}$$

$$\tilde{a}_2^n \simeq \tilde{a}_2^f \tag{5.6}$$

and

$$\varepsilon \tilde{m}^n \cdot \vec{d} \simeq \tilde{b}^f \cdot \vec{d}_{,\zeta} \tag{5.7}$$

With the aforementioned assumptions, Eq. (5.3) reduces to:

$$\tilde{a}_1^f \cdot \vec{d}_{,\xi} + \tilde{a}_2^f \cdot \vec{d}_{,\zeta} - \tilde{b}^f \cdot \vec{d}_{,\zeta\zeta} + \vec{c}(d,\xi,\zeta) = 0 \tag{5.8}$$

Although the above equation is a significantly simplified version of the original PNS equations, it is still difficult to study directly. As a further simplification, we choose to separately look at the viscous and inviscid limits of Eq. (5.8). We also note that as a minimum criterion of streamwise stability (which in this case, and for the class of PNS schemes based on the Schiff-Steger formulation, implies a marching-like character of the governing equations), the "simplified PNS equations" being studied have to be streamwise stable (i.e., marching-like in the streamwise direction) in the viscous as well as the inviscid limits. In the following sections we look into the streamwise stability (marching-like character) of the viscous and the inviscid limits of Eq. (5.8).

5.2. INVISCID LIMIT

The inviscid limit of Eq. (5.8) can be written as:

$$\tilde{a}_1^f \cdot \vec{d}_{,\xi} + \tilde{a}_2^f \cdot \vec{d}_{,\zeta} + \vec{c} = 0 \qquad (5.9)$$

This first-order system can be more simply studied if one could invert $\tilde{a}_1^f$ (i.e., if $\tilde{a}_1^{f\,-1}$ existed). This is where the coefficient θ comes into the picture. For $\theta=0$, $\tilde{a}_1^f$ is singular, and we have to study Eq. (5.9) as it is. Since one can not simultaneously diagonalize $\tilde{a}_1^f$ and $\tilde{a}_2^f$, studying Eq. (5.9) would become an extremely difficult (if not an impossible) task. By choosing θ as a very small number (of the order of

10^{-20} or smaller) we can make sure that the numerical solution remains essentially unchanged from the $\theta=0$ case. However, with $\theta\neq 0$, $\tilde{a}_1^f$ becomes non-singular and can be inverted. Thus, Eq. (47) can now be written as:

$$\vec{d}_{,\xi} + [\tilde{a}_1^{f\,-1}\tilde{a}_2^f]\cdot\vec{d}_{,\zeta} + \tilde{a}_1^{f\,-1}\vec{c} = 0 \qquad (5.10)$$

or

$$\vec{d}_{,\xi} + \tilde{N}_1\cdot\vec{d}_{,\zeta} + \vec{C} = 0 \qquad (5.11)$$

The aforementioned equation is now in a form which can be easily studied. For Eq. (5.11) to be stable, the ξ direction should be a valid marching direction. In other words, Eq. (5.11) has to be hyperbolic or marching-like always. This condition is satisfied if the eigenvalues of $\tilde{N}_1$ are all real. If for simplicity we assume that $w \ll u$, then an eigenvalue analysis gives the eigenvalues of $\tilde{N}_1$ as (see Appendix D):

$$\lambda_i = (1, w/u, w/u, w/u, w/u) \qquad (5.12)$$

Thus, we see that all the eigenvalues of $\tilde{N}_1$ are unconditionally real. That is to say, the "simplified PNS equations" being studied are unconditionally marching-like in the inviscid limit, and represent a stable marching scheme in the subsonic as well as the supersonic flow regions.

It is of interest to consider the case where (like conventional non-iterative PNS schemes) we do not uncouple the pressure terms. In such a case the form of $\tilde{a}_1^f$ is similar to the one studied by Schiff and Steger.[1] The only difference is that we have ρT as the independent variable rather than 'e'. The $\tilde{a}_1^f$ matrix for such a case is nonsingular and, thus, can be inverted. However, the eigenvalues of $\tilde{N}_1$ for such a case (where we do not uncouple the pressure) turn out to be complex in the subsonic flow regions, and the marching scheme becomes unstable (not marching-like; i.e., elliptic) unless methods such as the sublayer approximations of Ref. 1 or Ref. 3 are used.

5.3. VISCOUS LIMIT

In the viscous limit, Eq. (5.8) simplifies to

$$\tilde{a}_1^f \cdot \vec{d}_{,\xi} = \tilde{b}^f \cdot \vec{d}_{,\zeta\zeta} - \vec{c} \tag{5.13}$$

where the first-order convective derivatives in the ζ direction are much smaller than the viscous terms and have been neglected. If we use once again the fact that with $\theta \neq 0$, $\tilde{a}_1^f$ is nonsingular and can be inverted, we can re-write Eq. (5.13) as:

$$\vec{d}_{,\xi} = [\tilde{a}_1^{f\,-1} \tilde{b}^f] \cdot \vec{d}_{,\zeta\zeta} + \tilde{a}_1^{f\,-1} \cdot \vec{c} \tag{5.14}$$

or

$$\vec{d}_{,\xi} = \tilde{N}_2 \cdot \vec{d}_{,\zeta\zeta} + \vec{C} \qquad (5.15)$$

In this form, the stability analysis becomes much simpler. The criterion of a stable marching scheme requires that Eq. (5.15) should be parabolic. The parabolic character depends upon the eigenvalues of $\tilde{N}_2$, which should be real. Furthermore, in order to have positive diffusion effects in the ξ direction, these eigenvalues should also be positive. Thus, for the viscous limiting case to be stable, the eigenvalues of $\tilde{N}_2$ should be real and positive. An eigenvalue analysis of $\tilde{N}_2$ shows that the eigenvalues are (see Appendix D):

$$\sigma_i = (0,0,\varepsilon\mu/Pr\rho u, 4\varepsilon\mu/3\rho u, \varepsilon\mu/\rho u) \qquad (5.16)$$

Thus, the eigenvalues σ_i are always real; however, they are positive only if $u > 0$. That is to say, as long as no flow reversal occurs in the streamwise direction, the viscous limit of the "simplified PNS equations" is also unconditionally marching-like. Since flow reversal means axial separation, the aforementioned streamwise stability requirement actually tells us that a "single-sweep" solution of these "simplified PNS equations" can not be marched through regions of axial flow separation. Of course, this conclusion comes as no surprise and has been a well accepted fact in fluid mechanics for a long time. It may be of value to note that the viscous terms do not include any pressure terms and, thus, for the present scheme as well as the previous PNS schemes the viscous terms do not provide any speed-of-sound contribution to the eigenvalues

of the viscous limit. The speed-of-sound contributions to these eigenvalues for the viscous limit can come only from the jacobian matrix corresponding to the streamwise convective terms. For the classical PNS schemes (Ref. 1 and 3), this speed-of-sound contribution is the one which causes the problem of negative eigenvalues in the subsonic sublayer region. For the present PNS scheme, although the speed of sound does appear in the streamwise jacobian matrix $(\tilde{a}_1^f)$, it does not contribute to the eigenvalues in the viscous limit.

5.4. RELATIONSHIP WITH THE SUBLAYER APPROXIMATION

If we look into the sublayer approximation of Schiff and Steger,[1] we can identify that the object of their approach is, in a way, similar to the present approach. The main difference is that their approach splits the pressure terms only in the subsonic sublayer region and estimates the sonic pressure by extrapolating it from the previous marching steps. In the present scheme, the pressure is split over the entire shock layer, and is solved for in a coupled manner rather than just extrapolating it from the previous step. Thus, the present scheme not only seems to accomplish what the sublayer approximation tries to do, but also tends to maintain the accuracy of the solution without introducing any approximations resulting from extrapolating sublayer pressure.

CHAPTER VI. RESULTS AND DISCUSSION

6.1. TEST CASES

In order to substantiate the various ideas and claims made in the previous sections, the new implicit fully-iterative PNS scheme has been used to study the flow over a seven-deg sphere-cone reentry vehicle under two different flight altitude conditions. The nose radius for this sphere-cone test vehicle is 0.041667 ft and the vehicle is 200 nose radii long (see Fig. 3). Flight altitudes of 80 kft and 200 kft are considered, and the freestream Mach number is kept constant at 25. In the subsequent discussion, the 80 kft condition is called Case A and the 200 kft case condition is called Case B. The freestream conditions for these two cases are shown in Table 1, and the flow is considered to be fully laminar in both cases. Case A is chosen because the freestream Reynolds number for this case is quite large (2.92×10^5). On the other hand, the freestream Reynolds number for the Case B conditions is 1.72×10^3, which is much smaller than the usual limits of the non-iterative PNS schemes.

The wall temperature (T_w) for all cases is kept constant at 2000 °R. The ratio of wall temperature to the freestream total temperature is 0.040 for Case A and 0.035 for Case B. Thus, for these cases we expect to see a strong cold-wall effect, resulting in large temperature gradients and a temperature peak in the near-wall region. The cold-wall effect and the low-Reynolds number at the 200 kft altitude makes Case B an especially

tough set of conditions. The following sections discuss in detail the various results obtained for the Case A and Case B conditions.

6.2. SOLUTION ACCURACY AND CODE COMPARISONS

6.2.1. Case A Calculations

As mentioned earlier, Case A corresponds to a large Reynolds number flow so that we expect the non-iterative AFWAL PNS scheme to perform reasonably well under these conditions. Figures 4-7 show a comparison of the flowfield predictions for the Case A conditons using (a) the Viscous Shock-Layer (VSLPG) scheme of Ref. 17, (b) the axisymmetric version of the non-iterative AFWAL PNS code, (c) the present PNSPG scheme, and (d) the inviscid NOL3D scheme of Ref. 18. The VSLPG results are obtained using 101 body-normal grid points, the AFWAL PNS calculations use 50 axis-normal grid points and the PNSPG results are for 150 axis-normal grid points. Figure 4 shows the axial distribution of the wall pressure for Case A. These results show excellent agreement between the two PNS calculations and the inviscid predictions. The over-expansion and recompression predicted by the PNS schemes agrees very well with the inviscid calculations. The VSLPG calculations shown in this comparison are for the zeroth iteration and suggest that the solution needs to be globally iterated in the over expansion-recompression region. Except for this over expansion-recompression region, the wall pressures predicted by the VSLPG scheme are also in very good agreement with the other codes.

The skin-friction distributions for this case are shown in Fig. 5. These results show that there are slight differences in the skin-friction predictions. The AFWAL PNS results agree well with the PNSPG results only in the forebody region. In the afterbody region the AFWAL PNS results are significantly in error. Especially, towards the body end, the skin friction starts to show a peculiar and non-physical drop. The PNSPG results and the VSLPG results, on the other hand, are very smoothly behaved. The VSLPG skin-friction results are slightly higher than the PNSPG results in the afterbody region, especially in the overexpansion and recompression region. However, these differences are small and globally iterating the VSLPG was not considered necessary.

Figure 6 shows the corresponding predictions of the wall heat-transfer rates. Due to the cold-wall effect, we expect the greatest differences (if any) to occur in the wall heat-transfer rates. These results show that the agreement between the three viscous schemes is very good in the forebody region; however, in the afterbody region, the VSLPG and AFWAL PNS results are approximately 10% higher than the PNSPG results. Due to the fact that VSLPG results need to be globally iterated, and also because the PNSPG results are for a much finer grid, it is our opinion that the PNSPG results are more accurate and dependable.

Figure 7 shows the shock shape locations predicted by the inviscid NOL3D code and the two PNS schemes which use similar (but different) shock propagation approaches. The results show that for the Case A conditions (80 kft altitude) the flow is inviscid dominated, and the viscous as well

as the inviscid shock shapes are in excellent agreement. This result is completely consistent with the fact that the PNSPG wall pressures are also in complete agreement with the corresponding inviscid predictions.

The axial step-size distributions used for these Case A calculations are shown in Fig. 8. It should be noted that the VSLPG and the PNSPG schemes use automated step-size control procedures. The marching step size for the VSLPG scheme is controlled mainly by solution convergence constraints. The PNSPG scheme, however, uses constraints based on grid changes, shock-propagation accuracy and, also, solution convergence rates. The input step-size distribution for the AFWAL PNS scheme was chosen to closely resemble the step-size distribution of the PNSPG scheme.

6.2.2. Case B Calculations

The results of the Case B calculations are given in Figs. 9-12. At this altitude (200 kft), we expect noticeable viscous-induced effects on the flowfield as well as some of the wall-measurable quantities.

Figure 9 shows the wall-pressure distributions predicted for this case by the the VSLPG scheme and the present PNSPG scheme. The VSLPG and PNSPG calculations use the same grids as were used for the Case A calculations mentioned earlier (101 grid points for VSLPG and 150 grid points for PNSPG). These figures include the results of the zeroth VSL iteration (using the inviscid shock shape) and also the results of the first global iteration. This global iteration is necessary because the flow shows

significant viscous-induced effects, especially in the afterbody over-expansion and recompression region. Figure 9 also includes the inviscid surface pressures predicted by the NOL3D code, and shows that the inviscid calculations underpredict the wall pressures in the over expansion-recompression region by as much as 15-20%.

The zeroth iteration of VSLPG has very good agreement with the PNSPG results in the nose-dominated region as well as the afterbody region. However, the pressure recovery predicted by VSLPG in the afterbody recompression region is much slower and causes the wall pressures to be underpredicted by as much as 8%. Typically, in order to improve the accuracy of the VSLPG scheme for such viscous dominated flows, we need to globally iterate the solution by using the shock shape predicted by the zeroth VSLPG iteration. However, in this case the PNSPG results directly provide us with a good estimate of the viscous shock shape location. We use this information to (a) check the quality of the PNSPG solution and (b) cut down on the effort involved in repeated VSLPG global iterations. If the PNSPG results are really good, the VSLPG results based on the PNSPG shock shape should not require any further global iterations. The VSLPG results for this first iteration are also shown in Fig. 9, and are in very good agreement with the PNSPG results, clearly reflecting upon the accuracy of the PNSPG scheme.

Figures 10 and 11 show the skin-friction distributions and the wall heat-transfer rates predicted by the PNSPG and the VSLPG schemes. It can be seen that, in the over-expansion and recompression region, the

skin-friction and wall heat-transfer predictions of the zeroth VSLPG iteration are as much as 25% in error. However, the results of the first VSLPG iteration (using the PNSPG shock) are in excellent agreement with the PNSPG results. The reasons for these differences become even clearer when we consider Fig. 12, which compares the inviscid NOL3D shock shape with the predictions of the PNSPG scheme and also the shock shape predicted by the first VSLPG global iteration. (Interested readers are referred to Ref. 17 for the details of the VSLPG shock prediction scheme.) These results show that the viscous shock layer is approximately 10% thicker than the corresponding inviscid shock. Especially, in the expansion-recompression region (around 60-70 nose radii down the body length), the viscous shock slope is considerably larger and is the main cause for the thicker viscous shock in the afterbody region. Also, it should be noted that the shock predicted by the VSLPG scheme after the first global iteration is in excellent agreement with the original PNSPG predictions. These results clearly indicate that the PNSPG results are accurate and dependable even under these low-Reynolds number conditions. Also, by eliminating the need for global iterations, the present scheme becomes considerably more convenient to use in the afterbody region than the Viscous Shock-Layer schemes. The step-size distributions used for these Case B calculations are shown in Fig. 13.

It is to be noted that the above results for Case B conditions do not include the non-iterative AFWAL-PNS results. This is because, as expected, the non-iterative AFWAL PNS scheme completely failed under the high Mach number, low-Reynolds number conditions. Many attempts were made

with various axial step sizes; however, in the best case the non-iterative procedure marched just one step before it failed. Figure 14 shows the pressure profile across the shock layer at this marching step. The corresponding pressure profile from the PNSPG scheme is also shown in this figure.

These (Fig. 14) results show that the predictions of the non-iterative PNS scheme are, in general, good in the region near the outer bow shock; however, the solution clearly shows the onset of instabilities in the near-wall region. Furthermore, it should be noted that at the start of the sublayer region the solution oscillates suddenly and most severely. The PNSPG results, on the other hand, are very well behaved and smooth. The differences at the shock between the PNSPG results and the AFWAL PNS results (as seen in Fig. 14) are due to the differences in the shock-propagation schemes. It is worth noting that at this axial location the subsonic sublayer region is approximately 4% of the shock-layer thickness and contains approximately 50% of the grid points for the PNSPG as well as the AFWAL PNS schemes.

6.3. EFFECTS OF GRID DISTRIBUTION

When trying to solve problems where large gradients exist, it is important to have enough grid points to properly simulate these changes. Every differenced equation has an inherent truncation error which is solely dependent upon the grid spacing. This is especially true for central-differenced schemes where additional smoothing terms are added

to damp out solution oscillations. Thus, apart from numerical stability, an important criterion for a correct numerical scheme is that it should be consistent. In other words, any grid refinement on the scheme should result in increased accuracy and, furthermore, the effects of grid refinement should have a convergent trend. In order to study the effects of grid stretching and grid refinement, we studied Cases A and B with the PNSPG scheme using a sequence of 50, 100 and 150 grid points in the ζ direction. The grid stretching function used was the same as the one used in the AFWAL PNS scheme. These 50-, 100- and 150-point grids were generated such that the first point off the wall was located at a distance of 5×10^{-3}%, 1×10^{-3}% and 1×10^{-4}%, respectively, of the local shock standoff distance.

Figures 15-17 show the effects of grid distribution on the surface-measurable quantities for Case A conditions. The shock location is compared in Fig. 18, and Figs. 19-21 show comparisons of the pressure, temperature and velocity profiles across the shock layer at the body end. The wall pressures, as shown in Fig. 15, are the least affected by the grid refinement, because the afterbody pressure distributions do not have large gradients in the ζ direction (see Fig. 19). Figures 16 and 17 show that the skin-friction distributions and the surface heating rates in the afterbody region are, however, significantly affected by the ζ grid-size distribution. The reason is clearly shown in Figs. 20 and 21, which show the shock-layer temperature and u-velocity profiles at the body end. It can be seen that because of the cold-wall effect, there are large temperature gradients very near the wall, and the 50-point grid is not enough

to accurately resolve the temperature peak. Similarly, the velocity profile is also smoothed out near the wall with the 50-point grid. With finer grids, the modeling of these regions with large gradients improves significantly. It should also be noted that with increasing grid resolution the aforementioned results become less and less grid dependent and the solutions tend to approach a distinct final distribution.

Similar results for the Case B conditions are shown in Figs. 22-28. Figures 22-24 show the axial distributions of the surface-measurable quantities, Fig. 25 shows the shock shape locations, and Figs. 26-28 show the shock-layer profiles for pressure, temperature and u-velocity at the body end. In this case the differences between the results for the 50-, 100- and 150- point grids are much smaller than the Case A results. For Case B, the regions of large temperature and velocity gradients (see Fig. 27 and 28) are farther away from the wall. This behavior is consistent with the fact that at this altitude (200 kft) the flow is essentially viscous dominated and there is a thick viscous region near the wall.

These results for Cases A and B show that the present PNSPG scheme is not only stable but that it is also consistent in a mathematical sense. Thus, grid refinements (for improved accuracy) are possible and the results tend to approach a grid-independent solution. These results also emphasize the point that for all schemes using a fixed number of grid points to resolve the shock-layer profiles, proper grid resolution and refinement is very important for accurate results. Typically, grids which are accurate in the forebody region may cause significant errors in the

afterbody region where the shock layer is much thicker. This is especially important when using marching-type schemes for long bodies, because such schemes carry along with them any solution error, and it is very possible to obtain smooth results which are in fact significantly in error! It is important to point this out because the only way to resolve this problem is to use a more refined grid and get some idea about the effects of the grid distribution on the solution accuracy. The conventional non-iterative PNS schemes, in general, do not allow for an arbitrary grid refinement process because of the possibilty of departure solutions and instabilities. With the present PNSPG scheme; however, it is possible to use highly stretched and refined grids, so that one can always check the accuracy and grid-dependence of the solution by going to a finer grid.

6.4. CONVERGENCE RATES AND ITERATION HISTORY

The convergence characteristics of the present fully-iterative PNS scheme are also very good. If we define our maximum local percentage error at the n-th iteration (ψ^n) as:

$$\psi^n = 100\times[(\vec{q}^{n+1}-\vec{q}^{n})/\vec{q}^{n+1})]_{max} \qquad (6.1)$$

Then it is possible to correlate very accurately the convergence characteristics of the present scheme by the logarithmic correlation

$$\log(\psi^n) = mn + \text{constant} \qquad (6.2)$$

With a logarithmic curve as above, it is possible to define the convergence rate β as:

$$\beta = \psi^n/\psi^{n+1} = \exp(-m) \qquad (6.3)$$

where 'm' is the slope of the logarithmic curve. Thus, the convergence rate β is a true representation of the factor by which the errors decrease from one iteration to the next.

For the Case A and Case B conditions, in order to show the convergence rates, we can plot the $f(n)=\log(\psi^n)$ curves for the three grid distributions (50-, 100- and 150-point grids) at X/RN=10 location. These correlations are shown in Figs. 29 and 30, and Table 2 includes a tabulation of the estimated slope (m) of these curves. The corresponding convergence-rate (β) estimates are also given in Table 2, and the results show that the convergence rates increase with increasing grid points. Thus, from these results we see that, on the average, the present scheme shows at least a cubic convergence rate. The numerical values indicated in Table 2 are typical of the present scheme, even under other conditions that we have tried.

Typical computing-time histories for the various Case A and Case B results at X/RN = 10 are shown in Figs. 31 and 32. Comparisons of these time histories are given in Table 3. These results show that, in general, the computing times for each iteration after the first are 10-15% of the first iteration. This percentage reduction in time is the largest for

the 150-point grids (90% time reduction), followed by the 100-point grids (88% time reduction), and the 50-point grids have the smallest reduction (85% time reduction). In other words, the present solution becomes relatively more efficient as the number of grid points increase. Table 3 shows that computing times for the first iteration also show a similar trend. Thus, in an overall sense, when the number of grid points increases by a factor of 'κ', the computing time for each iteration increases by less than the factor 'κ'.

6.5. OVERALL COMPUTING TIMES

Tables 4 and 5 show the computing time comparisons for the full-body calculations with the present PNSPG scheme, the Viscous Shock-Layer calculations and the AFWAL PNS calculations. Table 4 is for the Case A calculations, whereas Table 5 is for the Case B calculations. Apart from the actual computing times 't^*', these tables also include the average computing times per grid point (τ^*) required by each of these schemes. Since different schemes involve a different number of axial steps as well a different number of grid points across the shock layer, probably τ^* is a better representation of the computing efficiency of a scheme. Tables 4 and 5 show that, on the average, the present fully-iterative PNS scheme requires 12% more computing effort at each grid point than the VSL scheme. However, it should be noted that convergence criteria used for the present PNSPG calculations were very small ($\psi^n < 10^{-6}$) as compared to the convergence criteria used in the VSL calculations ($\psi^n < 0.3$). This is in addition to the fact that under low-Reynolds number conditions, the VSL

solutions typically need to be globally iterated (as we have seen for the present Case B calculations). Thus, in terms of the real time and effort, the present PNS scheme becomes a lot more efficient than the viscous shock-layer approach.

Furthermore, despite the very low convergence criteria and the fully-iterative nature of the present PNS scheme, the scheme is only 30% slower than the non-iterative PNS scheme. However, with reasonable convergence criteria our estimates indicate that this time penalty can be easily reduced to a value of 15% or less. Of course, this is apart from the fact that the present PNS scheme is capable of accurately treating conditions which are beyond the limitations of the non-iterative PNS schemes.

CHAPTER VII. CONCLUSIONS

A new fast and accurate implicit fully-iterative Parabolized Navier-Stokes scheme has been developed to predict the axisymmetric reentry-type flows under low- to high-Reynolds number conditions. The new PNS scheme appears to be unconditionally stable in the subsonic as well as the supersonic flow regions and, thus, does not require any sub-layer approximation. This new PNS scheme is based on the idea that if we consider pressure as an additional unknown quantity and solve for the algebraic equation of state simultaneously with the differential equations governing the conservation of mass, momentum and energy, it appears to be possible to unconditionaly march the solution of these PNS equations in the streamwise direction. The new iterative approach involves a fast and efficient pseudo-time integration scheme. With this new approach, the computing times for the fully iterated solutions are only 30% larger than the conventional non-iterative PNS approaches. These computing times of the new scheme can be easily improved upon by choosing more realistic convergence criteria.

A new second-order accurate fully-implicit smoothing approach has been developed to help damp the solution oscillations caused by the central-differenced operators. Due to the apparent stability and time-like behavior of the involved marching scheme, and the use of the new smoothing approach, the new PNS scheme can be used to accurately predict the low-Reynolds number reentry flowfields which are beyond the

capabilities of the existing iterative or non-iterative PNS schemes. Furthermore, even under high-Reynolds number conditions, the new PNS scheme is more robust and the solutions are more accurate.

Apart from being stable, the new PNS scheme is also consistent and does not have the problem of departure solutions and associated instabilities. Due to this consistency and accuracy, it is possible to use highly refined grids near the wall and obtain grid-independent solutions. This scheme has been used to study the reentry flow around a seven-deg sphere-cone vehicle under low- and high-Reynolds number conditions. Two test cases, Case A and Case B, were chosen. Case A was chosen because its freestream Reynolds number was large (2.92×10^5), whereas Case B was chosen because its freestream Reynolds number (1.72×10^3) was much smaller than the usually accepted limit of applicability of the non-iterative PNS schemes. Furthermore, the results of Case B indicated that (as expected) the non-iterative AFWAL PNS scheme completely failed under these low Reynolds number conditions. On the other hand, the results of the present scheme were smooth, well-behaved and accurate.

In short, a new iterative ("single-sweep") PNS scheme has been developed which appears to be accurate, efficient and streamwise stable (departure free). The results substantiate the accuracy and stability claims of the scheme. The new fully-iterative PNS scheme also shows great promise for extension to study three-dimensional reentry flows under large angles of attack and with large cross-flow separated regions.

APPENDIX A. AXISYMMETRIC/2-D PNS EQUATIONS

The motion of viscous compressible fluids is described by the well known full Navier-Stokes (NS) equations (Ref. 19). If we assume (a) Newtonian fluid, (b) Stokes' Hypothesis, and (c) no body forces, we can write the three-dimensional NS equations as:

$$(\rho u)_{,x} + (\rho v)_{,y} + (\rho w)_{,z} = 0 \tag{A.1}$$

$$(\rho u^2+p)_{,x} + (\rho vu)_{,y} + (\rho wu)_{,z} = a_1 \tag{A.2}$$

$$(\rho uv)_{,x} + (\rho v^2+p)_{,y} + (\rho wv)_{,z} = a_2 \tag{A.3}$$

$$(\rho uw)_{,x} + (\rho vw)_{,y} + (\rho w^2+p)_{,z} = a_3 \tag{A.4}$$

$$(\rho u\Phi)_{,x} + (\rho v\Phi)_{,y} + (\rho w\Phi)_{,z} = a_4 \tag{A.5}$$

where

$$\Phi = T/(\gamma-1) + 0.5V^2 \tag{A.6}$$

$$a_1 = [2\mu u_{,x} - (2\mu/3)\vec{\nabla}\cdot\vec{V}]_{,x} + [\mu(u_{,y}+v_{,x})]_{,y} + [\mu(u_{,z}+w_{,x})]_{,z} \tag{A.7}$$

$$a_2 = [2\mu v_{,y} - (2\mu/3)\vec{\nabla}\cdot\vec{V}]_{,y} + [\mu(v_{,x}+u_{,y})]_{,x} + [\mu(v_{,z}+w_{,y})]_{,z} \tag{A.8}$$

$$a_3 = [2\mu w_{,z} - (2\mu/3)\vec{\nabla}\cdot\vec{V}]_{,z} + [\mu(w_{,x}+u_{,z})]_{,x} + [\mu(w_{,y}+v_{,z})]_{,y} \tag{A.9}$$

and

$$a_4 = \vec{\nabla}\cdot(k\vec{\nabla}T) + \vec{\nabla}\cdot(\vec{V}\cdot\tilde{\tau}) \qquad (A.10)$$

In here $\tilde{\tau}$ is the stress tensor for a Newtonian fluid, and is defined as (Ref. 15):

$$\tau_{ij} = \mu[u_{i,x_j} + u_{j,x_i} - (2/3)\delta_{ij}u_{k,x_k}] \qquad (A.11)$$

where $u_1=u$, $u_2=v$, $u_3=w$, $x_1=x$, $x_2=y$ and $x_3=z$.

Equation (A.1) corresponds to the conservation of mass; and Eqs. (A.2-A.4) correspond to the conservation of momentum in the x, y and z directions, respectively. Equation (A.5) corresponds to the conservation of energy, and these equations [Eqs. (A.1)-(A.5)] are closed through the use of equation-of-state for a perfect gas; i.e.,

$$\gamma p = \rho T \qquad (A.12)$$

The above equations have been written in a non-dimensional form, and the non-dimensionalization scheme used is:

$$
\begin{aligned}
u_i &= u_i^*/a_\infty^* \\
\rho &= \rho^*/\rho_\infty^* \\
T &= T^*/T_\infty^* \\
p &= p^*/(\rho_\infty^* a_\infty^{*2}) \\
\mu &= \mu^*/\mu_\infty^* \\
k &= k^*/k_\infty^* \\
x_i &= x_i^*/Rn^*
\end{aligned}
\qquad \text{(A.13))}
$$

Equations (A.1)-(A.5) and Eq. (A.12) can be combined together and written in the following vectorial form:

$$
\vec{E}_{1,x} + \vec{E}_{2,y} + \vec{E}_{3,z} = \varepsilon(\vec{G}_{1,x} + \vec{G}_{2,y} + \vec{G}_{3,z}) + \vec{P} \qquad \text{(A.14)}
$$

Using indicial notation we can write Eq.(A.14) as:

$$
(\vec{E}_i - \varepsilon \vec{G}_i)_{,x_i} = \vec{P} \qquad \text{(A.15)}
$$

Or

$$
\vec{K}_{i,x_i} = \vec{P} \qquad \text{(A.16)}
$$

Now consider the general coordinate transformation

$$
\xi_i = \xi_i(x_j) \qquad \text{(A.17)}
$$

where the orientation of our general curvilinear coordinate system is such that $\xi_1=\xi$ is measured along the body, $\xi_2=\zeta$ is measured from the body to the outer bow shock, and ξ_3 is the crossflow direction. Thus, derivatives in the transformed space are related to the derivatives in the physical space by

$$( )_{,\xi_i} = x_{j,\xi_i} ( )_{,x_j} \tag{A.18}$$

If 'J' represents the determinant of the Transformation-Jacobian for Eq. (A.17); i.e.,

$$J = \mathrm{Det}[(\xi_1,\xi_2,\xi_3)/(x_1,x_2,x_3)] \tag{A.19}$$

we can write Eq. (A.16) as

$$(1/J)(\xi_{j,x_i})(\vec{K}_{i,\xi_j}) = (1/J)\vec{P} \tag{A.20}$$

Equation (A.20) can be further expanded as

$$[(1/J)(\xi_{j,x_i})\vec{K}_i]_{,\xi_j} - \vec{K}_i[(1/J)(\xi_{j,x_i})]_{,\xi_j} = (1/J)\vec{P} \tag{A.21}$$

Viviand (Ref. 20) has shown that the Jacobian satisfies the identity

$$J_{,\alpha} = J(\xi_{j,\alpha})_{,\xi_j} \tag{A.22}$$

where 'α' is an arbitrary quantity. Equation (A.22) can be used to obtain

$$J_{,x_i} = J(\xi_{j,x_i})_{,\xi_j} \tag{A.23}$$

At the same time the chain rule of differentiation gives

$$J_{,x_i} = (\xi_{j,x_i})J_{,\xi_j} \tag{A.24}$$

Thus, we can see that by combining Eqs. (A.23) and (A.24) we can obtain yet another identity

$$(\xi_{j,x_i})_{,\xi_j} - (1/J)(\xi_{j,x_i})J_{,\xi_j} = 0 \tag{A.25}$$

The chain rule of differentiation also gives

$$[(1/J)\xi_{j,x_i}]_{,\xi_j} = (1/J)[(\xi_{j,x_i})_{,\xi_j} - (1/J)(\xi_{j,x_i})J_{,\xi_j}] \tag{A.26}$$

Thus, from Eqs. (A.25) and (A.26) we obtain

$$[(1/J)\xi_{j,x_i}]_{,\xi_j} = 0 \tag{A.27}$$

Substituting Eq. (A.27) in Eq. (A.21), we see that the NS equations in a general curvilinear coordinate system can be written as

$$[(1/J)\xi_{j,x_i}\vec{K}_i]_{,\xi_j} = (1/J)\vec{P} \tag{A.28}$$

If we use the notation

$$\vec{F}_j = (1/J)\xi_{j,x_i}\vec{E}_i \tag{A.29}$$

$$\vec{S}_j = (1/J)\xi_{j,x_i}\vec{G}_i \tag{A.30}$$

we can write the NS equations in a general curvilinear coordinate system as:

$$\vec{F}_{i,\xi_i} = \varepsilon\vec{S}_{i,\xi_i} + (1/J)\vec{P} \tag{A.31}$$

where

$$\vec{F}_i = (1/J)\begin{bmatrix} \rho U_i \\ \rho u U_i + \xi_{i,x} p \\ \rho v U_i + \xi_{i,y} p \\ \rho w U_i + \xi_{i,z} p \\ \{T/(\gamma-1) + 0.5V^2\}\rho U_i \\ 0 \end{bmatrix} \tag{A.32}$$

and

$$U_i = \xi_{i,x_j} u_j \tag{A.33}$$

Now, let us consider the case of axisymmetric/2-D flows. For such flows it can be shown that

$$U_3 = 0 \tag{A.34}$$

$$(\xi_{3,x})_{,\xi_3} = 0 \tag{A.35}$$

$$(\xi_{3,y})_{,\xi_3} = -\kappa(\mathrm{Sin}\phi/r) \tag{A.36}$$

$$(\xi_{3,z})_{,\xi_3} = -\kappa(\mathrm{Cos}\phi/r) \tag{A.37}$$

where r is tha axis-normal distance from the body axis, κ=0 for 2-D flows and κ=1 for axisymmetric flows, and ϕ is the circumferential angle measured from the windward plane of symmetry. If we consider only the windward pitch-plane (ϕ=0), we obtain

$$\vec{F}_{3,\xi_3} = (1/J) \begin{bmatrix} 0 \\ 0 \\ -\kappa p/z \\ 0 \\ 0 \end{bmatrix} \tag{A.38}$$

where r=z in the windward pitch-plane.

Furthermore, for axisymmetric/2-D flows the crossflow diffusion effects are zero; i.e.,

$$\vec{S}_{3,\xi_3} = 0 \tag{A.39}$$

Thus, if we define $\vec{H}$ as

$$\vec{H} = \vec{P} - \vec{F}_{3,\xi_3} \tag{A.40}$$

we obtain the axisymmetric/2-D Navier-Stokes equations in a general curvilinear coordinate system as:

$$\vec{F}_{1,\xi} + \vec{F}_{2,\zeta} = \varepsilon(\vec{S}_{1,\xi} + \vec{S}_{2,\zeta}) + \vec{H} \tag{A.41}$$

It should be noted that the third row of the above vectorial equation [Eq. (A.41)] consists of all zero terms and, thus, will be droped. In other words, the vectors appearing in Eq. (A.41) are re-defined such that third row is removed, and all other terms retain their form.

Now, in order to parabolize Eq. (A.41) we neglect all streamwise diffusion effects. With this assumption, the axisymmetric/2-D parabolized Navier-Stokes (PNS) equations in a general curvilinear coordinate system become

$$\vec{F}_{1,\xi} + \vec{F}_{2,\zeta} = \varepsilon\vec{S}_{,\zeta} + \vec{H} \tag{A.42}$$

where

$$\vec{F}_1 = (1/J)\begin{bmatrix} \rho U_1 \\ \rho u U_1 + \xi_{,x} p \\ \rho w U_1 + \xi_{,z} p \\ \{T/(\gamma-1)+0.5V^2\}\rho U_1 \\ 0 \end{bmatrix} \qquad (A.43)$$

$$\vec{F}_2 = (1/J)\begin{bmatrix} \rho U_2 \\ \rho u U_2 + \zeta_{,x} p \\ \rho w U_2 + \zeta_{,x} p \\ \{T/(\gamma-1)+0.5V^2\}\rho U_2 \\ 0 \end{bmatrix} \qquad (A.44)$$

$$\vec{S} = (\mu/J)\begin{bmatrix} 0 \\ m_0 u_{,\zeta} + 0.5(m_{xx} u_{,\zeta} + m_{xz} w_{,\zeta}) \\ m_0 w_{,\zeta} + 0.5(m_{zx} u_{,\zeta} + m_{zz} w_{,\zeta}) \\ \{m_0 T_{,\zeta}/Pr(\gamma-1) + m_0(uu_{,\zeta} + ww_{,\zeta}) + (1/3)(m_{xx} uu_{,\zeta} + m_{xz} uw_{,\zeta} + m_{xz} wu_{,\zeta} + m_{zz} ww_{,\zeta})\} \\ 0 \end{bmatrix} \qquad (A.45)$$

and

$$\vec{H} = \begin{bmatrix} 0 \\ 0 \\ \kappa p/Jz \\ 0 \\ \gamma p - \rho T \end{bmatrix} \qquad (A.46)$$

In the above equations $\kappa=0$ for two-dimensional flows and $\kappa=1$ for axisymmetric flows. Also, in the above equations

$$\begin{aligned} m_{xx} &= \zeta_{,x}\zeta_{,x} \\ m_{xz} &= \zeta_{,x}\zeta_{,z} \\ m_{zz} &= \zeta_{,z}\zeta_{,z} \\ m_0 &= m_{xx}+m_{zz} \end{aligned} \qquad A.47$$

and

$$V = (u^2+w^2)^{0.5} \qquad (A.48)$$

U_1 and U_2 are the contravariant velocity components in the ξ and ζ coordinate directions, respectively. These contravariant velocity components are defined as:

$$U_1=\xi_{,x}u+\zeta_{,x}w$$
$$U_2=\xi_{,z}u+\zeta_{,z}w \qquad \text{(A.49)}$$

APPENDIX B. ANALYSIS OF THE MODEL MARCHING PROBLEM

B.1. THE MODEL MIXED-TYPE PROBLEM

Consider the following model 'mixed-type' problem

$$\begin{aligned} \phi_{1,x} - \phi_{2,y} &= 0 \\ \phi_{2,x} - \phi_{1,y} + 2\phi_{2,y} + \phi_{3,y} &= 0 \\ a^2\phi_1 - \phi_3 &= 0 \end{aligned} \qquad \text{(B.1)}$$

with the initial conditions

$$\phi_1(0,y) = \phi_2(0,y) = y \qquad \text{(B.2)}$$

and the boundary conditions

$$\phi_{1,y}(x,0) = \phi_{2,y}(x,0) = 1 \qquad \text{(B.3)}$$

$$\phi_1(x,1) = 1 + x \qquad \text{(B.4)}$$

$$\phi_2(x,1) = 1 - (a^2+1)x \qquad \text{(B.5)}$$

The solution to this model problem, for these initial and boundary conditions, consists of bilinear functions; i.e.,

$$\phi_1(x,y) = y + x$$
$$\phi_2(x,y) = y - (a^2+1)x \qquad \text{(B.6)}$$
$$\phi_3(x,y) = a^2(y+x)$$

B.2. FORMULATION I

The approach used in Formulation I is that ϕ_3 is eliminated from Eq. (B.1) so that Eq. (B.1) reduces to a 2-by-2 system, rather than its original 3-by-3 form; i.e.,

$$\begin{aligned} \phi_{1,x} \qquad\qquad - \phi_{2,y} &= 0 \\ \phi_{2,x} + (a^2-1)\phi_{1,y} + 2\phi_{2,y} &= 0 \end{aligned} \qquad \text{(B.7)}$$

Thus,

$$\begin{bmatrix} \phi_{1,x} \\ \phi_{2,x} \end{bmatrix} + \begin{bmatrix} 0 & -1 \\ (a^2-1) & 2 \end{bmatrix} \begin{bmatrix} \phi_{1,y} \\ \phi_{2,y} \end{bmatrix} = \begin{bmatrix} 0 \\ 0 \end{bmatrix} \qquad \text{(B.8)}$$

Or

$$\vec{\phi}_{,x} + \tilde{A} \cdot \vec{\phi}_{,y} = 0 \qquad \text{(B.9)}$$

The eigenvalues of $\tilde{A}$ are given by

$$\begin{vmatrix} \lambda & 1 \\ -(a^2-1) & \lambda-2 \end{vmatrix} = 0$$

which reduces to

$$\lambda^2 - 2\lambda + (a^2-1) = 0 \qquad \text{(B.10)}$$

and gives the eigenvalues of $\tilde{A}$ as:

$$\begin{aligned} \lambda_1 &= 1 + (2-a^2)^{0.5} \\ \lambda_2 &= 1 - (2-a^2)^{0.5} \end{aligned} \qquad \text{(B.11)}$$

Suppose we define a matrix $\tilde{P}$ as:

$$\tilde{P} = \begin{vmatrix} 1 & 1 \\ -\lambda_1 & -\lambda_2 \end{vmatrix} \qquad \text{(B.12)}$$

The inverse of $\tilde{P}$ is:

$$\tilde{P}^{-1} = \begin{bmatrix} -\lambda_1 & -1 \\ \lambda_2 & 1 \end{bmatrix} / (\lambda_1 - \lambda_2) \qquad \text{(B.13)}$$

It can be verified that

$$\tilde{P}^{-1} \bullet \tilde{A} \bullet \tilde{P} = \begin{bmatrix} \lambda_1 & 0 \\ 0 & \lambda_2 \end{bmatrix} \qquad \text{(B.14)}$$

Now consider a new set of variables ψ_1 and ψ_2 such that

$$\begin{bmatrix} \phi_1 \\ \phi_2 \end{bmatrix} = \begin{bmatrix} 1 & 1 \\ -\lambda_1 & -\lambda_2 \end{bmatrix} \begin{bmatrix} \psi_1 \\ \psi_2 \end{bmatrix}$$

Or

$$\vec{\phi} = \tilde{P} \bullet \vec{\psi} \qquad \text{(B.15)}$$

Thus, we see that using Eq. (B.15) we can write Eq. (B.9) as:

$$\tilde{P} \bullet \vec{\psi}_{,x} + \tilde{A} \bullet \tilde{P} \bullet \vec{\psi}_{,y} = 0$$

Or

$$\vec{\psi}_{,x} + \tilde{P}^{-1} \cdot \tilde{A} \cdot \tilde{P} \vec{\psi}_{,y} = 0 \qquad \text{(B.16)}$$

From Eqs. (B.14) and (B.16) we see that Eq. (B.9) trnasforms to

$$\begin{bmatrix} \psi_{1,x} \\ \psi_{2,x} \end{bmatrix} + \begin{bmatrix} \lambda_1 & 0 \\ 0 & \lambda_2 \end{bmatrix} \begin{bmatrix} \psi_{1,y} \\ \psi_{2,y} \end{bmatrix} = \begin{bmatrix} 0 \\ 0 \end{bmatrix}$$

Or

$$\psi_{1,x} + \lambda_1 \psi_{1,y} = 0 \qquad \text{(B.17)}$$

$$\psi_{2,x} + \lambda_2 \psi_{2,y} = 0 \qquad \text{(B.18)}$$

Now, Eq. (B.17) is hyperbolic if λ_1 is real and non-zero, it is parabolic if λ_1=0, and it is elliptic if λ_1 is complex. Similarly, Eq. (B.18) is hyperbolic if λ_2 is real and non-zero, it is parabolic if λ_2=0, and it is elliptic if λ_2 is complex. Both hyperbolic and parabolic partial-differential equations qualify as 'time-like' partial-differential equations, and their numerical solutions can be 'marched' away from the initial conditions. The elliptic partial-differential equations, however, can not be 'marched' because such a marching solution does not allow for the inclusion of upstream influence and, thus, violates the nature of such partial-differential

equations. Furthermore, for a system of partial-differential equations to qualify as a 'time-like system' each one of the equations in that system has to be either hyperbolic or parabolic. If even one of the equations is not time-like, the system can not be solved with a marching-type numerical scheme. Thus, we see that according to this formulation the 2-by-2 system representd by Eq. (B.7) is conditionally time-like. In other words, if we attempt the solution to Eq. (B.1) by solving Eq. (B.7), we can use a marching-type numerical scheme only if $a^2 \leq 2$.

For the case when $a^2 \leq 2$, we see that the general solution to Eqs. (B.17) and (B.18) is

$$\psi_1(x,y) = a_1(y-\lambda_1 x) + a_2 \tag{B.19}$$

$$\psi_2(x,y) = b_1(y-\lambda_2 x) + b_2 \tag{B.20}$$

where a_1, a_2, b_1 and b_2 are constants. Using Eqs. (B.19), (B.20) and (B.15), we see that

$$\phi_1(x,y) = (a_1+b_1)y - (a_1\lambda_1+b_1\lambda_2)x + (a_2+b_2) \tag{B.21}$$

$$\phi_2(x,y) = -(a_1\lambda_1+b_1\lambda_2)y + (a_1\lambda_1^2+b_1\lambda_2^2)x - (a_2\lambda_1+b_2\lambda_2) \tag{B.22}$$

Or, simply speaking

$$\phi_1(x,y) = A_1 y + A_2 x + A_3$$

$$\phi_2(x,y) = B_1 y + B_2 x + B_3 \tag{B.23}$$

where A_1, A_2, A_3, B_1, B_2 and B_3 are constants. Thus, from Eq. (B.23), we see that Formulation I does indeed give the correct bilinear solution for ϕ_1 and ϕ_2

B.3. FORMULATION II

Consider the following small perturbation problem, which consists of a small perturbation on the original model problem of Eq. (B.1); i.e.,

$$\begin{aligned} \phi_{1,x} - \phi_{2,y} &= 0 \\ \phi_{2,x} - \phi_{1,y} + \phi_{2,y} + \phi_{3,y} &= 0 \\ \varepsilon\phi_{3,x} &= a^2\phi_1 - \phi_3 \end{aligned} \tag{B.24}$$

where

$$\varepsilon \geq 0 \tag{B.25}$$

The initial conditions for this perturbation problem are the same as the initial conditions for our actual model problem [Eq. (B.2)]; i.e.,

$$\begin{aligned} \phi_1(0,y) &= y \\ \phi_2(0,y) &= y \\ \phi_3(0,y) &= a^2 y \end{aligned} \tag{B.26}$$

The boundary conditions for Eq. (B.24) are

$$\begin{aligned}
\phi_{1,y}(x,0) &= 1 \\
\phi_{2,y}(x,0) &= 1 \\
\varepsilon\phi_{3,x}(x,0) &= a^2\phi_1(x,0) - \phi_3(x,0)
\end{aligned} \tag{B.27}$$

and

$$\begin{aligned}
\phi_1(x,1) &= 1 + x \\
\phi_2(x,1) &= 1 - (a^2+1)x \\
\varepsilon\phi_{3,x}(x,1) &= a^2\phi_1(x,1) - \phi_3(x,1)
\end{aligned} \tag{B.28}$$

The small perturbation problem of Eq. (B.24) can also be written as the following 3-by-3 system

$$\begin{bmatrix} \phi_{1,x} \\ \phi_{2,x} \\ \phi_{3,x} \end{bmatrix} + \begin{bmatrix} 0 & -1 & 0 \\ -1 & 2 & 1 \\ 0 & 0 & 0 \end{bmatrix} \begin{bmatrix} \phi_{2,y} \\ \phi_{2,y} \\ \phi_{3,y} \end{bmatrix} = (1/\varepsilon) \begin{bmatrix} 0 & 0 & 0 \\ 0 & 0 & 0 \\ a^2 & 0 & -1 \end{bmatrix} \begin{bmatrix} \phi_1 \\ \phi_2 \\ \phi_3 \end{bmatrix} \tag{B.29}$$

Or

$$\vec{\phi}_{,x} + \tilde{A}\cdot\vec{\phi}_{,y} = (1/\varepsilon)\tilde{B}\cdot\vec{\phi} \tag{B.30}$$

The eigenvalues of $\tilde{A}$ are given by

$$\begin{vmatrix} \lambda & 1 & 0 \\ 1 & \lambda-2 & -1 \\ 0 & 0 & \lambda \end{vmatrix} = 0$$

Or

$$\lambda(\lambda^2 - 2\lambda - 1) = 0 \tag{B.31}$$

Thus, the eigenvalues are:

$$\begin{aligned} \lambda_1 &= 1 + \sqrt{2} \\ \lambda_2 &= 1 - \sqrt{2} \\ \lambda_3 &= 0 \end{aligned} \tag{B.32}$$

Suppose we define a matrix $\tilde{P}$ such that

$$\tilde{P} = \begin{vmatrix} 1 & 1 & 1 \\ -\lambda_1 & -\lambda_2 & 0 \\ 0 & 0 & 1 \end{vmatrix} \tag{B.33}$$

where the inverse of $\tilde{P}$ is

$$\tilde{P}^{-1} = \begin{pmatrix} -\lambda_2 & -1 & \lambda_2 \\ \lambda_1 & 1 & -\lambda_1 \\ 0 & 0 & (\lambda_1-\lambda_2) \end{pmatrix} / (\lambda_1-\lambda_2) \qquad \text{(B.34)}$$

It can be confirmed that

$$\tilde{P}^{-1} \bullet \tilde{A} \bullet \tilde{P} = \begin{pmatrix} \lambda_1 & 0 & 0 \\ 0 & \lambda_2 & 0 \\ 0 & 0 & 0 \end{pmatrix} \qquad \text{(B.35)}$$

Now, if we define a new set of variables ψ_1, ψ_2 and ψ_3 such that

$$\begin{bmatrix} \phi_1 \\ \phi_2 \\ \phi_3 \end{bmatrix} = \begin{pmatrix} 1 & 1 & 1 \\ -\lambda_1 & -\lambda_2 & 0 \\ 0 & 0 & 1 \end{pmatrix} \begin{bmatrix} \psi_1 \\ \psi_2 \\ \psi_3 \end{bmatrix} \qquad \text{(B.36)}$$

Or

$$\vec{\phi} = \tilde{P} \bullet \vec{\psi} \qquad \text{(B.37)}$$

Substituting Eqs. (B.37) and (B.35) in Eq. (B.30) we get

$$\begin{bmatrix} \psi_{1,x} \\ \psi_{2,x} \\ \psi_{3,x} \end{bmatrix} + \begin{bmatrix} \lambda_2 & 0 & 0 \\ 0 & \lambda_2 & 0 \\ 0 & 0 & 0 \end{bmatrix} \begin{bmatrix} \psi_{1,y} \\ \psi_{2,y} \\ \psi_{3,y} \end{bmatrix} = (1/\varepsilon)\tilde{P}^{-1}\cdot\tilde{B}\cdot\tilde{P}\cdot\vec{\psi} \qquad \text{(B.38)}$$

If we use the notation

$$\vec{f}(\psi) = [a^2(\psi_1+\psi_2) + (a^2-1)\psi_3]/(\lambda_1-\lambda_2) \qquad \text{(B.39)}$$

we can varify that

$$\tilde{P}^{-1}\cdot\tilde{B}\cdot\tilde{P}\cdot\vec{\psi} = \begin{bmatrix} \lambda_2 \\ -\lambda_1 \\ (\lambda_1-\lambda_2) \end{bmatrix} \vec{f}(\psi) \qquad \text{(B.40)}$$

Thus, using Eqs. (B.39) and (B.40) we can write Eq. (B.38) as:

$$\psi_{1,x} + \lambda_1\psi_{1,y} - \lambda_2 \vec{f}(\psi)/\varepsilon = 0 \qquad \text{(B.41)}$$

$$\psi_{2,x} + \lambda_2\psi_{2,y} + \lambda_1 \vec{f}(\psi)/\varepsilon = 0 \qquad \text{(B.42)}$$

$$\psi_{3,x} - (\lambda_1-\lambda_2)\vec{f}(\psi)/\varepsilon = 0 \qquad \text{(B.43)}$$

Since λ_1 and λ_2 are real for this case, we see that Eqs. (B.41) and (B.42) are always hyperbolic and Eq. (B.43) is always parabolic. Thus, we see that Eqs. (B.41-B.43) are always time-like and can be unconditionally marched in the increasing x direction. Equations (B.41-B.43) include terms of the form '$\vec{f}(\psi)/\varepsilon$', and the question arises --- "Is the solution to Eqs. (B.41-B.43) singular for $\varepsilon \to 0^+$?". It will be shown in the following discussion that '$\vec{f}(\psi)/\varepsilon = \vec{\psi}_{,x}/(\lambda_1-\lambda_2)$' is bounded for all '$\varepsilon \to 0^+$'; and, consequently, Eqs. (B.41-B.43) do not appear to be singular. This argument may be substantiated by looking at the analytic solution of Eqs. (B.41-B.43).

The analytic solution of Eqs. (B.41-B.43) can be obtained by re-writing these equations as:

$$\psi_{1,x} + \lambda_1\psi_{1,y} - \lambda_2\psi_{3,x}/(\lambda_1-\lambda_2) = 0 \qquad \text{(B.44)}$$

$$\psi_{2,x} + \lambda_2\psi_{2,y} + \lambda_1\psi_{3,x}/(\lambda_1-\lambda_2) = 0 \qquad \text{(B.45)}$$

$$\varepsilon\psi_{3,x} - a^2(\psi_1+\psi_2) - (1-a^2)\psi_3 = 0 \qquad \text{(B.46)}$$

Equations (B.44) and (B.45) can be written as:

$$[\psi_1 - \lambda_2\psi_3/(\lambda_1-\lambda_2)]_{,x} = -\lambda_1\psi_{1,y} = \text{constant} = c_1 \qquad \text{(B.47)}$$

$$[\psi_2 + \lambda_1\psi_3/(\lambda_1-\lambda_2)]_{,x} = -\lambda_2\psi_{2,y} = \text{constant} = c_2 \qquad \text{(B.48)}$$

This implies that

$$\psi_1(x,y) = -c_1 y/\lambda_1 + g_1(x)$$
$$\psi_2(x,y) = -c_2 y/\lambda_2 + g_2(x) \qquad \text{(B.49)}$$

Also,

$$\psi_1 - \lambda_2\psi_3 = c_1 x + d_1 y + e_1$$
$$\psi_2 + \lambda_1\psi_3 = c_2 x + d_2 y + e_2 \qquad \text{(B.50)}$$

where d_1, d_2, e_1 and e_2 are constants, and $g_1(x)$ and $g_2(x)$ are arbitrary functions of 'x'.

From Eq. (B.50) we can see that

$$\psi_1 + \psi_2 = -\psi_3 + (c_1+c_2)x + (d_1+d_2)y + (e_1+e_2) \qquad \text{(B.51)}$$

Substituting Eq. (B.51) in Eq. (B.28), we get the following non-homogeneous partial differential equation for ψ_3; i.e.,

$$\varepsilon\psi_{3,x} + \psi_3 = a^2[(c_1+c_2)x + (d_1+d_2)y + (e_1+e_2)] \qquad \text{(B.52)}$$

The homogeneous solution of Eq. (B.52) is

$$\psi_3{}^h(x,y) = A(y)\ \exp(-x/e) \qquad \text{(B.53)}$$

where A(y) is some arbitrary function of y.

The right-hand side of Eq. (B.52) is of a bilinear form, so that we look for a particular solution of the form:

$$\psi_3^{p}(x,y) = b_1 x + b_2 y + b_3 \tag{B.54}$$

Substituting Eq. (B.54) into Eq. (B.52) we can find

$$\begin{aligned} b_1 &= a^2(c_1+c_2) \\ b_2 &= a^2(d_1+d_2) \\ b_3 &= a^2[(e_1+e_2) - \varepsilon(c_1+c_2)] \end{aligned} \tag{B.55}$$

Thus, our general solution for ψ_3 becomes

$$\begin{aligned} \psi_3(x,y) &= \psi_3^{h}(x,y) + \psi_3^{p}(x,y) \\ &= A(y)\ \exp(-x/\varepsilon) + a^2[(c_1+c_2)x \\ &\qquad + (d_1+d_2)y + (e_1+e_2) - \varepsilon(c_1+c_2)] \end{aligned} \tag{B.56}$$

Using the transformation of Eq. (B.37) we can write

$$\vec{\psi} = \tilde{P}^{-1} \cdot \vec{\phi} \tag{B.57}$$

We can transform the initial and boundary conditions of this small perturbation problem and obtain the following initial and boundary conditions on ψ_1, ψ_2 and ψ_3; i.e.,

$$\psi_1(0,y) = [\ \lambda_2\psi_3(0,y) - (1+\lambda_2)y]/(\lambda_1-\lambda_2) \tag{B.58}$$

$$\psi_2(0,y) = [-\lambda_1\psi_3(0,y) + (1+\lambda_1)y]/(\lambda_1-\lambda_2) \tag{B.59}$$

$$\psi_3(0,y) = a^2y \tag{B.60}$$

$$\psi_{1,y}(x,0) = [\ \lambda_2\psi_{3,y} - (1+\lambda_2)]/(\lambda_1-\lambda_2) \tag{B.61}$$

$$\psi_{2,y}(x,0) = [-\lambda_1\psi_{3,y} + (1+\lambda_1)]/(\lambda_1-\lambda_2) \tag{B.62}$$

$$\psi_1(x,1) = \{-[\lambda_2-(a^2+1)]x - 1 - \lambda_2 + \lambda_2\psi_3\}/(\lambda_1-\lambda_2) \tag{B.63}$$

$$\psi_2(x,1) = \{\ [\lambda_1-(a^2+1)]x + 1 + \lambda_1 - \lambda_1\psi_3\}/(\lambda_1-\lambda_2) \tag{B.64}$$

The boundary conditions on ψ_3 are automatically satisfied as they are the same as the governing equation.

Using these initial and boundary conditions, we can evaluate c_1, c_2, d_1, d_2, e_1, e_2 and A(y) as:

$$c_1 = -(\lambda_2-a^2-1)/(\lambda_1-\lambda_2) \tag{B.65}$$

$$c_2 = (\lambda_1-a^2-1)/(\lambda_1-\lambda_2) \tag{B.66}$$

$$d_1 = -(1+\lambda_2)/(\lambda_1-\lambda_2) \tag{B.67}$$

$$d_2 = (1+\lambda_1)/(\lambda_1-\lambda_2) \tag{B.68}$$

$$e_1 = 0 \tag{B.69}$$

$$e_2 = 0 \tag{B.70}$$

and

$$A(y) = a^2\varepsilon = \text{constant} \tag{B.71}$$

Thus, the solution becomes

$$\psi_3(x,y) = a^2(x+y) - a^2\varepsilon[1-\exp(-x/\varepsilon)] \qquad (B.72)$$

$$\psi_1(x,y) = c_1x + d_1y - \lambda_2\psi_3(x,y)/(\lambda_1-\lambda_2) \qquad (B.73)$$

$$\psi_2(x,y) = c_2x + d_2y - \lambda_1\psi_3(x,y)/(\lambda_1-\lambda_2) \qquad (B.74)$$

Using the transformation of Eq. (B.37), along with Eqs. (B.72-B.74), we get the analytic solution to our small perturbation problem as:

$$\phi_1(x,y) = y + x \qquad (B.75)$$

$$\phi_2(x,y) = y - (a^2+1)x \qquad (B.76)$$

$$\phi_3(x,y) = a^2(x+y) - a^2\varepsilon[1-\exp(-x/\varepsilon)] \qquad (B.77)$$

where $\varepsilon \geq 0$.

From Eq. (B.75) it is clear that for the right-hand limit of ε; i.e.,

$$\varepsilon \rightarrow 0^+ \qquad (B.78)$$

we get

$$\text{£im}(x\rightarrow 0^+) \quad a^2\varepsilon[1-\exp(-x/\varepsilon)] \rightarrow 0 \qquad (B.79)$$

Thus, we see that the solution to our small perturbation problem does not appear to be singular for $\varepsilon \geq 0$, and the small perturbation problem and its solution seem to correctly approaches the solution to our model marching problem in the limit $\varepsilon \rightarrow 0^+$. Furthermore, the solution to the

aforementioned small perturbation problem also appears to be valid for $\varepsilon=0$, because in this case

$$1-\exp(-x/\varepsilon) \to 0 \qquad \text{for } \varepsilon=0 \tag{B.80}$$

and, consequently,

$$a^2\varepsilon[1-\exp(-x/\varepsilon)] = 0 \qquad \text{for } \varepsilon=0 \tag{B.81}$$

It should be noted that for the aforementioned small-perturbation problem

$$\vec{f}(\psi)/\varepsilon = \vec{\psi}_{,x}/(\lambda_1-\lambda_2) = a^2[1-\exp(-x/\varepsilon)]/(\lambda_1-\lambda_2) \tag{B.82}$$

Thus, using Eqs. (B.80) and (B.82) we see that

$$\mathfrak{Lim}(\varepsilon\to 0^+)\ \vec{f}(\psi)/\varepsilon \to a^2/(\lambda_1-\lambda_2) \tag{B.83}$$

In other words '$\vec{f}(\psi)/\varepsilon$' is bounded [has a limiting value of $a^2/(\lambda_1-\lambda_2)$] as $\varepsilon \to 0^+$, which was the result stated earlier to suggest that the small-perturbation problem of Eqs. (B.41-B.43) does not appear to be singular for $\varepsilon \geq 0$.

APPENDIX C. EXPRESSIONS FOR THE JACOBIAN MATRICES

The parabolized Navier-Stokes (PNS) equations for axisymmetric/2-D flows in a general curvilinear coordinate system, at the j+1 marching step and at the n+1 iteration level, can be written in the following vectorial form:

$$\vec{F}_{1,\xi}^{\,j+1,n+1} + \vec{F}_{2,\zeta}^{\,j+1,n+1} = \varepsilon \vec{S}_{,\zeta}^{\,j+1,n+1} + \vec{H}^{j+1,n+1} \qquad (C.1)$$

Using a first-order Taylor series expansion around the previous iteration, we can write

$$\begin{aligned}
\vec{F}_1^{\,j+1,n+1} &\simeq \vec{F}_1^{\,j+1,n} + \tilde{A}_1^{\,j+1,n} \cdot \vec{\Delta q}^{\,n+1} \\
\vec{F}_2^{\,j+1,n+1} &\simeq \vec{F}_2^{\,j+1,n} + \tilde{A}_2^{\,j+1,n} \cdot \vec{\Delta q}^{\,n+1} \\
\vec{S}^{\,j+1,n+1} &\simeq \vec{S}^{\,j+1,n} + \tilde{M}^{\,j+1,n} \cdot \vec{\Delta q}^{\,n+1} \\
\vec{H}^{\,j+1,n+1} &\simeq \vec{H}^{\,j+1,n} + \tilde{A}_0^{\,j+1,n} \cdot \vec{\Delta q}^{\,n+1}
\end{aligned} \qquad (C.2)$$

where

$$\vec{\Delta q}^{\,n+1} = \vec{q}^{\,j+1,n+1} - \vec{q}^{\,j+1,n} \qquad (C.3)$$

The matrices $\tilde{A}_0$, $\tilde{A}_1$, $\tilde{A}_2$, and $\tilde{M}$ are called the jacobian matrices, and have the following form:

$$\tilde{A}_1 = (1/J)\begin{bmatrix} 0 & \xi_{,x} & \xi_{,z} & 0 & 0 \\ -uU_1 & \xi_{,x}u+U_1 & \xi_{,z}u & 0 & \xi_{,x} \\ -wU_1 & \xi_{,x}w & \xi_{,z}w+U_1 & 0 & \xi_{,z} \\ -\Phi U_1 & \xi_{,x}\Phi+uU_1 & \xi_{,z}\Phi+wU_1 & U_1 & 0 \\ 0 & 0 & 0 & 0 & 0 \end{bmatrix} \qquad (C.4)$$

$$\tilde{A}_2 = (1/J)\begin{bmatrix} 0 & \zeta_{,x} & \zeta_{,z} & 0 & 0 \\ -uU_2 & \zeta_{,x}u+U_2 & \zeta_{,z}u & 0 & \zeta_{,x} \\ -wU_2 & \zeta_{,x}w & \zeta_{,z}w+U_2 & 0 & \zeta_{,z} \\ -\Phi U_2 & \zeta_{,x}\Phi+uU_2 & \zeta_{,z}\Phi+wU_2 & U_2 & 0 \\ 0 & 0 & 0 & 0 & 0 \end{bmatrix} \qquad (C.6)$$

$$\tilde{M} = (\mu/J)\begin{bmatrix} 0 & 0 & 0 & 0 & 0 & 0 \\ m_{21} & m_{22} & m_{23} & 0 & 0 & 0 \\ m_{31} & m_{32} & m_{33} & 0 & 0 & 0 \\ m_{41} & m_{42} & m_{43} & m_{44} & 0 & 0 \\ 0 & 0 & 0 & 0 & 0 & 0 \end{bmatrix} \qquad (C.7)$$

$$\tilde{A}_0 = \begin{bmatrix} 0 & 0 & 0 & 0 & 0 & 0 & 0 \\ 0 & 0 & 0 & 0 & 0 & 0 & 0 \\ 0 & 0 & 0 & 0 & 0 & 0 & -\kappa/Jz \\ 0 & 0 & 0 & 0 & 0 & 0 & 0 \\ 0 & 0 & 0 & 0 & 0 & -1 & \gamma \end{bmatrix} \qquad (C.8)$$

where

$$\Phi = T/(\gamma-1) + 0.5v^2 \qquad (C.9)$$

$$m_{21} = -(1/3)[(3m_0+m_{xx})(u/\rho)_{,\zeta}+m_{xz}(w/\rho)_{,\zeta}] \qquad (C.10)$$

$$m_{22} = (1/3)[(3m_0+m_{xx})(1/\rho)_{,\zeta}] \qquad (C.11)$$

$$m_{23} = (1/3)[m_{xz}(1/\rho)_{,\zeta}] \qquad (C.12)$$

$$m_{31} = -(1/3)[(3m_0+m_{zz})(w/\rho)_{,\zeta}+m_{xz}(u/\rho)_{,\zeta}] \qquad (C.13)$$

$$m_{32} = (1/3)[m_{xz}(1/\rho)_{,\zeta}] \qquad (C.14)$$

$$m_{33} = (1/3)[(3m_0+m_{zz})(1/\rho)_{,\zeta}] \qquad (C.15)$$

$$m_{41} = -(1/3)[3(T/\rho)_{,\zeta}/Pr(\gamma-1) + (3m_0+m_{xx})(u^2/\rho)_{,\zeta} + (3m_0+m_{zz})(w^2/\rho)_{,\zeta} + m_{xz}(2uw/\rho)_{,\zeta}] \quad (C.16)$$

$$m_{42} = (1/3)[(3m_0+m_{xx})(u/\rho)_{,\zeta} + m_{xz}(w/\rho)_{,\zeta}] \quad (C.17)$$

$$m_{43} = (1/3)[(3m_0+m_{xx})(w/\rho)_{,\zeta} + m_{xz}(u/\rho)_{,\zeta}] \quad (C.18)$$

$$m_{44} = m_0(1/\rho)_{,\zeta}/P\rho(\gamma-1) \quad (C.19)$$

$$m_{xx} = \zeta_{,x}\zeta_{,x} \quad (C.20)$$

$$m_{xz} = \zeta_{,x}\zeta_{,z} \quad (C.21)$$

$$m_{zz} = \zeta_{,z}\zeta_{,z} \quad (C.22)$$

and

$$m_0 = m_{xx} + m_{zz} \quad (C.23)$$

Also, $\kappa=0$ for 2-D flows and $\kappa=1$ for axisymmetric flows.

APPENDIX D. ON THE EIGENVALUES OF THE SIMPLIFIED PNS EQUATIONS

If we assume

(a) two-dimensional flow

(b) an evenly spaced square grid such that $\xi_{,x}=\zeta_{,z}=1$ a and $\xi_{,z}=\zeta_{,x}=0$

(c) equation-of-state approximated as

$$\gamma p - \rho T + \theta(p_{,\xi}+p_{,\zeta}) = 0 \qquad (D.1)$$

where the coefficient 'θ' is chosen such that $\theta \approx 0$ for all practical purposes; i.e.,

$$\theta p_{,\xi}+\theta p_{,\zeta}+\gamma p-\rho T \approx \gamma p-\rho T$$

(c) $w_{,\zeta} << u_{,\zeta}$ and $w << u$

we can write the simplified parabolized Navier-Stokes (PNS) equations as:

$$\vec{f}_{1,\xi}^{\,n+1} + \vec{f}_{2,\zeta}^{\,n+1} = \varepsilon \vec{s}_{,\zeta}^{\,n+1} + \vec{h}^{n+1} \qquad (D.2)$$

where

$$\vec{f}_1 = \begin{bmatrix} \rho u \\ \rho u^2+p \\ \rho w u \\ \{T/(\gamma-1)+0.5V^2\}\rho u \\ \theta p \end{bmatrix} \qquad (D.3)$$

$$\vec{f}_2 = \begin{bmatrix} \rho w \\ \rho u w \\ \rho w^2+p \\ \{T/(\gamma-1)+0.5V^2\}\rho w \\ \theta p \end{bmatrix} \qquad (D.4)$$

$$\vec{s} = \mu \begin{bmatrix} 0 \\ u_{,\zeta} \\ 4w_{,\zeta}/3 \\ \{ T_{,\zeta}/Pr(\gamma-1) + uu_{,\zeta} \} \\ 0 \end{bmatrix} \qquad (D.5)$$

and

$$\vec{h} = \begin{bmatrix} 0 \\ 0 \\ 0 \\ 0 \\ \gamma p - \rho T \end{bmatrix} \qquad (D.6)$$

Using a Taylor-Series expansion we can expand $\vec{f}_1$ and $\vec{f}_2$ around the previous iteration as:

$$\vec{f}_1^{\,n+1} \simeq \vec{f}_1^{\,n} + \tilde{a}_1^{n} \cdot \Delta\vec{q} \qquad (D.7)$$

$$\vec{f}_2^{\,n+1} \simeq \vec{f}_2^{\,n} + \tilde{a}_2^{n} \cdot \Delta\vec{q} \qquad (D.8)$$

where

$$\tilde{a}_1^{n} = \begin{bmatrix} 0 & 1 & 0 & 0 & 0 \\ -u^2 & 2u & 0 & 0 & 1 \\ -uw & w & u & 0 & 0 \\ -\Phi_1 u & \Phi_2 + u^2 & (\gamma-1)uw & u & 0 \\ 0 & 0 & 0 & 0 & \theta \end{bmatrix} \qquad (D.9)$$

and

$$\tilde{a}_2^n = \begin{bmatrix} 0 & 0 & 1 & 0 & 0 \\ -uw & w & u & 0 & 0 \\ -w^2 & 0 & 2w & 0 & 1 \\ -\Phi_1 w & (\gamma-1)uw & \Phi_2+w^2 & w & 0 \\ 0 & 0 & 0 & 0 & \theta \end{bmatrix} \tag{D.10}$$

In the above expressions

$$\Phi_1 = T + (\gamma-1)V^2 \tag{D.11}$$

$$\Phi_2 = T + (\gamma-1)(V^2/2+u^2) \tag{D.12}$$

In order to obtain a similar expression for the viscous vector $\vec{(s)}$, consider the following derivative expressions

$$u_{,\zeta} = (1/\rho)(\rho u)_{,\zeta} - (u/\rho)\rho_{,\zeta} \tag{D.13}$$

$$uu_{,\zeta} = (u/\rho)(\rho u)_{,\zeta} - (u^2/\rho)\rho_{,\zeta} \tag{D.14}$$

and

$$T_{,\zeta} = (1/\rho)(\rho T)_{,\zeta} - (T/\rho)\rho_{,\zeta} \tag{D.15}$$

Thus, using Eqs. (D.13-D.15) and Eq. (D.5), we can write

$$\vec{s}^{n+1} \simeq \tilde{m}^{n+1} \cdot (\vec{q}_{,\zeta})^{n+1} \tag{D.16}$$

Linearizing Eq. (D.16) around the previous iteration gives

$$\vec{s}^{n+1} \simeq \vec{s}^{n} + \tilde{m}^{n} \cdot \vec{d}_{,\zeta} \tag{D.17}$$

where

$$\tilde{m}^{n} = (\mu/\rho) \begin{vmatrix} 0 & 0 & 0 & 0 & 0 \\ -u & 1 & 0 & 0 & 0 \\ -4w/3 & 0 & 4/3 & 0 & 0 \\ \alpha_1 & u(\gamma-1) & 0 & 1/Pr & 0 \\ 0 & 0 & 0 & 0 & 0 \end{vmatrix} \tag{D.18}$$

$$\vec{d} = \Delta \vec{q}^{n+1} \tag{D.19}$$

and

$$\alpha_1 = -[T/Pr + (\gamma-1)u^2] \tag{D.20}$$

If we represent

$$\tilde{b}^{n} = \varepsilon \tilde{m}^{n} \tag{D.21}$$

we can write Eq. (D.2) as

$$(\tilde{a}_1^n \cdot \vec{d})_{,\zeta} + (\tilde{a}_2^n \cdot \vec{d})_{,\xi} - (\tilde{b}^n \cdot \vec{d}_{,\zeta})_{,\zeta} + \vec{R} = 0 \qquad \text{(D.22)}$$

Using a frozen coefficient approach, we assume that the jacobian matrices $\tilde{a}_1^n$, $\tilde{a}_2^n$ and $\tilde{b}^n$ do not change with ξ and ζ; i.e.,

$$\tilde{a}_1^n \simeq \tilde{a}_1^f \qquad \text{(D.23)}$$

$$\tilde{a}_2^n \simeq \tilde{a}_2^f \qquad \text{(D.24)}$$

and

$$\tilde{b}^n \simeq \tilde{b}^f \qquad \text{(D.25)}$$

With this frozen coefficient assumption Eq. (D.18) reduces to:

$$\tilde{a}_1^f \cdot \vec{d}_{,\xi} + \tilde{a}_2^f \cdot \vec{d}_{,\zeta} - \tilde{b}^f \cdot \vec{d}_{,\zeta\zeta} + \vec{R}(d,\xi,\zeta) = 0 \qquad \text{(D.26)}$$

Thus

$$\vec{d}_{,\xi} + \tilde{a}_1^{f\,-1} \cdot \tilde{a}_2^f \cdot \vec{d}_{,\zeta} - \tilde{a}_1^{f\,-1} \cdot \tilde{b}^f \cdot \vec{d}_{,\zeta\zeta} + \tilde{a}_1^{f\,-1} \cdot \vec{R} = 0$$

Or

$$\vec{d}_{,\xi} + \tilde{N}_1 \cdot \vec{d}_{,\zeta} - \tilde{N}_2 \vec{d}_{,\zeta\zeta} + \vec{C} = 0 \qquad \text{(D.27)}$$

Here, the inverse of $\tilde{a}_1^f$ is defined as:

$$\tilde{a}_1^{f\,-1} = \begin{bmatrix} 2/u & 1/u^2 & 0 & 0 & 1/\theta u^2 \\ 1 & 0 & 0 & 0 & 0 \\ w/u & -w/u^2 & 1/u & 0 & w/\theta u^2 \\ \Phi_1/u & -\Phi_3/u^2 & -(\gamma-1)w/u & 1/u & \Phi_3/\theta u^2 \\ 0 & 0 & 0 & 0 & 1/\theta \end{bmatrix} \qquad (D.28)$$

where

$$\Phi_3 = T + (\gamma-1)u^2 \qquad (D.29)$$

Also, with the approximation that $w \ll u$, the expressions for $\tilde{N}_1$ become

$$\tilde{N}_1 = \begin{bmatrix} w/u & -w/u^2 & 1/u & 0 & 1/u^2 \\ 0 & 0 & 1 & 0 & 0 \\ 0 & -w^2/u^2 & 2w/u & 0 & 1/u \\ 0 & wT/u^2 & T/u & w/u & \Phi_3/u^2 \\ 0 & 0 & 0 & 0 & 1 \end{bmatrix} \qquad (D.30)$$

and

$$\tilde{N}_2 = (\varepsilon\mu/\rho)\begin{bmatrix} 1/u & -1/u^2 & 0 & 0 & 0 \\ 0 & 0 & 0 & 0 & 0 \\ \beta_1 & -\beta_1/u & 4/3u & 0 & 0 \\ \beta_2 & -T/u^2 & \beta_3 & 1/Pru & 0 \\ 0 & 0 & 0 & 0 & 0 \end{bmatrix} \tag{D.31}$$

where

$$\beta_1 = -w/3u \tag{D.32}$$

$$\beta_2 = [T(1+1/Pr) + 2(\gamma-1)/3]/u \tag{D.33}$$

and

$$\beta_3 = -4(\gamma-1)w/3u \tag{D.34}$$

The eigenvalues of $\tilde{N}_1$ [Eq. (D.30)] are given by

$$(\lambda-1)(\lambda-w/u)[\lambda(\lambda-2w/u)(\lambda-w/u)+(\lambda-w/u)w^2/u^2] = 0$$

Or

$$(\lambda-1)(\lambda-w/u)^2[\lambda^2-2\lambda w/u+w^2/u^2] = 0 \tag{D.35}$$

Thus

$$\lambda_i = (1, w/u, w/u, w/u, w/u) \tag{D.36}$$

Similiarly, the eigenvalues of $\tilde{N}_2$ [Eq. (B.31)] are given by

$$\sigma^2(\sigma - \varepsilon\mu/Pr\rho u)(\sigma - 4\varepsilon\mu/3\rho u)(\sigma - \varepsilon\mu/\rho u) = 0 \tag{D.37}$$

Thus, we obtain the eigenvalues of $\tilde{N}_2$ as

$$\sigma_i = (0, 0, \varepsilon\mu/Pr\rho u, 4\varepsilon\mu/3\rho u, \varepsilon\mu/\rho u) \tag{D.38}$$

REFERENCES

1. Schiff, L. B., and Steger, J.L., "Numerical Simulation of Steady Supersonic Viscous Flows," AIAA Paper No. 79-0130, Jan. 1979.

2. Shanks, S.P., Srinivasan, G.R., and Nicolet, W.E., "AFWAL Parabolized Navier-Stokes Code: Formulation and User's Manual," AFWAL-TR-82-3034,

3. Vigneron, Y.C., Rakich, J.V., and Tannehill, J.C., "Calculation of Supersonic Viscous Flow Over Delta Wings with Sharp Subsonic Leading Edges," AIAA Paper No. 78-1137, July 1978. Air Force Flight Dynamics Laboratory, Wright-Patterson AFB, OH, June 1982.

4. Chaussee, D.S., Patterson, J.L., Kutler, P., Pulliam, T.H., and Steger, J.L., "A Numerical Simulation for Hypersonic Viscous Flows Over Arbitrary Geometries at High Angle of Attack," AIAA Paper No. 81-0050, Jan. 1981.

5. Lubard, S.C., and Helliwell, W.S., "Calculation of the Flow on a Cone at High Angle Attack," Report No. RDA-TR-150, R & D Associates, Santa Monica, CA 90403, Feb. 1973).

6. Helliwell, W.S., Dickinson, R.P., and Lubard, S.C., "Viscous Flow Over Arbitrary Geometries at High Angles of Attack," AIAA Paper No. 80-0064, Jan. 1980.

7. Lin, T.C., and Rubin, S.G., "A Numerical Scheme for Supersonic Viscous Flow Over a Slender Reentry Vehicle," AIAA Paper No. 79-0205, Jan. 1979.

8. Rubin, S.G., and Lin, A., "Marching with the PNS Equations," Israel Journal of Technology, Vol. 18, March 1980, pp. 21-31.

9. Lin, A., and Rubin, S.G., "Three-Dimensional Supersonic Viscous Flow over a Cone at Incidence," AIAA Journal, Vol. 20, Nov. 1982, pp. 1500-1507.

10. Kim, M.D., and Lewis, C.H., "Computation of Hypersonic Viscous Flows over a Body with Mass Transfer and/or Spin," Journal of Spacecraft and Rocket, Vol. 20, March-April 1983, pp. 101-107.

11. Kim, M.D., Thareja, R.R., and Lewis, C.H., "Three-Dimensional Viscous Flowfield Computations in a Streamline Coordinate System," Journal of Spacecraft and Rocket, Vol. 19, Jan.-Feb. 1983, pp. 41-46.

12. Thompson, R.A., Lewis, C.H., and Kautz, II, F.A., "Comparitive Analysis of Viscous Flows Over Complex Geometries During Reentry," AIAA Paper No. 82-1304, August, 1982.

13. Thompson, R.A., Lewis, C.H., and Kautz, II, F.A., "Comparison Techniques for Predicting 3-D Viscous Flows Over Ablated Shapes," AIAA Paper 8-0345, Jan. 1983.

14. Bhutta, B.A., Lewis, C.H., and Kautz, II, F.A., "Influence of Aerodynamic Prediction Methodology on the Performance Evaluation of Reentry Vehicle Configurations," AIAA Paper No. 83-1799, July 1983.

15. Kautz, II, F.A., Bhutta, B.A., and Lewis, C.H., "Improvements in Reentry Vehicle Aerodynamic Performance Through use of Multiconic Configurations," AIAA Paper No. 83-1800, July 1983.

16. Peyret, R., and Viviand H., "Computations of Viscous Compressible Flows Based on the Navier-Stokes Equations," AGARD-AG-212, 1975.

17. Murray, A.L., Lewis, C.H., "Hypersonic Three-Dimensional Viscous Shock-Layer Flows over Blunt Bodies," AIAA Journal, Vol. 16, Dec. 1978, pp. 1279-1286.

18. Solomon, J.M., Ciment, M., Ferguson, R.E., Bell, J.B., and Wardlaw, Jr., A.B., "A Program for Computing Steady Inviscid Three-Dimensional Supersonic Flow on Reentry Vehicles, Vol. I, Analysis and Programming," Report No. NSWC/WOL/Tr 77-28, Naval Surface Weapons Center, White Oak Laboratory, Silver Spring, Maryland, Feb. 1977.

19. White, F.M., Viscous Fluid Flow, McGraw-Hill Book Company, NY, 1974.

20. Viviand, H., "Conservative Forms of Gas Dynamic Equations," La Recherche Aerospatiale, No. 1, Jan.-Feb., 1974, pp. 65-68.

Table 1. Freestream Conditions

		Case A	Case B
Altitude	(kft)	80.000	200.000
Mach Number		25.000	25.000
Reynolds Number		2.92E+5	1.72E+3
Pressure	(lbs/ft^2)	58.562	0.417
Density	($slug/ft^3$)	8.64E-5	5.34E-7
Temperature	($^\circ R$)	395.067	455.381
Velocity	(ft/sec)	2.44E+4	2.62E+4

Table 2. Convergence Rates at X/RN=10. Location for Various Grid Distributions

Case	ζ Grid Points	m	β
	50	-1.00	2.7
A	100	-1.20	3.3
	150	-1.30	3.7
	50	-0.95	2.6
B	100	-1.20	3.3
	150	-1.30	3.7

Table 3. Computing Time[(a)] studies for the Solution at X/RN=10. Location

Case	ζ-Points	t^{1*} (sec)	(b) t^1	(c) t_t^* (sec)	(d) t_t
A	50	0.14	1.00	2.12	1.00
	100	0.28	2.00	2.09	1.97
	150	0.43	3.00	2.02	2.85
B	50	0.15	1.00	2.17	1.00
	100	0.28	1.87	1.95	1.68
	150	0.42	2.80	2.18	2.81

(a) On IBM 3081 with H-compiler and OPT=2 optimization
(b) Time for the first iteration scaled with respect to the 50-point value
(c) Total time for the marching step
(d) Total time for the marching step scaled with respect to the 50-point value

Table 4. Comparison of Total Computing Times[a] for Case A

Code	X/RN From-to		Grid ξ	Grid ζ	t^* (m:s)	τ^* (sec)	τ (b)
NOL3D	0.	500.	475	10	0:06	0.00001	0.002
VSLPG	0.	2.	33	101	0:22	0.00660	1.000
VSLPG	2.	200.	60	101	0:35	0.00580	0.879
PNSPG	2.	200.	124	150	2:03	0.00660	1.000
AFWAL	2.	200.	123	50	0:29	0.00472	0.715

(a) On IBM 3081 with H-compiler and OPT=2 optimization

(b) Scaled with respect to the τ^* value for PNSPG code

Table 5. Comparison of Total Computing Times[a] for Case B

Code	X/RN From-to		Grid ξ	Grid ζ	t^* (m:s)	τ^* (sec)	τ (b)
NOL3D	0.	500.	475	10	0:06	0.00001	0.002
VSLPG	0.	2.	33	101	0:22	0.00660	1.031
VSLPG-0	2.	200.	219	101	2:04	0.00561	0.877
VSLPG-1	2.	200.	218	101	2:02	0.00552	0.863
PNSPG	2.	200.	126	150	2:01	0.00640	1.000

(a) On IBM 3081 with H-compiler and OPT=2 optimization

(b) Scaled with respect to the τ^* value for PNSPG code

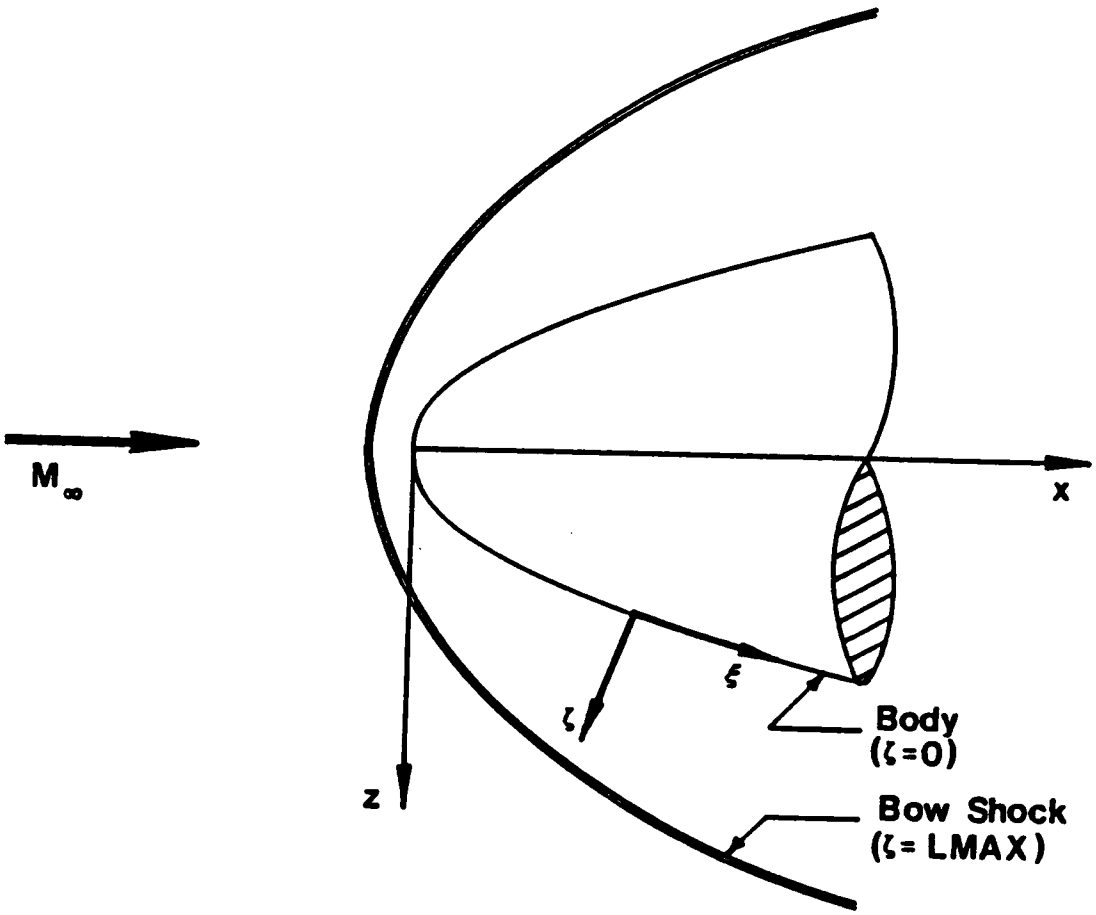

Figure 1. Coordinate system

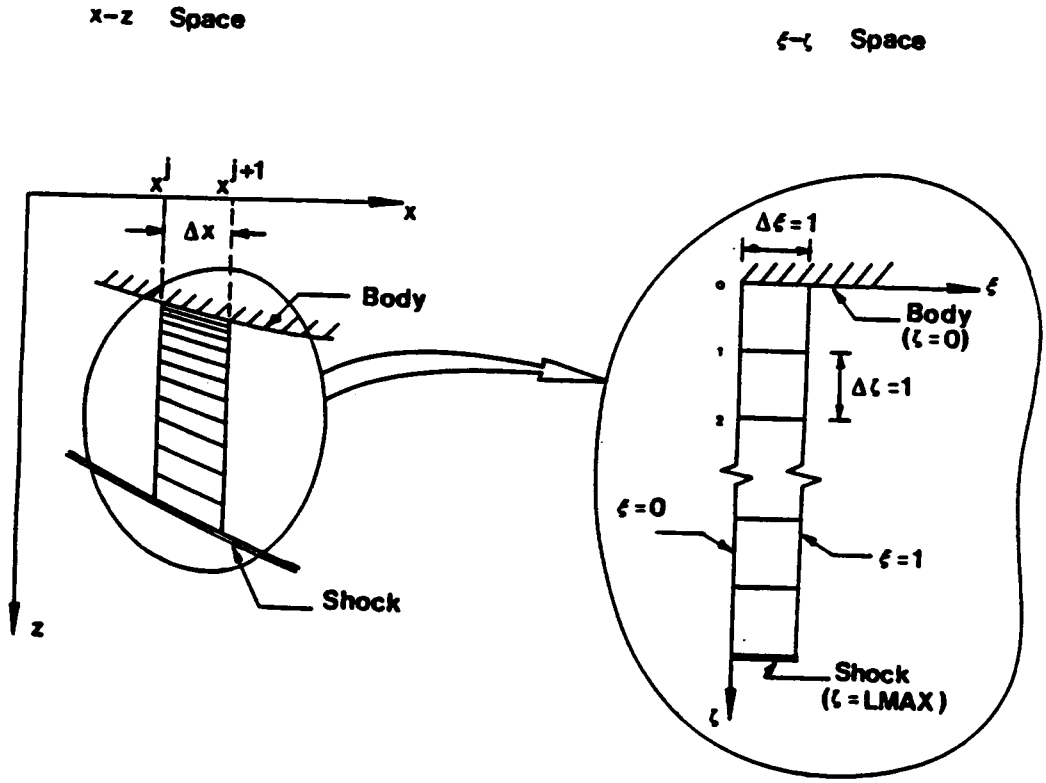

Figure 2. Transformation from the physical to the computational space

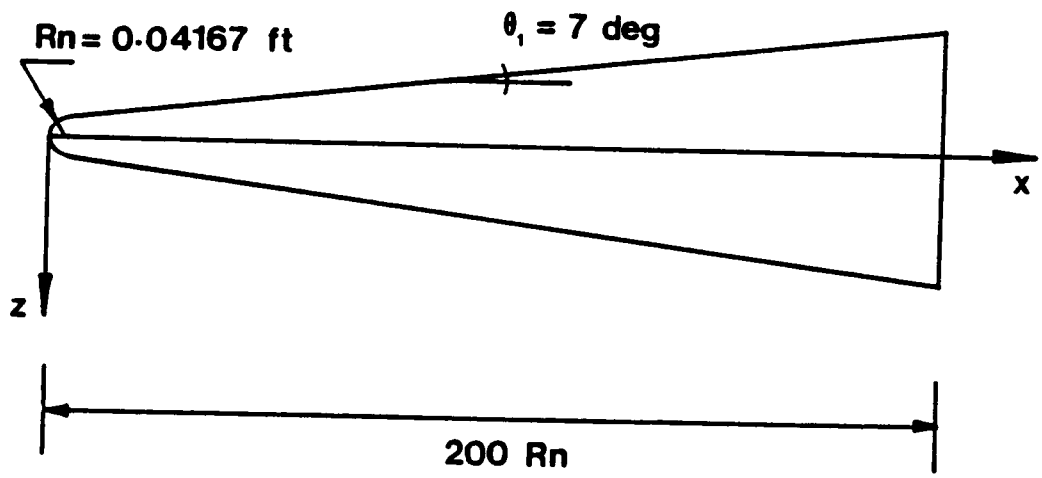

Figure 3. Vehicle geometry

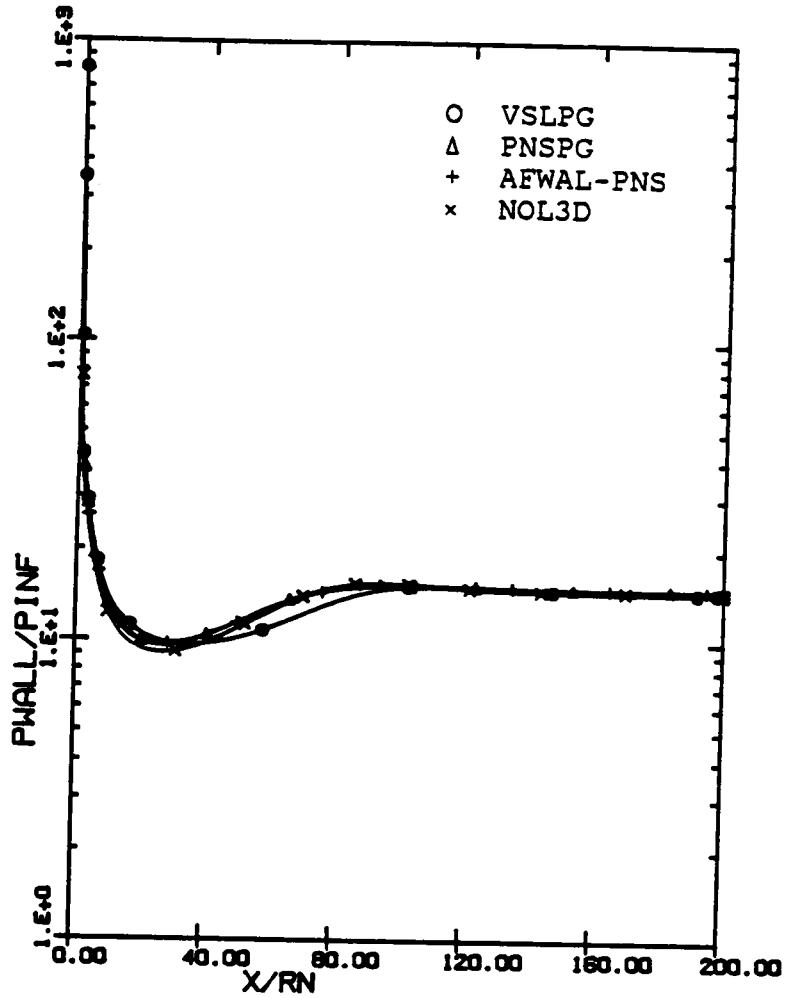

Figure 4. Axial distribution of wall pressures for Case A

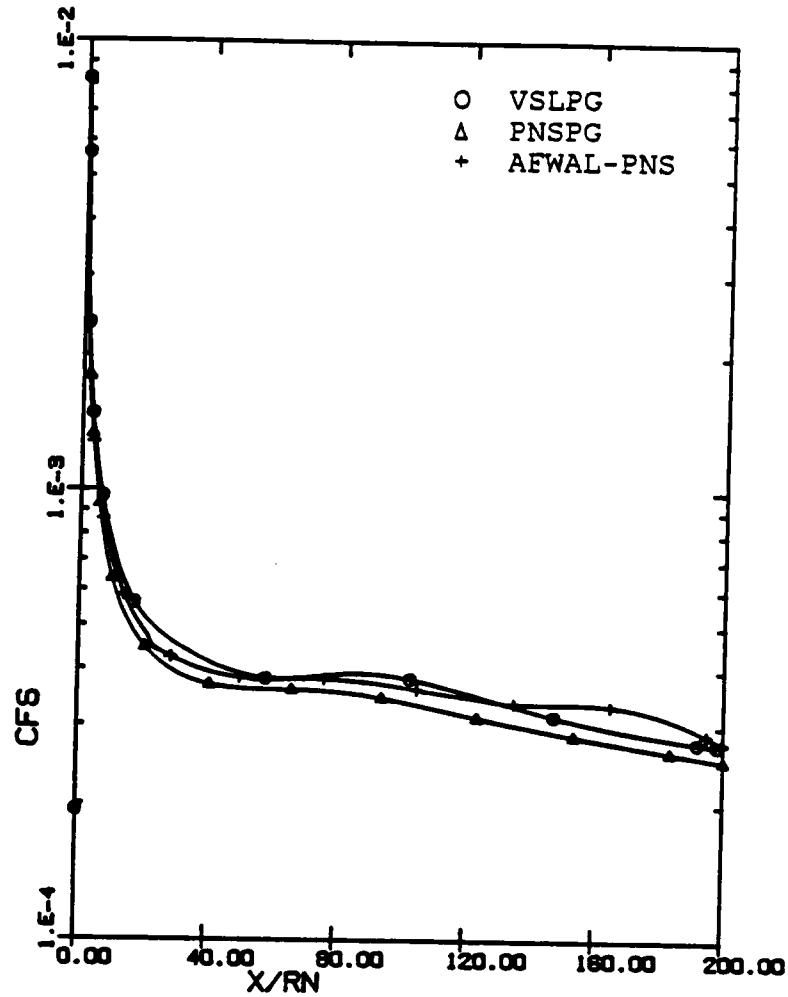

Figure 5. Axial distribution of skin friction for Case A

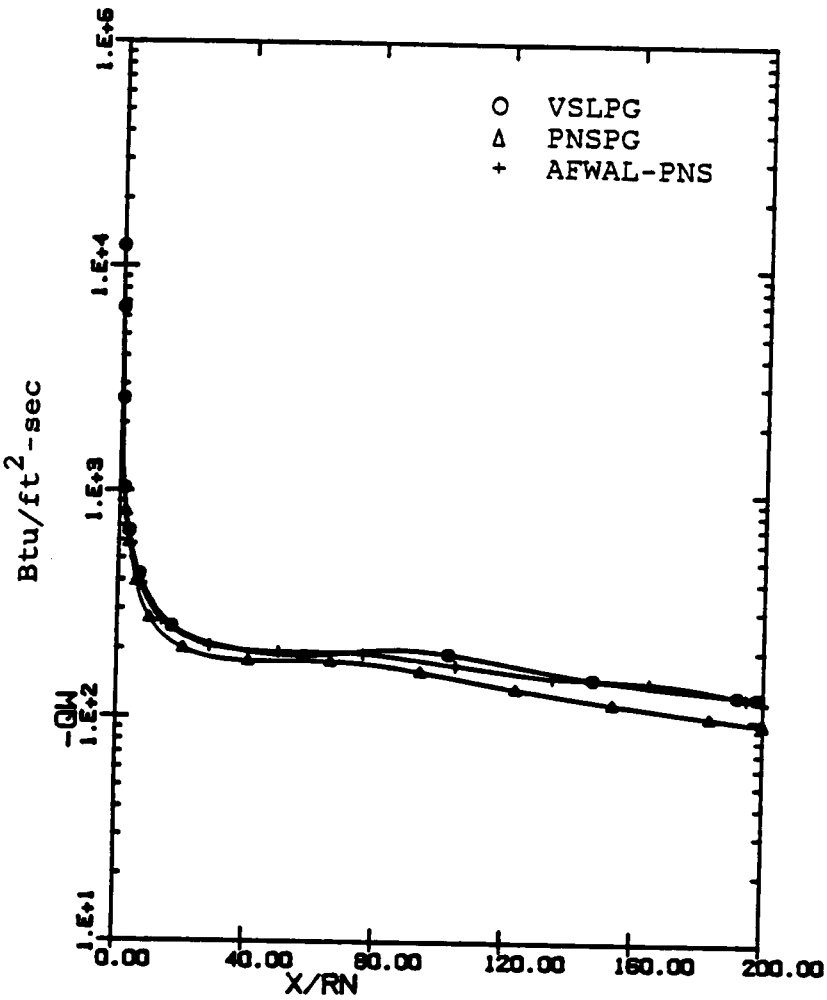

Figure 6. Axial distribution of wall heat- transfer rates for Case A

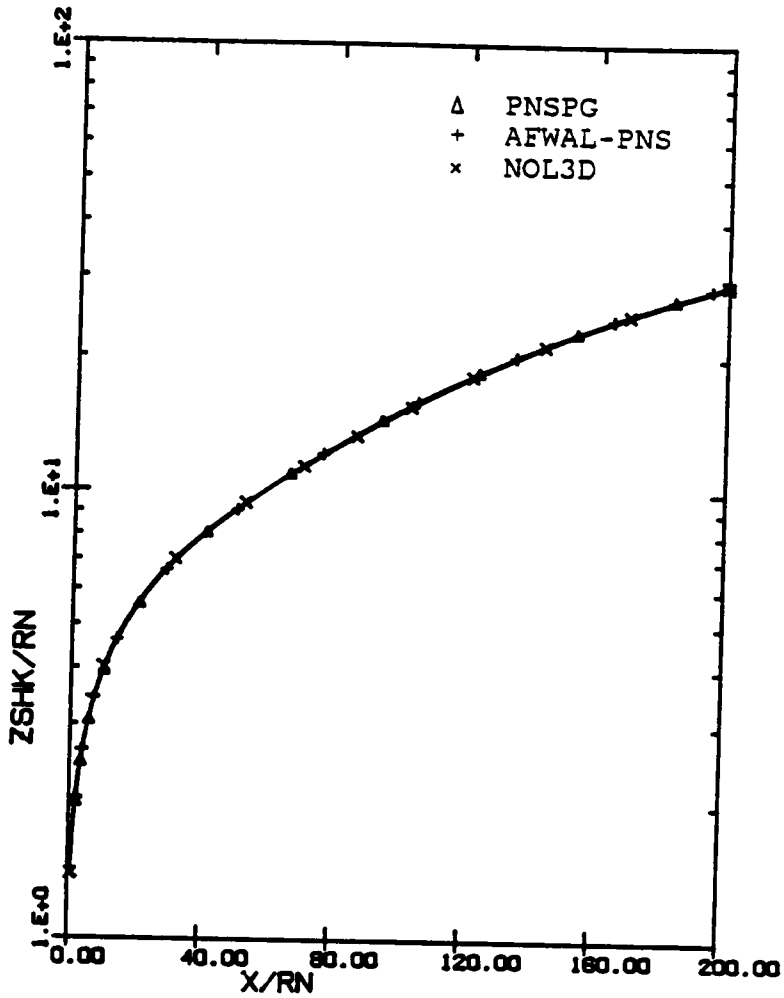

Figure 7. Bow shock shape for Case A

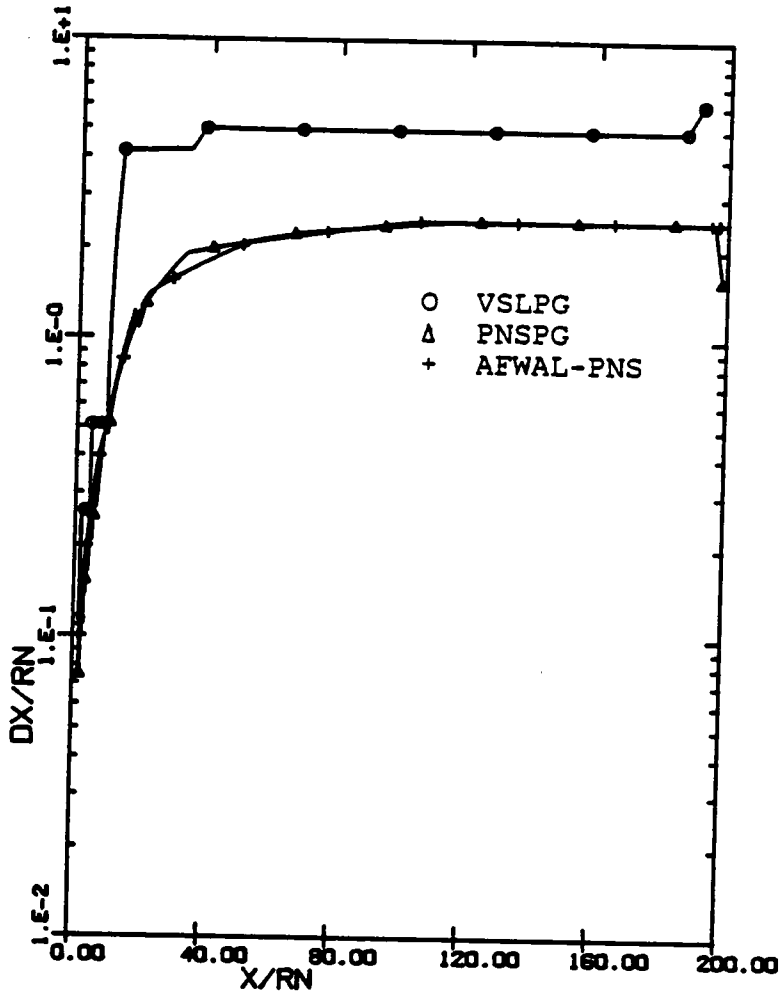

Figure 8. Step-size distributions used for Case A calculations

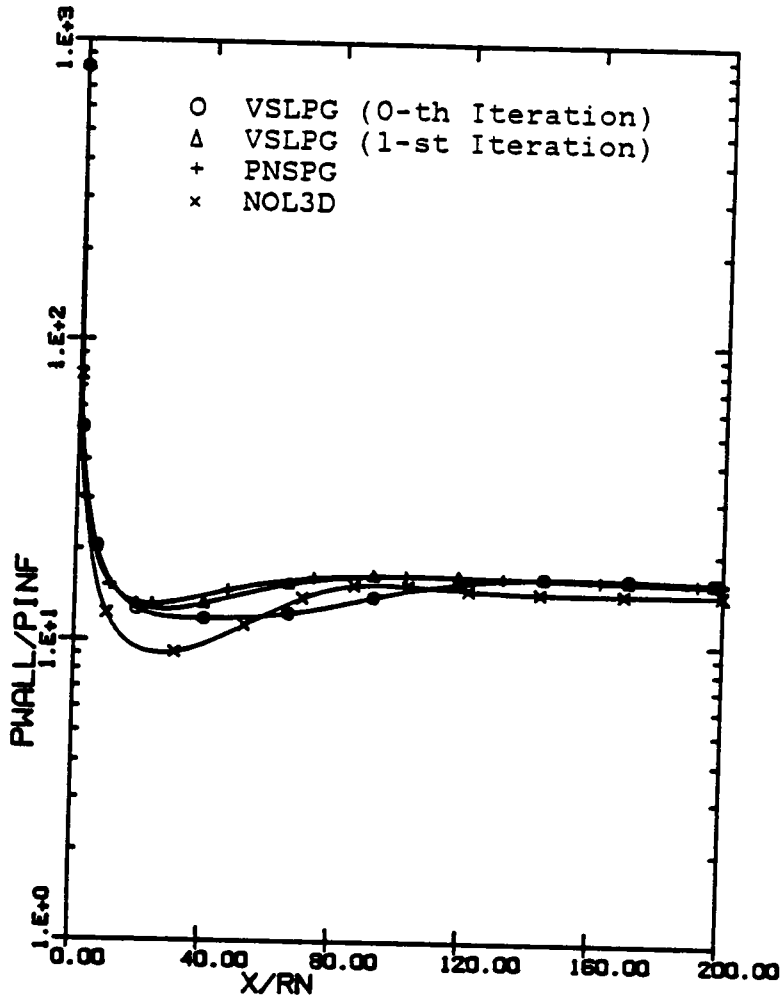

Figure 9. Axial distribution of wall pressures for Case B

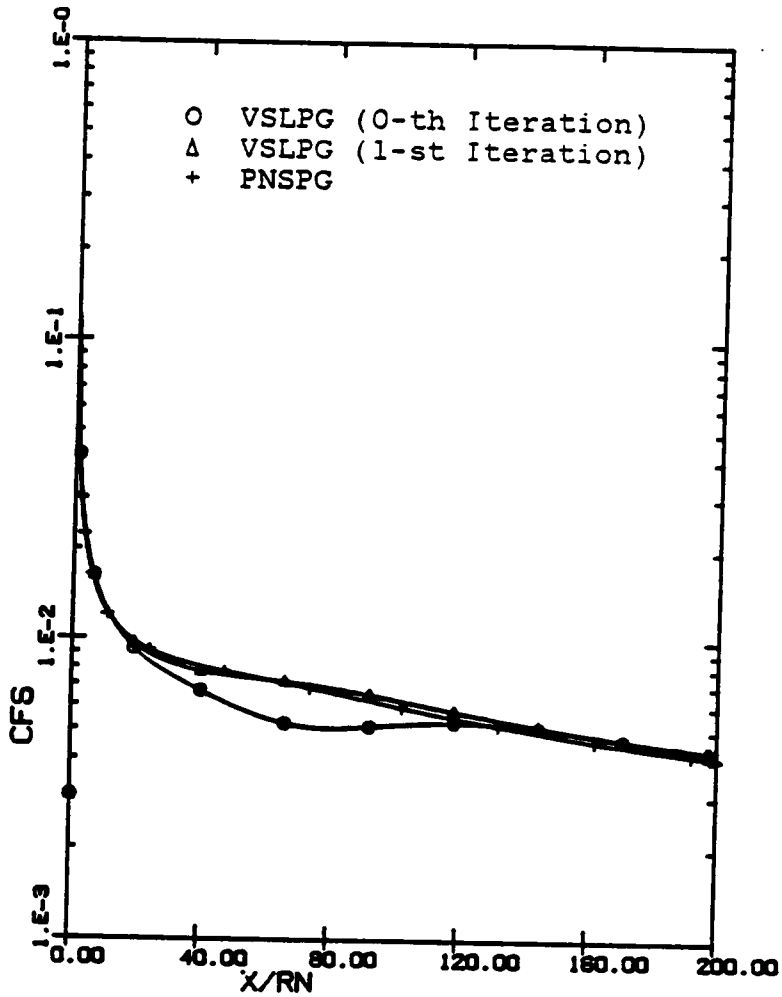

Figure 10. Axial distribution of skin friction for Case B

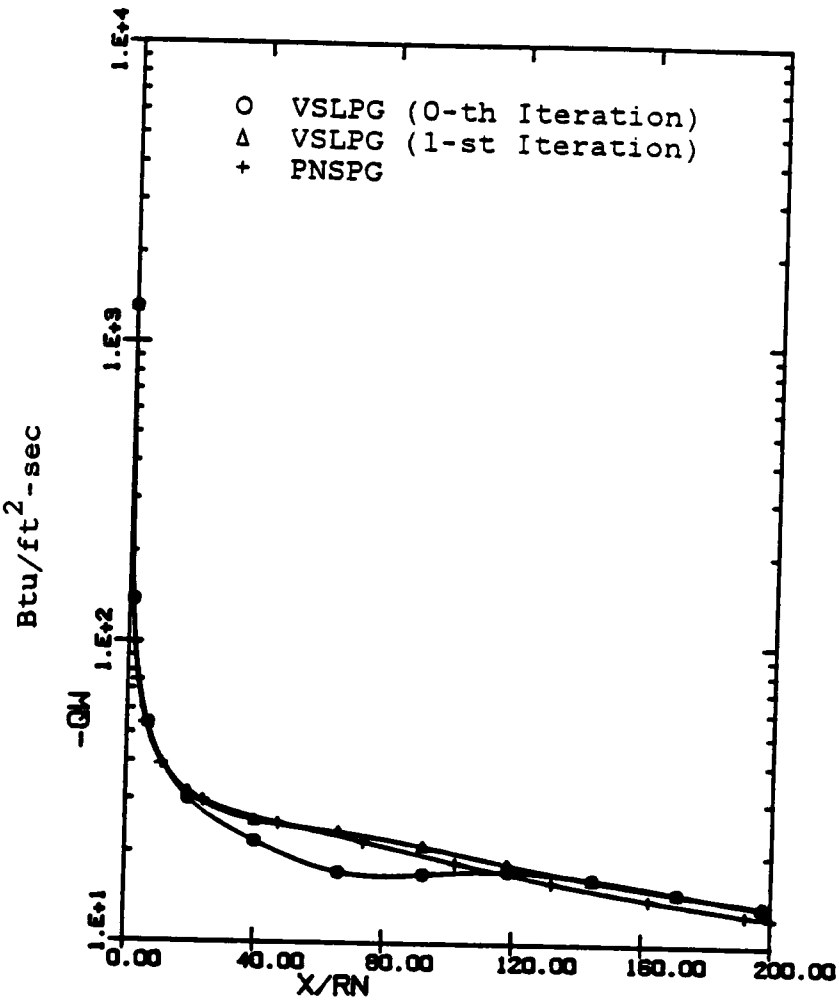

Figure 11. Axial distribution of wall heat-transfer rates for Case B

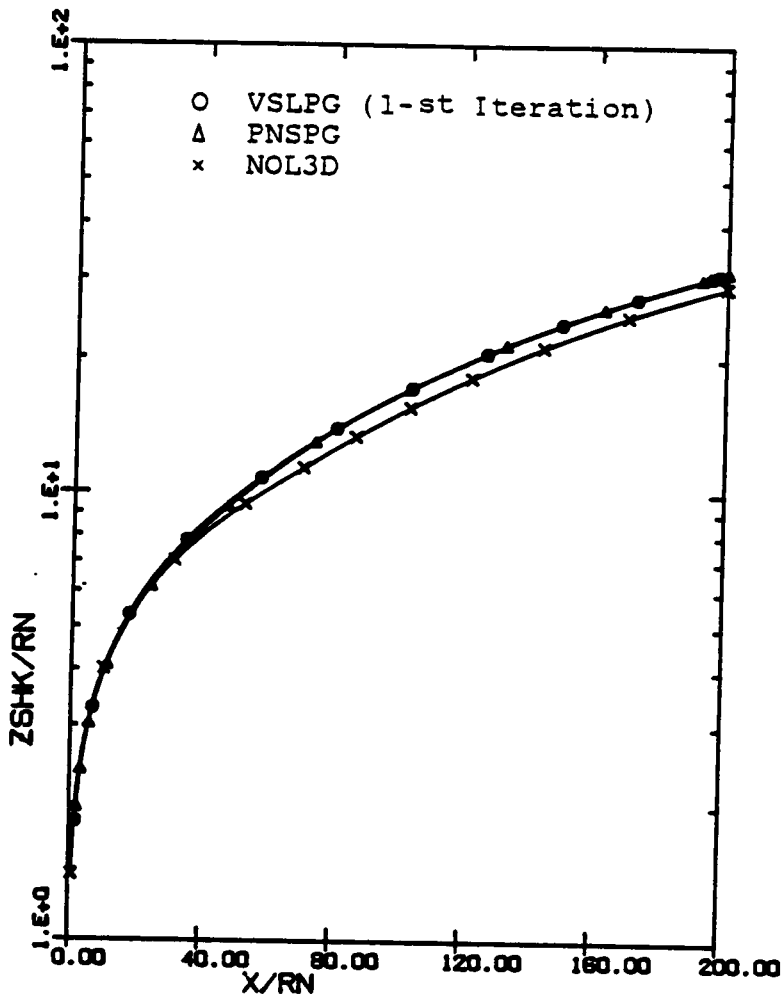

Figure 12. Bow shock shape for Case B

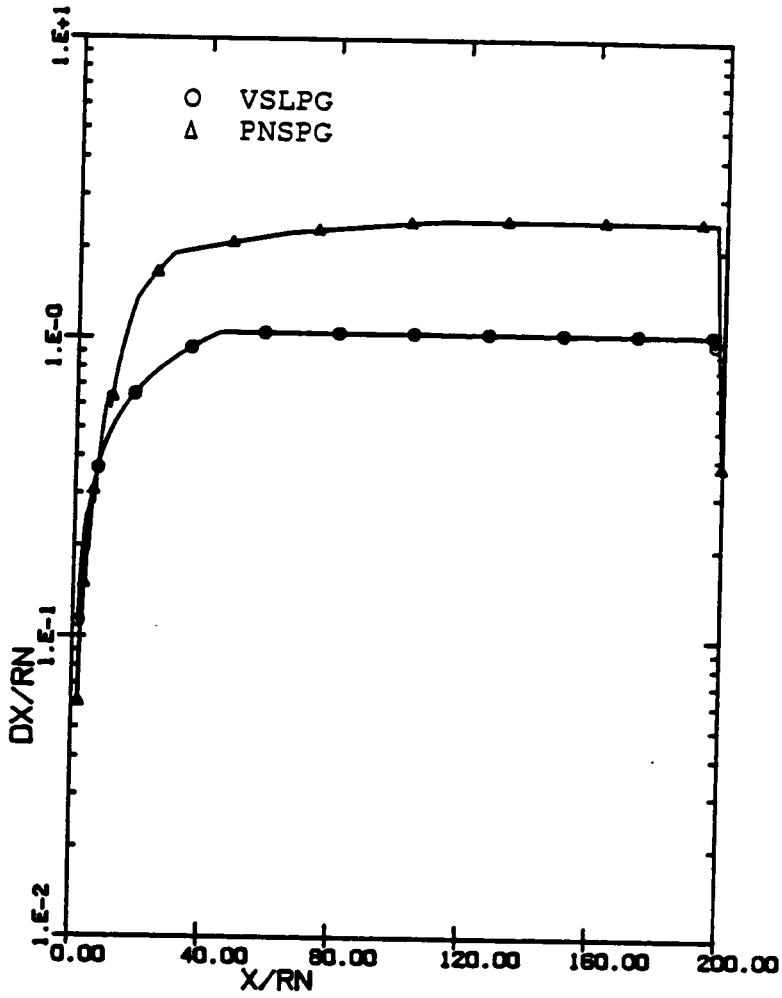

Figure 13. Step-size distributions used for Case B calculations

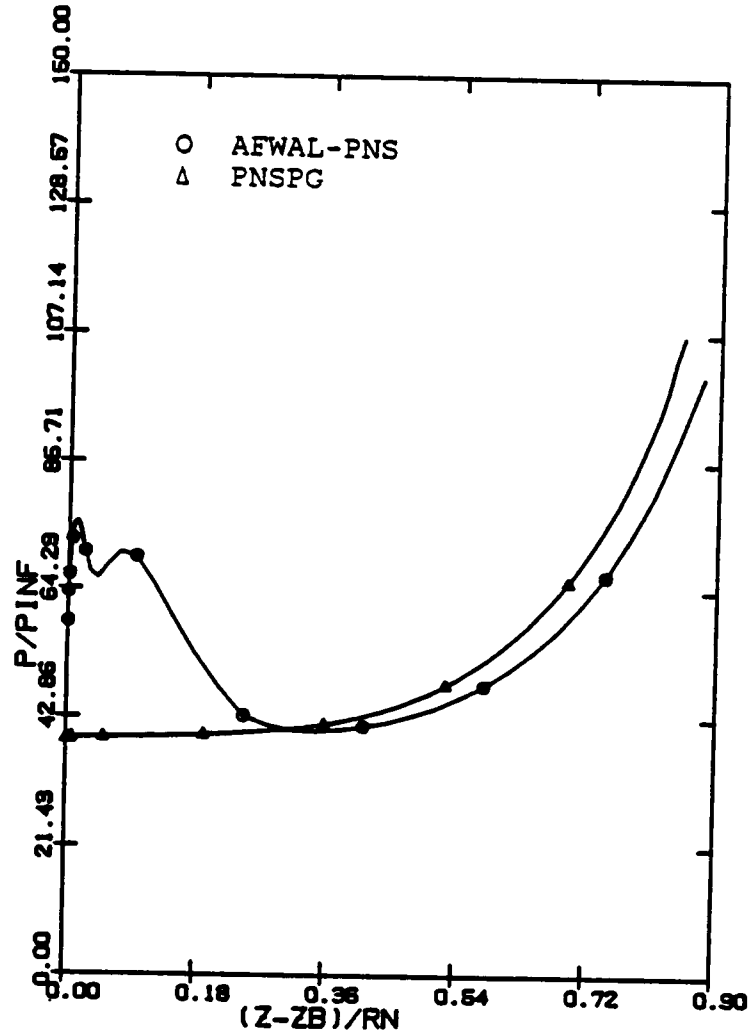

Figure 14. Comparison of PNSPG and AFWAL PNS pressure profile for Case B at X/RN=2.1

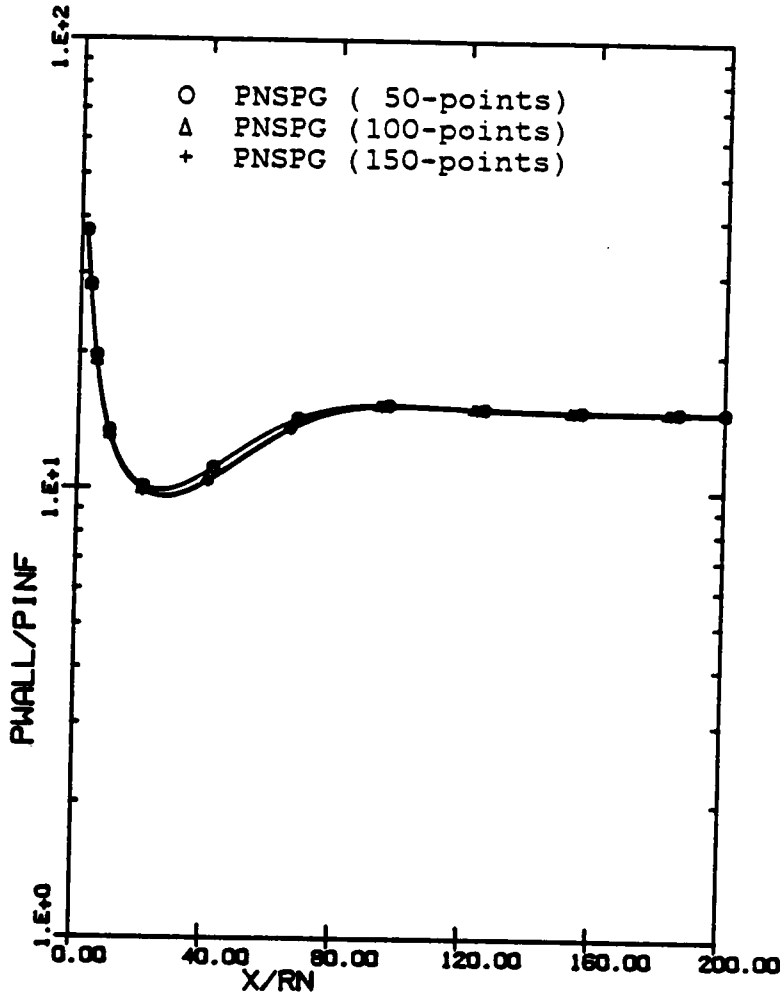

Figure 15. Effects of grid distribution on wall pressures for Case A

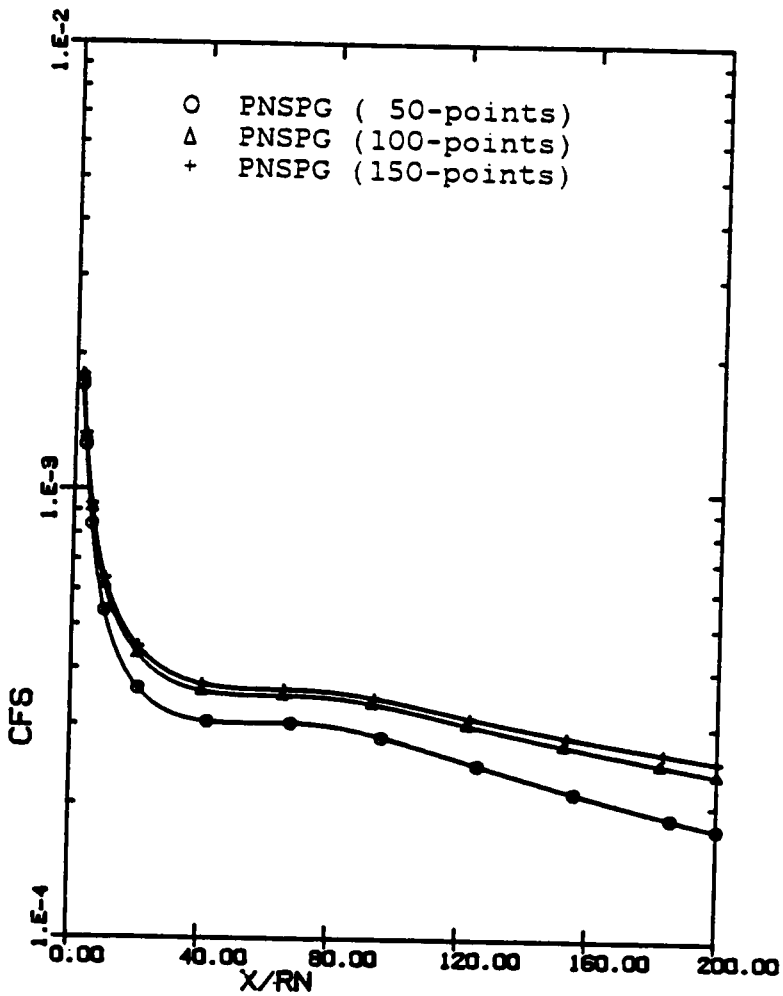

Figure 16. Effects of grid distribution on skin friction for Case A

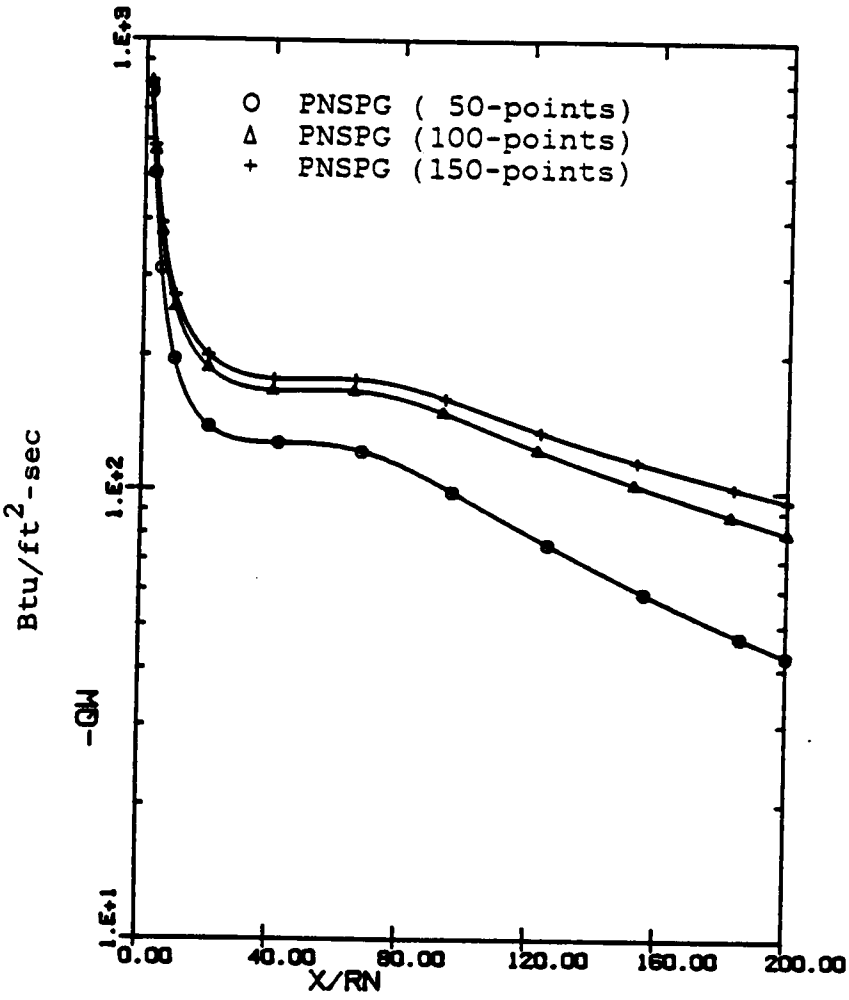

Figure 17. Effects of grid distribution on wall heat-transfer rates for Case A

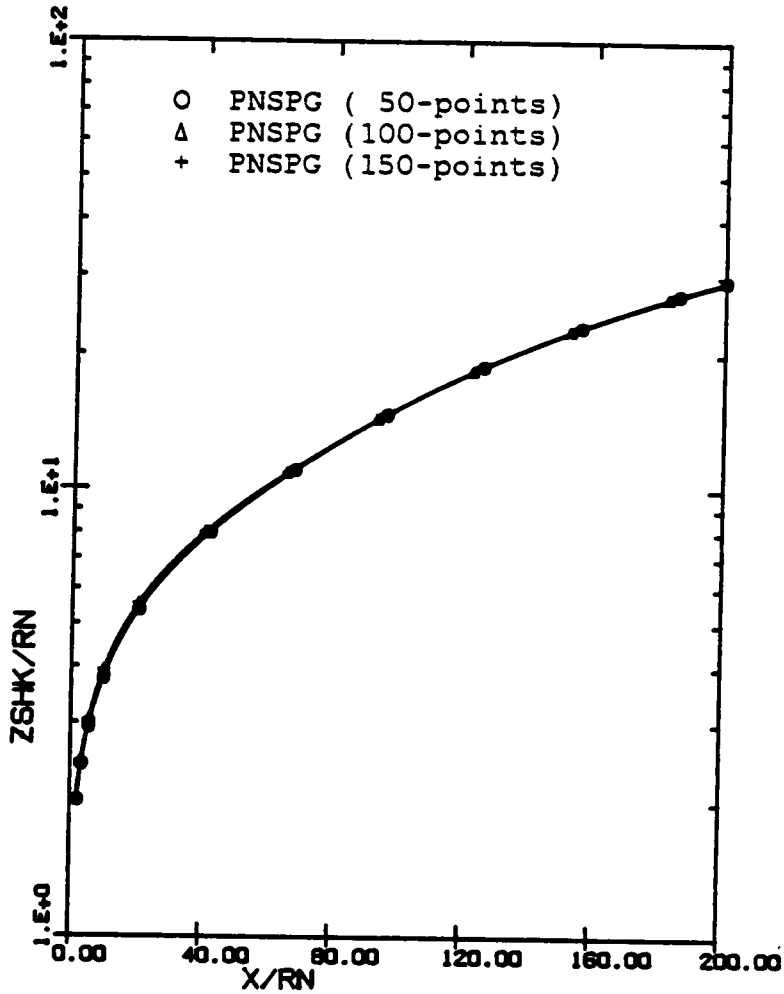

Figure 18. Effects of grid distribution on bow shock shape for Case A

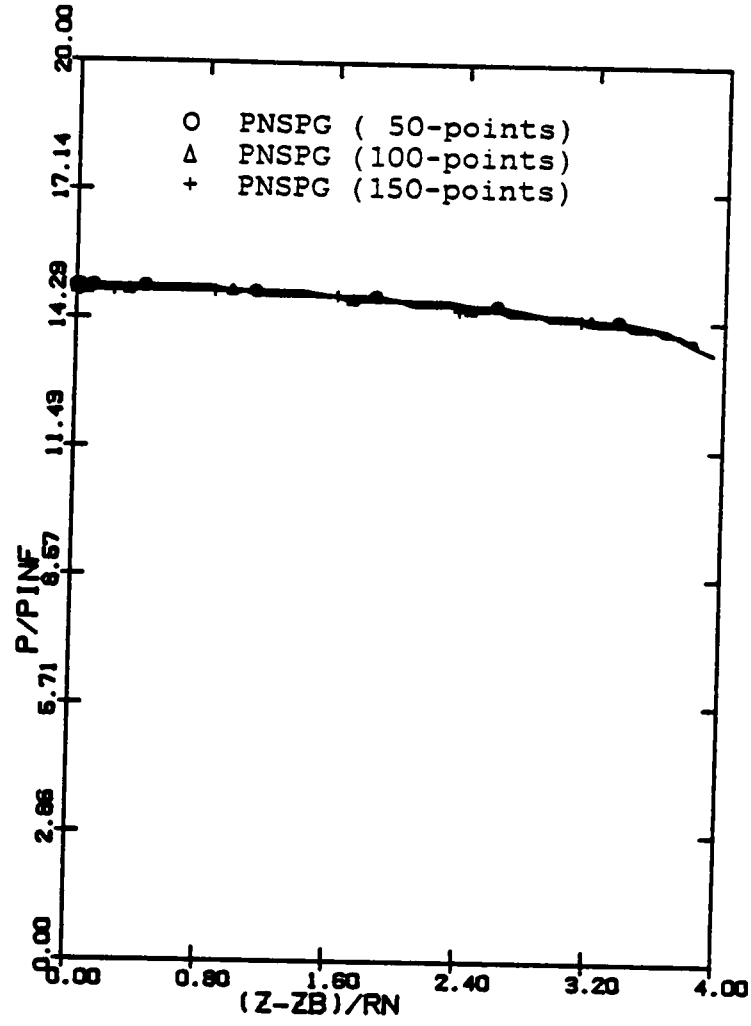

Figure 19. Effects of grid distribution on pressure profile at X/RN=200 for Case A

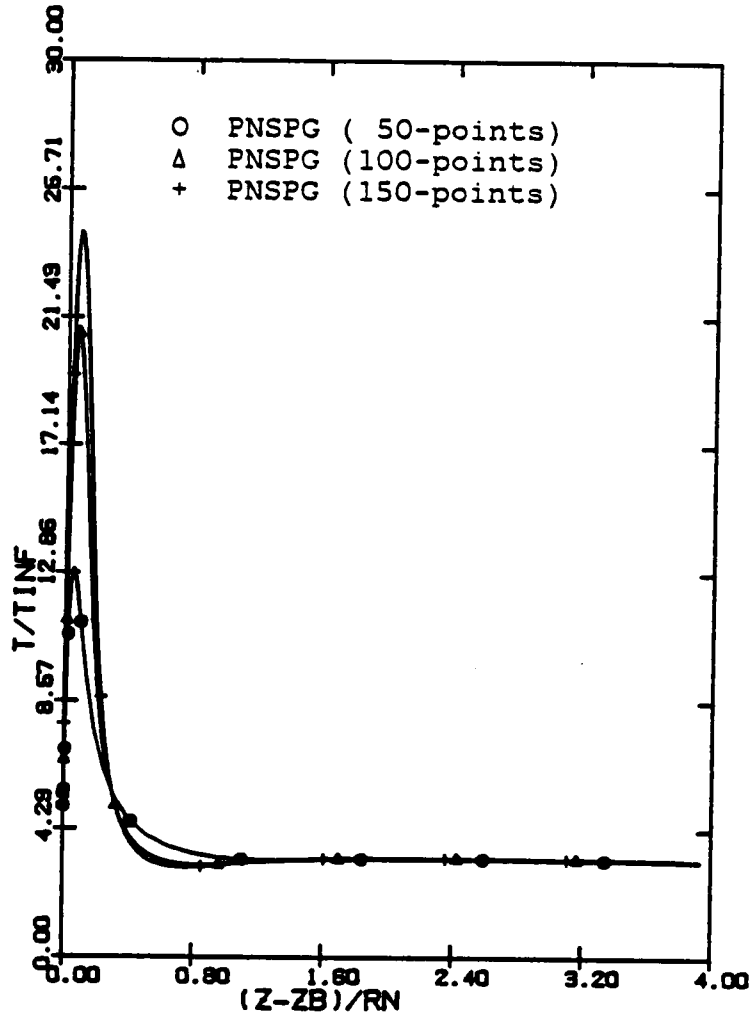

Figure 20. Effects of grid distribution on temperature profile at X/RN=200 for Case A

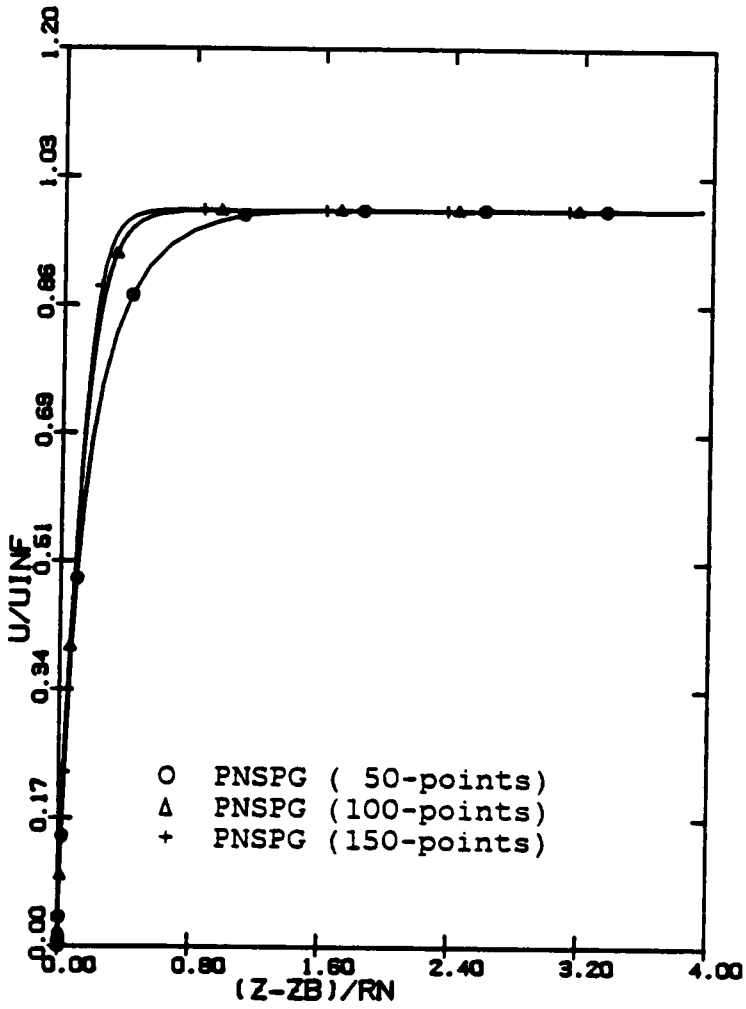

Figure 21. Effects of grid distribution on u-velocity profile at X/RN=200 for Case A

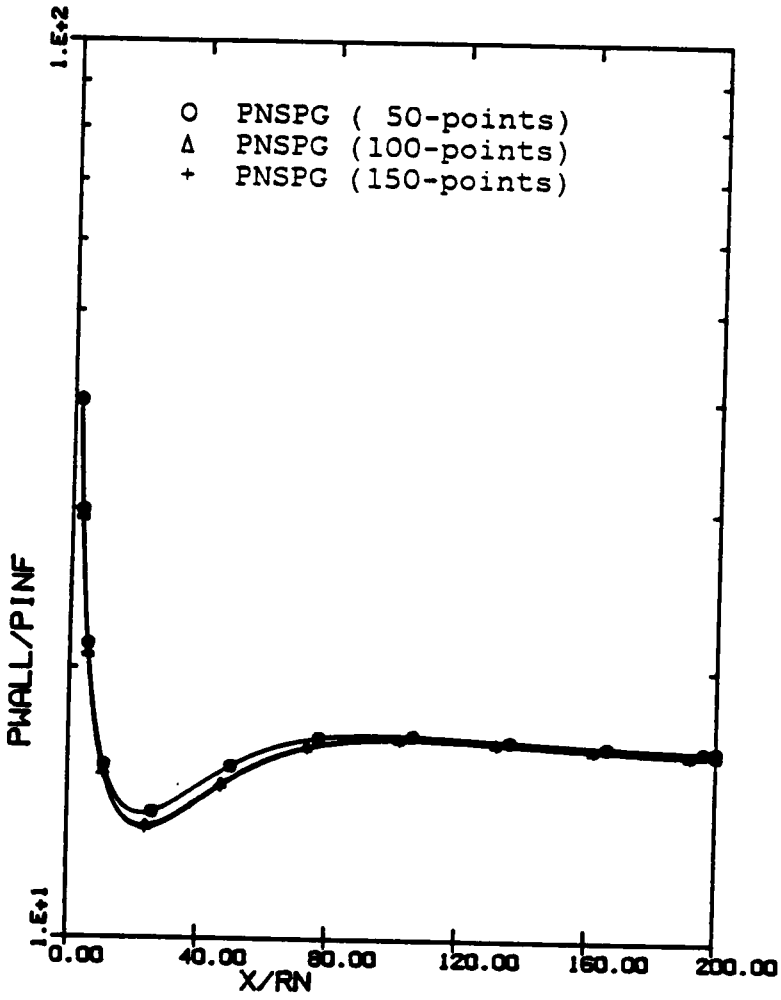

Figure 22. Effects of grid distribution on wall pressures for Case B

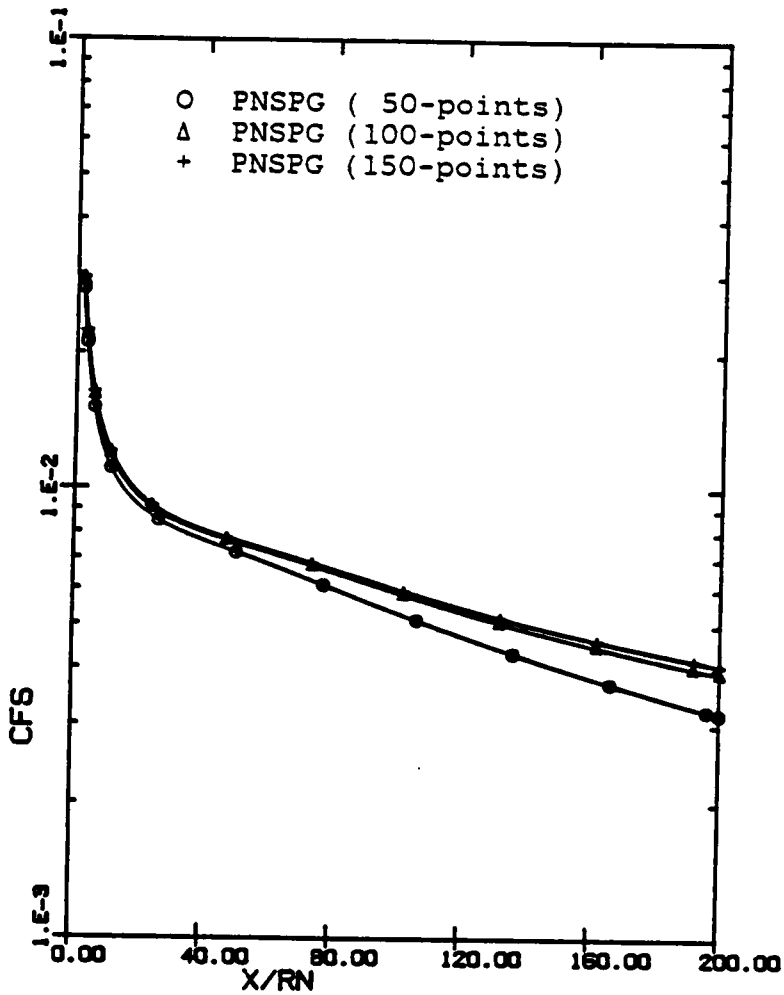

Figure 23. Effects of grid distribution on skin friction for Case B

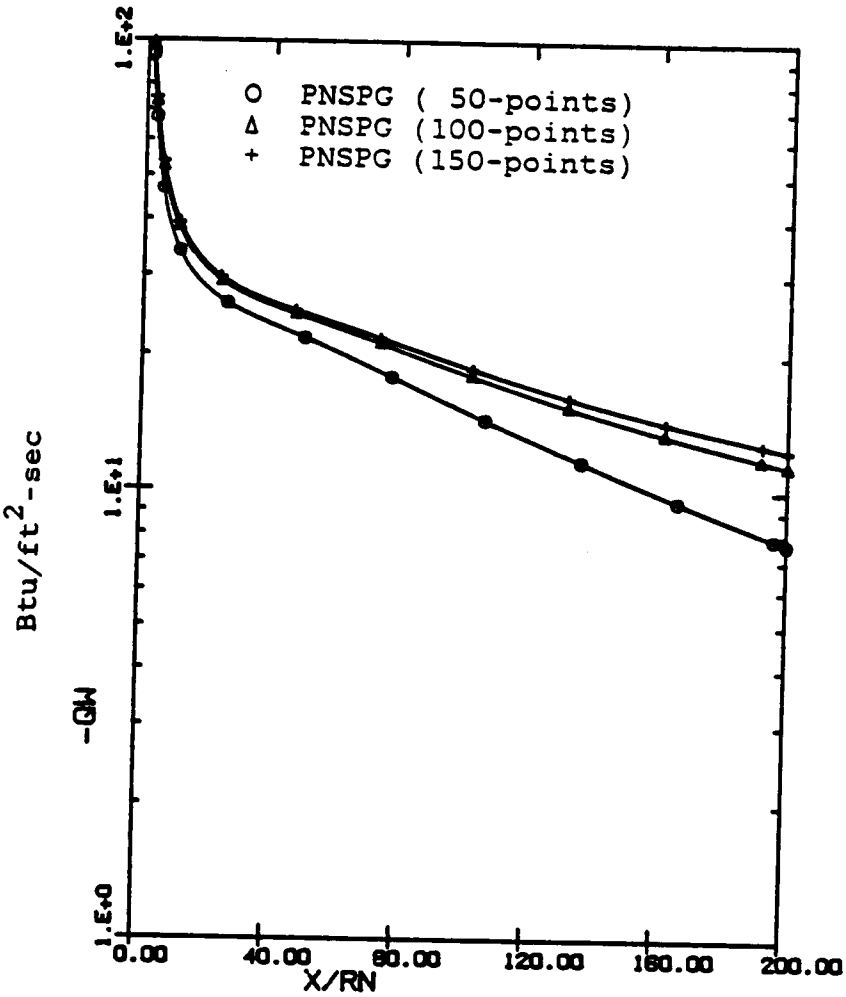

Figure 24. Effects of grid distribution on wall heat-transfer rates for Case B

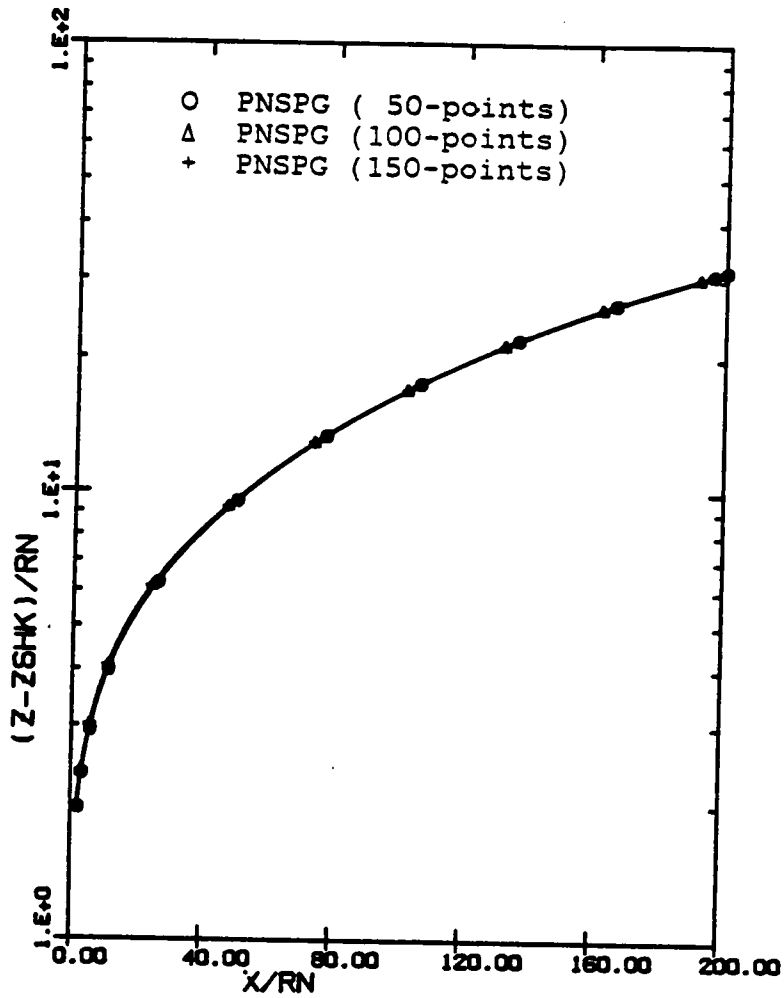

Figure 25. Effects of grid distribution on bow shock shape for Case B

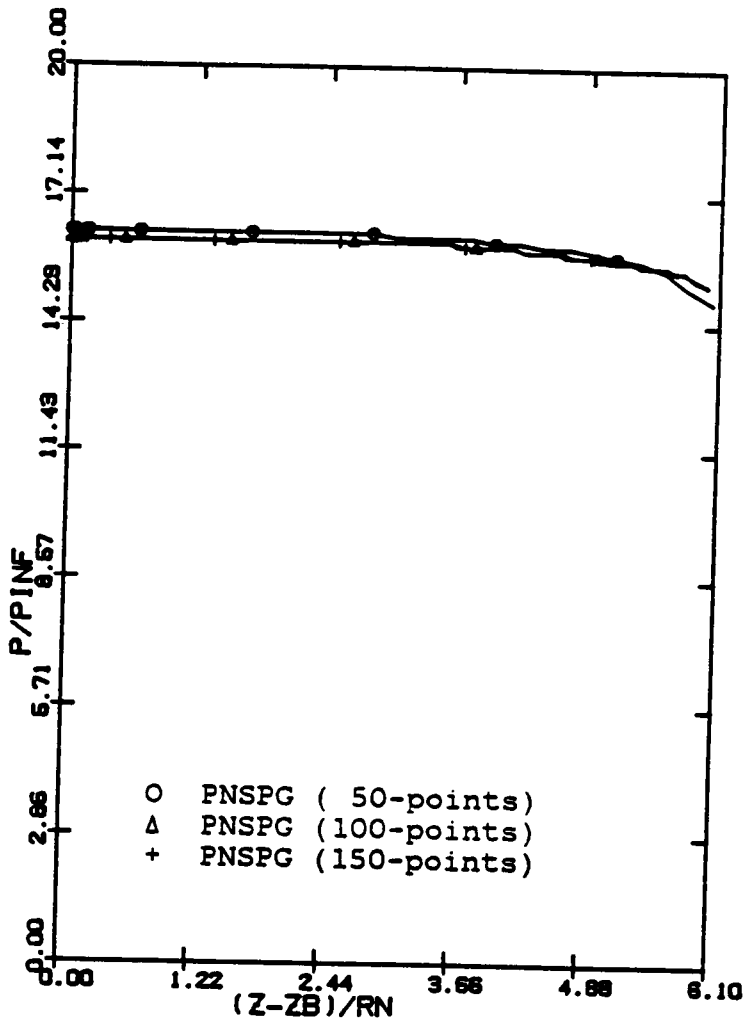

Figure 26. Effects of grid distribution on pressure profile at X/RN=200 for Case B

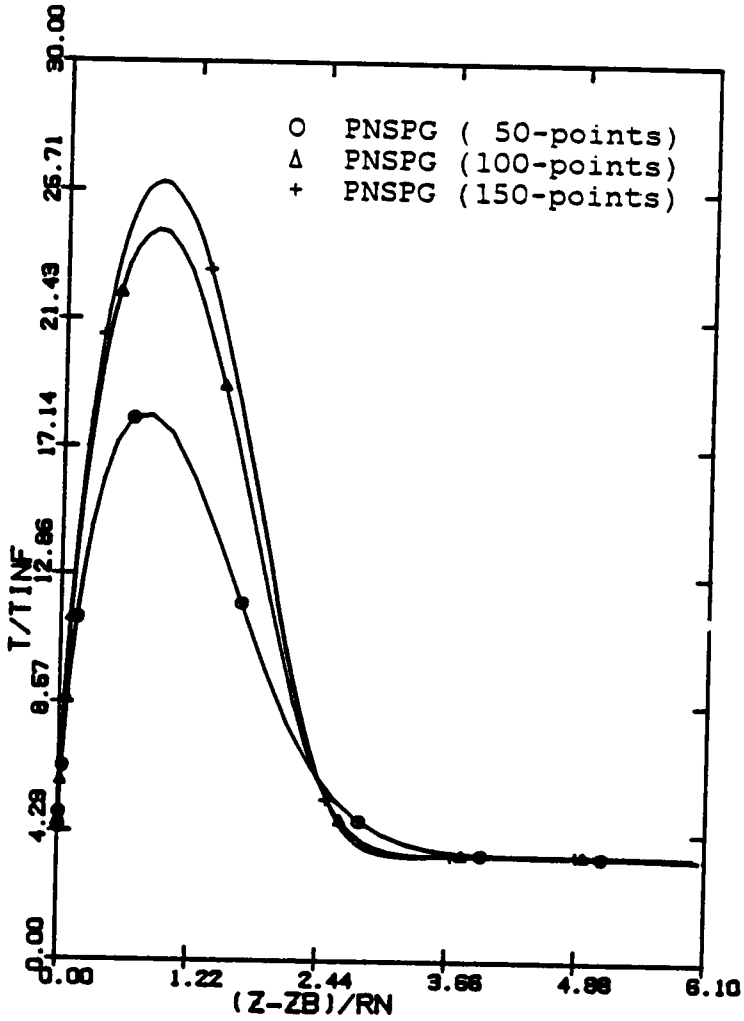

Figure 27. Effects of grid distribution on temperature profile at X/RN=200 for Case B

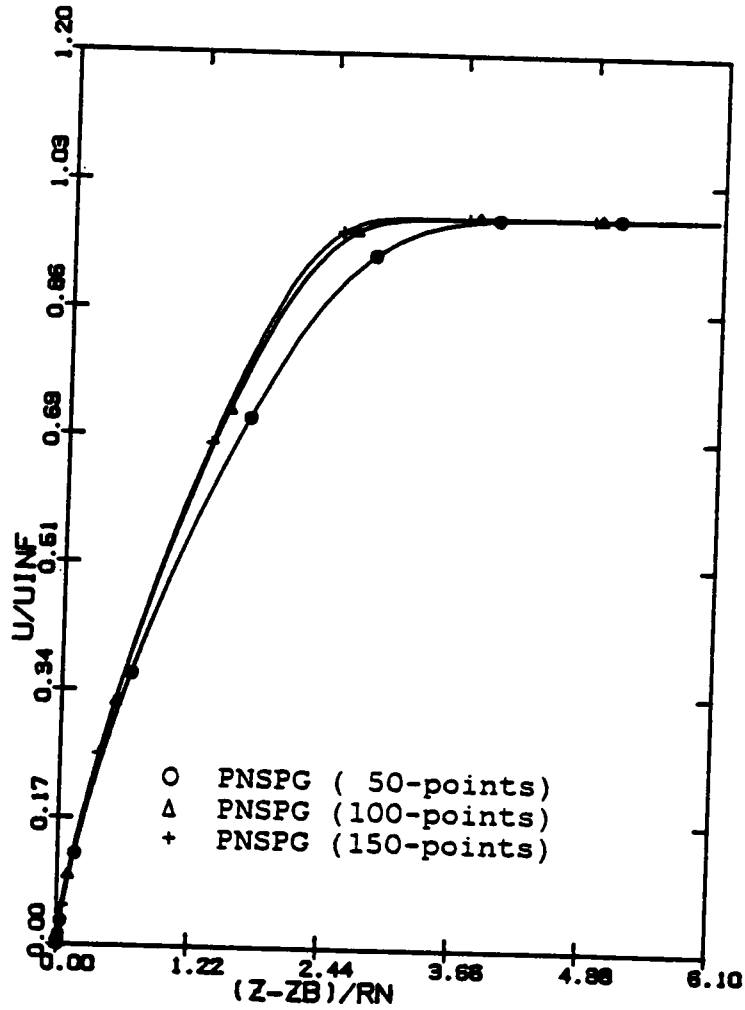

Figure 28. Effects of grid distribution on u-velocity profile at X/RN=200 for Case B

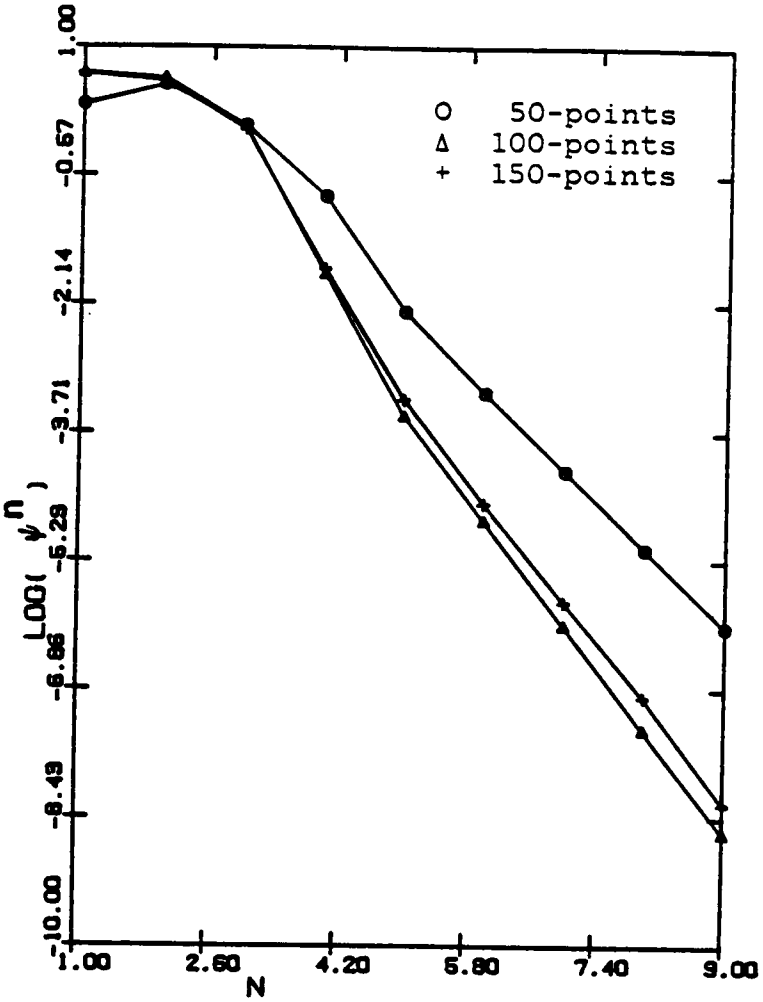

Figure 29. Error-reduction histories for Case A at X/RN=10

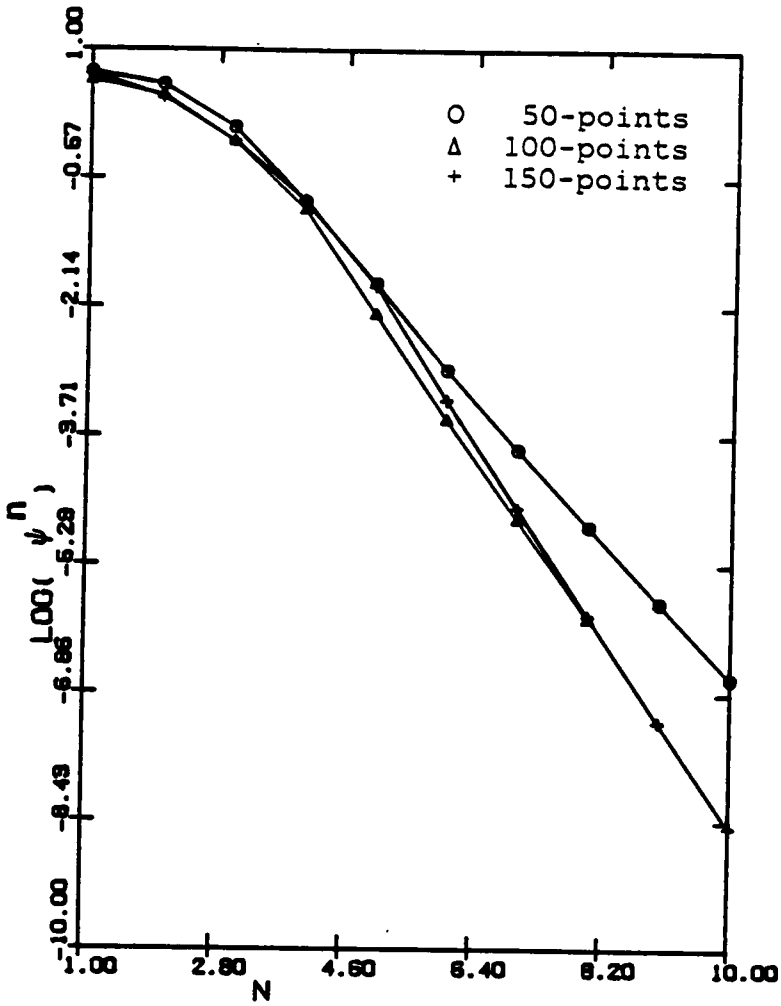

Figure 30. Error-reduction histories for Case B at X/RN=10

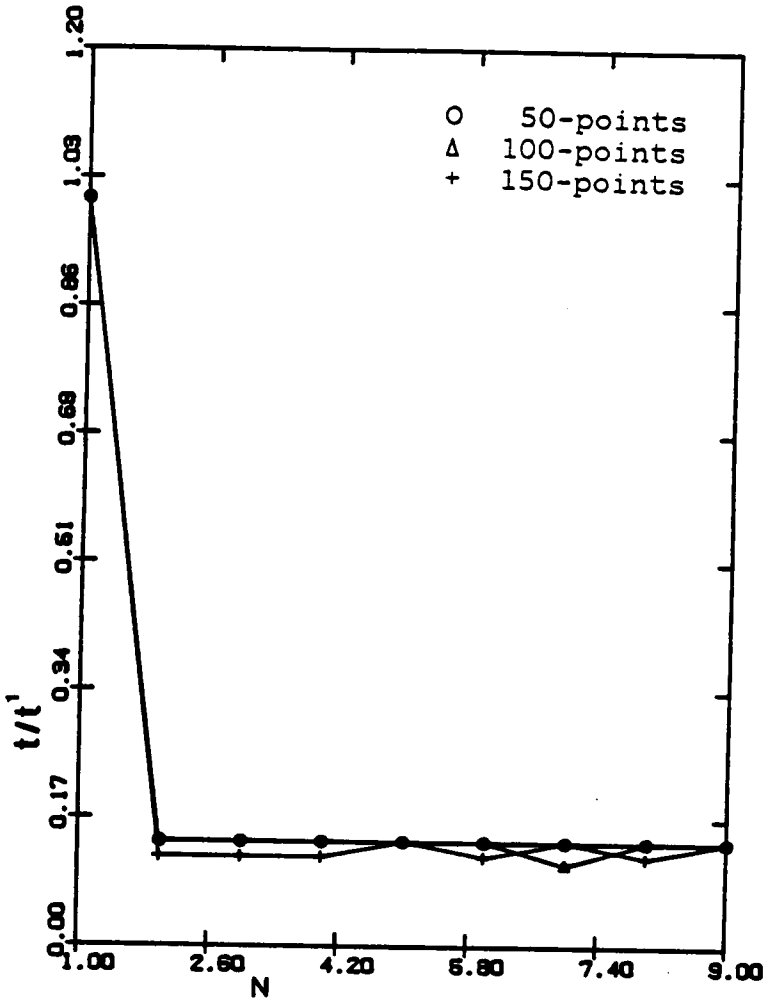

Figure 31. Computing-time histories for Case A at X/RN=10

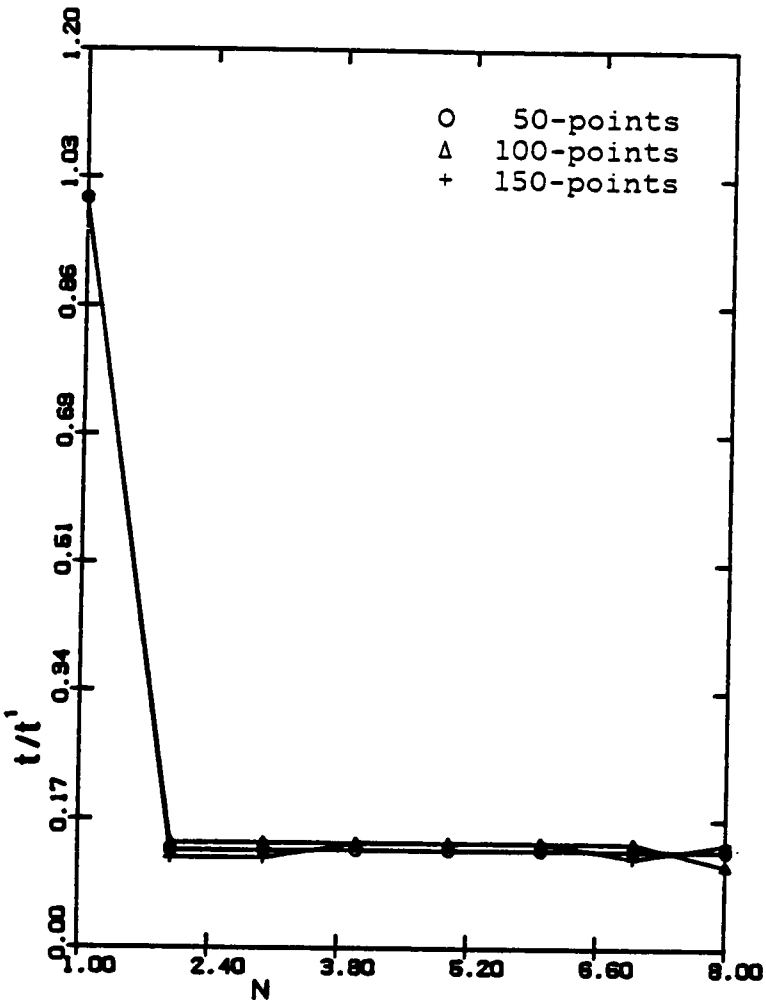

Figure 32. Computing-time histories for Case B at X/RN=10

The vita has been removed from the scanned document